LBL-3240 c.2

FRACTURE OF BRITTLE SOLIDS UNDER MULTIAXIAL AND DYNAMIC LOADING

Oktem Vardar
(Ph. D. thesis)

February 1975

Prepared for the U. S. Atomic Energy Commission
under Contract W-7405-ENG-48
and
With the financial support of the National Science
Foundation (RANN) under NSF Grant AG-393

TWO-WEEK LOAN COPY

This is a Library Circulating Copy which may be borrowed for two weeks. For a personal retention copy, call Tech. Info. Division, Ext. ~~5545~~ 5716

LAWRENCE BERKELEY LABORATORY
UNIVERSITY OF CALIFORNIA
BERKELEY

LBL-3240 c.2

DISCLAIMER

This document was prepared as an account of work sponsored by the United States Government. While this document is believed to contain correct information, neither the United States Government nor any agency thereof, nor the Regents of the University of California, nor any of their employees, makes any warranty, express or implied, or assumes any legal responsibility for the accuracy, completeness, or usefulness of any information, apparatus, product, or process disclosed, or represents that its use would not infringe privately owned rights. Reference herein to any specific commercial product, process, or service by its trade name, trademark, manufacturer, or otherwise, does not necessarily constitute or imply its endorsement, recommendation, or favoring by the United States Government or any agency thereof, or the Regents of the University of California. The views and opinions of authors expressed herein do not necessarily state or reflect those of the United States Government or any agency thereof or the Regents of the University of California.

FRACTURE OF BRITTLE SOLIDS UNDER MULTIAXIAL AND DYNAMIC LOADING

Table of Contents iii

Abstract v

Acknowledgment vii

Nomenclature ix

I. Introduction 1

II. Multiaxial Static Loading 5

2.1 Development of the statistical theory of Weibull . . 5

2.2 Limitations of the statistical theory of Weibull . . 9

2.3 Other formulations for brittle solids 13

2.4 Application of the statistical theory on disk tests . 16

III. Uniaxial Dynamic Loading 26

3.1 Introduction 26

3.2 Crack Initiation 27

3.3 Crack Propagation 33

3.4 A new theory of dynamic fracture 38

IV. Analysis of Electron Beam Tests 45

4.1 Introduction 45

4.2 Thermal crater analysis 46

4.3 Shock spalling analysis 47

V. Conclusion 53

References 55

Tables 61

Figures 66

Appendix: An extension of the dynamic model 105

FRACTURE OF BRITTLE SOLIDS UNDER MULTIAXIAL AND DYNAMIC LOADING

Öktem Vardar

Lawrence Berkeley Laboratory
University of California
Berkeley, California 94720

February 1975

ABSTRACT

Weibull's statistical treatment is employed in studying the behavior of brittle solids under static multiaxial loading in the first part of the thesis. Later, the response of cracks to short duration tensile loading is examined, and a new theory is developed for predicting failure in brittle solids due to uniaxial dynamic loading.

It is pointed out that the Weibull multiaxial treatment of brittle strength contains limitations which are not present in the more familiar uniaxial formulation. Provided these limitations are satisfied, it is possible to use tension or bending data to predict multiaxial behavior when at least one principal stress is tensile. This is illustrated for the Brazilian disk test (diametral compression of a disk). Predictions based on bending tests agree well with observed strength values in disk tests on two types of rocks.

The failure mechanism of brittle solids under very short duration loading is basically different from that under static loading. Many cracks have to be initiated and propagated at the same time so that they can link up and create a fracture surface before the pulse is over. A simple, new theory is proposed which relates the strength of brittle

solids to the duration of the applied loading. Results from the experiments in which rocks are exposed to intense short duration electron beams are predicted successfully using this theory.

ACKNOWLEDGMENT

The author wishes to express his gratitude to Professor Iain Finnie for his help, encouragement, and support during the preparation of this thesis and during the entire graduate career of the author. The author also wishes to express his sincere thanks to Professors D. B. Bogy and T. L. Brekke for their help during his research and for their review of this thesis, and to Dr. R. T. Avery for his stimulating suggestions and for procuring the rock samples.

The author acknowledges with appreciation the financial support of the National Science Foundation under NSF Grant AG-393.

NOMENCLATURE

a	crack half length
a_0	initial crack half length
b	thickness of rectangular beams
c	crack speed
c_1	dilatational wave speed $[(\lambda+2\mu)/\rho]^{\frac{1}{2}}$
c_2	shear wave speed $[\mu/\rho]^{\frac{1}{2}}$
c_R	Rayleigh wave speed
D	diameter of solid disks
d	half mean path (see Sect. 3.4)
E	Young's modulus
F	individual failure probability
G	cumulative distribution of failure
g	probability density function; ratio of $g(c)/g(0)$
$g(0)$	energy release rate at zero crack speed
$g(c)$	energy release rate at a crack speed of c
$g_c(0)$	critical energy release rate at zero crack speed
$g_c(c)$	critical energy release rate at a crack speed of c
h	height of rectangular beams; depth of the volume subject to stress pulse
Δh	depth of a single layer (see Sect. 3.4)
K_I	stress intensity factor
K_{Ic}	critical stress intensity factor ($\equiv$ fracture toughness)
K_{Id}	stress intensity factor due to dynamic loading
ℓ	number of layers in the volume subjected to stress pulse

L	length of rectangular beams
m	Weibull parameter
N	number of cracks; number of specimens
p	pressure
p_m	mean pressure
P	load
P-wave	Primary (dilatational) wave
R	radius of solid disks
S	cumulative distribution of survival
S-wave	Secondary (shear) wave
T	temperature
t	thickness of disks
u	displacement
V	total volume of the specimen
α	half of the angle over which pressure is applied in solid disks; linear thermal coefficient of expansion
Γ	gamma function
λ	Lamé constant; wave length
μ	Lamé constant; coefficient of friction
ν	Poisson's ratio
ρ	mass density
$\sigma_1,\sigma_2,\sigma_3$	principal stresses
σ_0	scaling parameter in Weibull's theory; a stress level
σ_u	zero strength (stress, below which no failure occurs)
σ_n	normal stress
σ_m	mean stress

σ_c	critical stress
τ	duration of the stress pulse; time to fracture

CHAPTER ONE: INTRODUCTION

Brittle solids were the materials of antiquity and indeed the very survival of our prehistoric ancestors depended on their ability to shape stones into tools and weapons. By contrast, in the past century with the development of steel, mechanical engineers have been concerned primarily with design based on the properties of ductile metals. However, interest in brittle solids has revived in recent years for several reasons. They are the materials with the highest theoretical strength. While this strength is not realized in bulk specimens because of inherent flaws, it is approached in microscopic whiskers. The use of these materials in composites is attracting considerable attention. Also, these solids which we term brittle -oxides, carbides, nitrides, graphite - have the greatest strength at elevated temperature. With the growing emphasis on fuel economy, there is a need to increase operating temperatures and extensive research on ceramic gas turbines is under way. Certain brittle solids are also of interest because of special properties such as transparency or corrosion resistance. The compressive strength of brittle solids is much greater than their tensile strength. For this reason, design with brittle solids such as concrete or masonry is usually aimed at keeping them in compression with generous safety factors being allowed.

Another area which has led to great interest in brittle solids is that of tunneling and excavation of rock. With the growing emphasis on improving the environment by providing underground rapid transit systems, underground power plants, etc., much attention has been given to novel tunneling techniques. Unfortunately most drilling or tunneling

techniques load the rock in compression rather than exploiting the comparatively low tensile strength of this type of material.

Having given these general reasons for an interest in brittle solids, we will now summarize our present state of knowledge and point out the areas which appear to need further study. By "brittle solids" we mean materials which show essentially no platic deformation before failure in conventional strength tests. This means that these materials are extremely sensitive to small imperfections since local stresses cannot be relieved by plastic flow. It is believed that this is the basic reason for the discrepancy between the theoretical strength of about E/10 (where E is Young's modulus) and the usual strength of about E/1000 observed in testing bulk specimens. Unfortunately, the powerful analytical tools of linear elastic fracture mechanics which relate strength to flaw size cannot, at present, be applied to typical brittle solids. Because the toughness (strength in the presence of a flaw) of these materials is so low, the cracks responsible for strength are extremely small and cannot be detected non-destructively. In some materials such as rocks the inherent flaws can probably be detected as grain boundary cracks. In other cases such as glass, the inherent flaws have never been observed directly to our knowledge. Thus in most cases we can only infer that a distribution of inherent flaws is present in the material. This conclusion is supported by the large variability in strength of nominally identical specimens as well as by the discrepancy between the theoretical and actual strengths. In addition, the increase in average fracture stress which is observed when the specimen size is decreased is consistent with the decreased probability of finding a large flaw in a smaller specimen. The preceding comments relate to failure under tensile states of stress and static

loading conditions. Here the flaws may be regarded as links in a chain with failure of the part being governed by failure of the weakest link. By contrast in compressive loading and also, as we will see, in very short duration tensile loading, many flaws may have to initiate prior to final fracture of the part.

Fortunately, for static loading under tensile states of stress, an approach developed by Weibull allows many useful predictions to be made. Given the distribution of strength from tests on a number of specimens, Weibull's approach allows the effects of specimen size and stress distribution to be predicted. For example, test results in bending can be used to predict behavior in other situations such as thermal shock and for different sizes of specimens. Almost all of the attention given to Weibull's formulation has been for uniaxial states of stress. Little has been done to study multiaxial stress although Weibull in his original work suggested an approach to this problem. For this reason the problem of predicting strength under multiaxial loading will be examined in the first part of the thesis. Some limitations of the Weibull approach will be pointed out. It will be shown that if these are recognized, satisfactory predictions may be made for multiaxial behavior. This is illustrated by using bending data to predict the fracture of a disk under line loading at opposite ends of a diameter (the Brazilian disk test). Surprisingly, although this is a very common test it has never been subjected to a complete analysis using the Weibull approach.

As already mentioned, the compressive strength of a brittle solid is much greater than its tensile strength. Basically, this is because many cracks must initiate before final failure occurs. Although of

fundamental interest, we have chosen not to study compressive strength because it presents less of a problem in design or in optimizing tunneling operations than the tensile strength.

Another problem in which many cracks may have to initiate before final separation occurs is that of very short duration tensile loading. In this case, the propagation rather than the initiation phase of fracture may be the dominant one. That is, a single crack can travel only a limited distance in the time of loading and this may not be enough to produce complete separation of the part. Present theories for this type of fracture are almost completely empirical and have been developed in connection with spalling problems. Recently a novel method of tunneling has been proposed by Avery et al. [1-1]. This utilizes short duration bursts of energetic electrons and subjects the rock to very short duration tensile pulses. To understand the mechanism of removal in this novel process it is important to obtain a better understanding of tensile failure under very short duration loading. For this reason, in the second part of this thesis, a detailed study of this problem is undertaken. A new theory for this type of fracture is developed which is believed to be more rational than existing theories and is in good agreement with experimental results.

CHAPTER TWO: MULTIAXIAL STATIC LOADING

2-1 Development of the statistical theory of Weibull

Based on the assumptions that brittle solids are homogeneous, isotropic,* and contain uniformly distributed randomly oriented flaws, Weibull [2-1] formulated in 1939 his statistical treatment of failure in brittle solids. Although it is not based on a rigorous, analytic derivation, it shows great ingenuity and predicts the behavior of - at least a group of - brittle solids remarkably well.

It is necessary to review the Weibull treatment as applied to uniaxial stress states in order to get a better understanding of multiaxial stress states. The theoretical basis of the theory is well developed by Oh and Finnie [2-2] . Observations show that brittle solids can be approximated most effectively by the series model. It is assumed that there is no interaction of flaws and failure occurs when the strength of the worst flaw is reached. (The chain is as strong as its weakest link.) Only tensile stress is assumed to cause failure; any effect of compressive stress is neglected. No detailed analysis is made as to the size, shape, or number of the existing flaws.

Considering a chain of N links in which the individual failure probabilities at a given stress σ are $F_i(\sigma)$, the survival probability $S(\sigma)$ for the whole chain is

$$S(\sigma) = \prod_{i=1}^{N} \left[1 - F_i(\sigma) \right]$$

---

*Although some brittle solids are very heterogeneous on a microscale, they can be approximated well on a macroscale as homogeneous and isotropic.

and

$$\ln S = \sum_{i=1}^{N} \ln (1-F_i) = - \sum_{i=1}^{N} (F_i + \frac{F_i^2}{2} + \frac{F_i^3}{3} + \cdots)$$

$$\cong - \sum_{i=1}^{N} F_i$$

if F_i is sufficiently small or if N is sufficiently large. It is reasonable to assume that F_i for each link is proportional to its volume and some function of stress; Weibull chose, based on existing experimental evidence,

$$F_i(\sigma) = (\sigma/\sigma_0)^m dV$$

which leads to the failure probability

$$G = 1 - S = 1 - \exp\left[-\int (\sigma/\sigma_0)^m dV\right] \qquad (2\text{-}1)$$

which turns out to be a logical choice for representing the results of strength tests on brittle solids as long as the number of flaws present is large. Oh and Finnie have shown that provided the individual probability distribution of cracks, $F(\sigma)$, behaves like σ^m as σ approaches zero from above, the distribution in strength of the specimens will always converge toward Eq.(2-1), independent of the form of $F(\sigma)$.

To ensure that σ_0 has units of stress, it is more convenient to write Eq.(2-1) as

$$G = 1 - \exp\left[- \int (\frac{\sigma}{\sigma_0})^m \frac{dV}{V_0} \right]$$

where V_o is a unit volume. On the other hand, it is inconvenient to carry along an extra quantity in the formulation. Therefore, in the rest of the thesis "V_0" will be omitted with the understanding that dV is a dimensionless quantity and stands for (dV/V_0), where V_0 is taken as 1 in^3 ($1m^3$).

The integral in Eq.(2-1) is called "risk of rupture". It is to be taken over the region where the acting stresses are tensile. Depending on the nature of the flaws, it may be a volume, area, or line element. The parameters m, σ_0 are assumed to be properties of the particular material in question and are determined experimentally.

It is more realistic to admit a third parameter, σ_u, which would mark the stress below which no failure occurs. The three parameter formulation as given by

$$G = 1 - \exp(-B)$$

$$B = \int (\sigma - \sigma_u)^m/\sigma_0 \; dV \qquad \text{for } \sigma \geq \sigma_u$$

$$= 0 \qquad \text{for } \sigma < \sigma_u$$

has to be employed if interest lies in very small probabilities. For mean (or median) fracture stresses, however, the advantage of three parameter is questionable, especially in the face of difficulties connected with parameter estimation in multiaxial stress states.

Following the assumption of tensile stress being the only cause of failure, Weibull replaced "σ" of the one-dimensional stress state by the normal stress acting on a crack, " σ_n", in multiaxial cases. He then considered all possible orientations of cracks and summed up their

contribution to the "risk of rupture". It is worth noting here that this is not an averaging process but includes all disjoint events. Thus,

$$G = 1 - \exp\left[-B\right]$$

$$B = \int_V \left\{ K \int_{A_{\text{unit sphere}}} \sigma_n^m \, dA \right\} dV . \tag{2-2}$$

In principal stress space, as shown in Fig.2-1,

$$\sigma_n = \cos^2\phi \, (\sigma_1 \cos^2\psi + \sigma_2 \sin^2\psi) + \sigma_3 \sin^2\phi$$

$$dA = \frac{1}{4\pi} \cos\phi \, d\psi \, d\phi \tag{2-3}$$

and the integration is carried out over the range of angles for which σ_n is tensile. Thus, we are not able to treat stress states which induce triaxial compression. In particular, where $\sigma_3 \equiv 0$, the limits reduce to $-\pi/2 \leq \phi \leq \pi/2$ and $-\psi_0 \leq \psi \leq \psi_0$, where

$$\psi_0 = \begin{cases} \pi/2 & \text{if } \sigma_2 \geq 0 \\ \arctan\left(-\dfrac{\sigma_1}{\sigma_2}\right)^{\frac{1}{2}} & \text{if } \sigma_2 < 0 . \end{cases} \tag{2.4}$$

Using Eqs.(2-2) and (2-3), setting $\sigma_2 = \sigma_3 = 0$, and comparing with Eq.(2-1),

$$K = 2 \, (2m + 1)/\sigma_0^m . \tag{2-5}$$

The difficulties involved in using three parameter distribution can be discussed now. One, which is common to both uniaxial and multiaxial treatment, is that the uncertainty involved in fitting three parameters to data is a great deal greater than when only two parameters are involved.

The other difficulty with the three parameter distribution in the multiaxial case is what Weibull called the "risk of rupture", B in Eq.(2-2), does not reduce to its value for the uniaxial case. Thus, the parameters deduced from uniaxial tests cannot be applied to the multiaxial case. We see this by writing

$$B = \int_V \left\{ K \int_{A_{\text{unit sphere}}} (\sigma_n - \sigma_u)^m \, dA \right\} dV$$

$$B = \int_V \left\{ \frac{K}{4\pi} \iint_{\psi\phi} \left[\cos^2\phi \, (\sigma_1 \cos^2\psi + \sigma_2 \sin^2\psi) + \sigma_3 \sin^2\phi - \sigma_u \right]^m \cos\phi \, d\phi \, d\psi \right\} dV.$$

This reduces for uniaxial stress states only to

$$B = \int_V \left\{ \frac{K}{4\pi} \iint_{\psi\phi} \left[\cos^2\phi \, \cos^2\psi \, \sigma_1 - \sigma_u\right]^m \cos\phi \, d\phi \, d\psi \right\} dV \qquad (2\text{-}6)$$

which is not a function of $(\sigma_1 - \sigma_u)^m$.

Several attempts have been made to overcome this limitation of the three parameter distribution for multiaxial stresses. They are discussed in some detail in Section 2.3.

2.2 Limitations of the statistical theory of Weibull

For uniaxial stress states, the Weibull treatment has been applied successfully to a wide variety of brittle solids [2-2 to 2-6]. The multiaxial formulation, however, has seen relatively little application. This may be due to the fact that the limitations of the theory are not

yet fully recognized. Some of these limitations are restricted to multiaxial cases and lead to important consequences. An attempt is made here to list the limitations of the Weibull theory.

(i) A knowledge of the complete stress field is necessary; there is a finite probability of failure associated with each point in the body where the normal stress is tensile. (It is generally much easier to determine maximum stresses and their location, and this is sufficient for most other failure theories.)

(ii) The Weibull formulation, as discussed here, makes no provisions for anisotropic behavior. Although Weibull attacked this problem in his second paper [2-7], he could not estimate the parameters from experimental data except through a complicated trial and error procedure.

(iv) A number of investigators have obtained biaxial data in both the tension-tension and tension-compression regions. At first sight, the results appear contradictory with some materials showing weakening in biaxial tension, relative to uniaxial tension, while other materials show just the opposite effect. As a generalization, materials which would be expected to have sharp flaws (alumina [2-8], titania [2-9], silicon carbide [2-10], cast iron [2-11], and glass [2-12]), are in the former category. Materials which might be expected to have more nearly spherical flaws (porous zirconia [2-13], hydrostone plaster [2-24]) show the latter behavior. Thus, not surprisingly, the shape of the inherent flaw appears to have a strong influence on the form of the fracture envelope for multiaxial stress. The Weibull multiaxial formulation considers only the normal tensile stress on all planes at each point in a solid. Thus, it

would be expected to apply primarily to cases in which the flaws are sharp, flat cracks. For such a flaw, normal stresses in directions lying in the plane of the crack do not contribute to the stress singularity. By contrast, for more nearly spherical flaws, all normal stress components affect the maximum local stress at the surface of the flaw.

To extend the formulation to elliptical cracks, we can replace σ_n in Eq.(2-2) by an equivalent stress $\bar{\sigma}_n$ which is a combination of the stresses acting normal to the crack plane (σ_n) and parallel to it (σ_{n^*}) (Fig. 2-2). Here we assume that mode I fracture (opening mode) exists alone and fracture will start at the very tip of the crack. Then, from the Inglis' solution [2-15], shear stress τ has no effect on the tangential stress at the tip, $\sigma_{\eta\eta}$, and we can write

$$\bar{\sigma}_n = \sigma_n - f\sigma_{n^*}$$

where f is a factor reflecting the relative effects of σ_n and σ_{n^*} at the tip; it depends on the shape of the ellipse and varies from zero, for a line crack, to approximately 1/3 for spherical voids with $\nu = 0.3$.

Using Euler's parametric specification of rotations around a point [2-16], we can express the normal stresses in the principal stress space as

$$\sigma_n = (\sigma_1\cos^2\psi + \sigma_2\sin^2\psi)\cos^2\phi$$

$$\sigma_{n^*} = \sigma_1(n_1^*)^2 + \sigma_2(n_2^*)^2$$

$$n_1^* = (\sin^2\psi + \sin\phi\ \cos^2\psi)\cos\Theta + \sin\psi\ \cos\psi(\sin\phi - 1)\sin\Theta$$

$$n_2^* = \sin\psi\ \cos\psi(\sin\phi - 1)\cos\Theta + (\cos^2\psi + \sin\phi\ \sin^2\psi)\sin\Theta$$

where ψ, ϕ are shown on Fig. 2-1 and Θ is the angle of the crack tip, as measured from a convenient datum line, in the plane of the crack. As Θ is changed from $-\pi/2$ to $\pi/2$, all cracks having the same normal ($\underset{\sim}{n}$) are covered. Thus, for a uniform stress field

$$B = KV \int_{-\pi/2}^{\pi/2} \int_{-\pi/2}^{\pi/2} \left\{ \int_{-\Theta_0}^{\Theta_0} \left[\bar{\sigma}_n(\phi,\psi,\Theta) \right]^m \frac{d\Theta}{2\pi} \right\} \cos\phi \frac{d\psi d\phi}{4\pi}$$

where Θ_0 is such that $\bar{\sigma}_n > 0$.

For purposes of illustration the above equation is evaluated for certain special cases ($m = 5$, $f = 0.01$; 0.1; 0.3), and the fracture envelope for the mean is plotted in Fig. 2-3. It is very clear that the shape of the flaws is crucial for multiaxial cases whereas it practically does not change results for uniaxial stress states. For an elliptical flaw with semi-major to semi-minor axis ratio (b/a) approximately equal to 4.5 (i.e $f \cong 0.1$), the Weibull treatment introduces an error of 43% for $\sigma_2/\sigma_1 = -9$, 11% for $\sigma_2/\sigma_1 = -2$, but only 1% for the uniaxial stress state. Thus, although the Weibull treatment is applicable to all homogeneous, isotropic brittle solids in uniaxial stress states, it can be employed in multiaxial cases only for materials with sharp cracks, i.e., where $b/a > 50$ approximately.

(v) Weibull's analysis assumes in the very beginning that the number of inherent flaws in the specimen is large. Hence, care has to be taken to apply this statistical treatment to regions where flaw population is expected to be high.

2.3 Other formulations for brittle solids

Statistical extreme value theory predicts that there are only three general types of asymptotic distributions for the smallest or largest value in an increasingly large sample. And only one of them is used generally in strength predictions since the other two of these three forms correspond to cases where the range of the parent distribution has no lower bound. But it has been pointed out by McClintock [2-17] that the distribution of strengths does not necessarily tend to an asymptote as the size of the sample is increased. In fact, he chose a more physical model where the distribution of the crack lengths follows an extreme value distribution, and he showed that the resulting distributions of strength do not follow any of the three asymptotic distributions. Using a model with uniform grain size and examining the probability of one or more grain boundary cracking, McClintock arrived at the same size distribution as proposed by Fisher and Hollomon in 1946. The cumulative distribution of failure for individual cracks then turned out to be $K' \exp(K''/\sigma^2)$ as opposed to Weibull's choice of $K\sigma^m$. McClintock's theory was proposed recently and no comparison with experimental data is yet available. Although it is based on reasonable physical grounds, it has not yet been extended to treat multiaxial stress states. It is not at all clear how such an extension could be carried out.

Batdorf [2-18,19] attempted to formulate directly a multiaxial theory. He assumed that the density of cracks having a critical stress less than or equal to σ_{cr} can be given as a polynomial, $\sum_{j=1}^{N} b_j \sigma_{cr}^j$; similar to Weibull and McClintock, he also looked at sharp cracks without specifying their detailed shape or size and considered the normal stress on a crack

as the only determining factor for fracture. The estimation of the coefficients in the density distribution function proves to be straightforward for materials with surface flaws, but rather difficult for materials with volume flaws; a set of N linear simultaneous equations have to be solved using N of the experimental data points obtained from uniaxial tests. Based on Oh's [2-20] data, Batdorf's prediction for glass failure is good only at very low probabilities (Fig. 2-4). Weibull's theory is much easier to apply and predicts a better correlation at the mean or median (Fig. 2-5).

The difficulties involved in using three parameter Weibull distribution were pointed out in Section 3.1. Dukes [2-21] used numerical techniques to overcome these. He wrote Eq. (2-6) as

$$B = \int_V \left\{ \frac{K_1 \sigma_1^{m_1}}{4\pi} \int_\phi \int_\psi \left[\cos^2\phi \cos^2\psi - \frac{\sigma_u}{\sigma_1} \right]^{m_1} \cos\phi \, d\psi \, d\phi \right\} dV$$

and compared with the uniaxial formulation

$$B = \int_V K \sigma_1^{\,m} \left[1 - \frac{\sigma_u}{\sigma_1} \right]^m dV \ .$$

Through numerical evaluation, he found out that the parameters in the multiaxial formulation $(m_1 K_1, \sigma_u)$ can be approximately determined from the uniaxial parameters (m, K, σ_u) using the relations

$$m_1 = m - 1$$

$$K_1 = 4\pi\sigma_1 K/I_0$$

$$I_0 = \int_{-\pi/2}^{\pi/2}\int_{-\pi/2}^{\pi/2} \left[\cos^2\phi\cos^2\psi\right]^{m_1} \cos\phi d\psi d\phi$$

as long as $2 < m_1 \leq 10$ and $0 \leq \sigma_u/\sigma_1 \leq 0.8$. He plotted the quantity I_0 as a function of m_1 as a convenience to the designer.

For cases where the stress field is uniform, the risk of rupture can be expressed, using the above relations, as

$$B = \frac{K_1 V \sigma_1^{m_1}}{4\pi} \int_{\psi}\int_{\phi} \left[\cos^2\phi(\cos^2\psi + \frac{\sigma_2}{\sigma_1}\sin^2\psi) + \frac{\sigma_3}{\sigma_1}\sin^2\phi - \frac{\sigma_u}{\sigma_1}\right]^{m_1} \cos\phi d\psi d\phi$$

$$B = KV\sigma_1^m \left[I/I_0\right].$$

He evaluated the term in brackets numerically and plotted it for various values of σ_2/σ_1, σ_3/σ_1, σ_u/σ_1 and m_1.

Duke's efforts were mainly towards simplifying the use of the multi-axial Weibull formulation; although he made no original contribution to the subject, his plots may prove very convenient in practical design procedures.

Fairhurst, Hardy and Hudson [2-22,23,24] took a completely different approach. They assumed that brittle solids, mainly rocks, can be characterized by an "effective crack length" and a "work of fracture", and then they applied the linear elastic fracture mechanics approach. The method is based on calculating the change in compliance with crack length using finite element method for any given geometry. The energy release

rate g can be given as

$$g = \frac{P^2}{2B} \frac{dC}{da} \tag{2-7}$$

where C is the compliance and B is the thickness of the specimen. Since the energy release rate g equals its critical value g_c at fracture, the critical load in an experiment can be found from Eq. (2-7) when g_c of that particular material is known. It is to be noted that since energy release rate g is a function of loads, geometry, and crack length, the critical crack length has to be known to evaluate dC/da. To estimate the material properties "a" and " g_c", they used diametral compression tests. From finite element calculations they determined that the failure load in a ring test is independent of the effective crack size, so that Eq. (2-7) could be used to get g_c. To evaluate the crack size, the disk test proved handy since it is quite sensitive to a central crack.

At this stage, it is hard to evaluate the assumption that material behavior can be fully described by an "effective crack length" and a "work of fracture". The experimental results of Hardy [2-23] are not conclusive either; predictions based on other tests for the failure of beams in three point bending are in error by as much as 31%.

2.4 Application of the statistical theory on disk tests

In studying brittle solids such as ceramics and rocks, conventional tension tests present difficulty both in specimen preparation and in alignment during the test. As an alternative, bending tests are often made but in addition, a large number of less conventional specimens have been proposed for measurement of tensile strength [2-25] . One of the more interesting of these is the diametral compression of a solid disk,

shown in Fig. 2-6a, for the specimen is simple to prepare and to load. In this specimen there is an extensive region along the axis of loading where the stress transverse to the loading axis is tensile and constant with magnitude about one-third that of the compressive stress in the loading direction. This test was first proposed, apparently, by Carniero and Barcellos [2-26] and since then has often been referred to as the Brazilian Disk test.

Despite the attention which the Brazilian disk test has received [2-27 to 2-30], it appears that no detailed analysis has been made to compare its results with more conventional strength tests. We will show, at least for a certain class of brittle solids, that behavior in this test may be predicted from that in bending tests by using the Weibull multiaxial treatment of brittle strength.

We consider disks which are thin enough relative to their diameter to be treated as a case of generalized plane stress. Thus, the stress components to be considered are $\sigma_r, \sigma_\Theta, \tau_{r\theta}$. Rather than point loading as shown in Fig. 2-6a to avoid local crushing, it is preferable to flatten the disk slightly at the loading points and work with the shape shown in Fig. 2-6b. An exact stress analysis for the configuration shown in Fig. 2-6c has been given by Hondros [2-31]. When the angle 2α over which pressure is applied is small, we would expect the stresses in cases (b) and (c) to be essentially identical a short distance away from the loaded surface.

Most workers have considered only the stress state at the center of the specimen or along the loaded diameter. However, depending on the combination of stress and flaw location, fracture in this test may start

away from the centerline. The attraction of the Weibull formulation is that it takes care of this aspect by integrating a function of stress over the entire stressed volume.

For the case shown in Fig. 2-6c, the cummulative distribution of failure may be written as

$$G(p) = 1 - \exp\left[-B(p)\right]$$
$$B(p) = t\int_{A_{disk}} \left\{ K \int_{A_{unit\ sphere}} \left[\sigma_n(p)\right]^m dA \right\} dA \qquad (2\text{-}8)$$

where p is the applied pressure and t the thickness of the disk.

To evaluate B(p) I have taken the first twenty terms in the series expansion given by Hondros [2-31]

$$\sigma_r = -\frac{2p}{\pi}\left\{\alpha + \sum_{n=1}^{\infty}\left[1 - (1 - \frac{1}{n})\ (\frac{r}{R})^2\right](\frac{r}{R})^{2n-2} \sin 2n\alpha \cos 2n\Theta\right\}$$

$$\sigma_\Theta = -\frac{2p}{\pi}\left\{\alpha - \sum_{n=1}^{\infty}\left[1 - (1 + \frac{1}{n})\ (\frac{r}{R})^2\right](\frac{r}{R})^{2n-2} \sin 2n\alpha \cos 2n\Theta\right\} \qquad (2\text{-}9)$$

$$\tau_{r\Theta} = \frac{2p}{\pi}\left\{\sum_{n=1}^{\infty}\left[1 - (\frac{r}{R})^2\right](\frac{r}{R})^{2n-2} \sin 2n\alpha \sin 2n\Theta\right\}.$$

The quantities in these equations are defined in Fig. 2-6c.

The mean pressure at failure is given by

$$p_m = \int_0^\infty p \cdot g(p)\,dp$$

where $g(p)$ is the probability density function. Noting that $g(p) = \frac{dG(p)}{dp}$ and the cummulative distribution of survival $S(p) = 1 - G(p)$

$$p_m = \int_0^1 p\,dG = -\int_1^0 p\,dS = \int_0^\infty S\,dp$$

since S approaches zero more rapidly than p does infinity. Using Eq.(2-8) and Eq.(2-3),

$$p_m = \int_0^\infty \exp\left\{ -t \int_{A_{disk}} \left[\frac{K}{4\sqrt{\pi}} \frac{\Gamma(m+1)}{\Gamma(m+1.5)} \sigma_1^m(p) \int_{-\psi_0}^{\psi_0} \left(\cos^2\psi + \frac{\sigma_2}{\sigma_1} \sin^2\psi \right)^m d\psi \right] dA \right\} dp$$

where the limit of integration ψ_0 is as given in Eq.(2-4), and Γ is the gamma function. As it is obvious from Eq.(2-9), the principal stresses can be written

$$\sigma_1 = p \cdot H_1(r/R,\Theta,\alpha)$$

$$\sigma_2 = p \cdot H_2(r/R,\Theta,\alpha) \ .$$

Hence, the expression for mean pressure reduces to

$$p_m = \int_0^\infty \exp(-p^m q)\ dp = \Gamma\left(1+\frac{1}{m}\right)/q^{1/m}$$

where

$$q = \frac{Kt}{4\sqrt{\pi}} \frac{\Gamma(m+1)}{\Gamma(m+1.5)} \int_{A_{disk}} \left\{ \left[H_1(r/R,\Theta,\alpha) \right]^m \int_{-\psi_0}^{\psi_0} \left(\cos^2\psi + \frac{H_2}{H_1} \sin^2\psi \right)^m d\psi \right\} dA$$

and using Eq.(2-5)

$$\frac{p_m V^{1/m}}{\sigma_0} = \Gamma(1+\frac{1}{m}) \left\{ K' \int_0^1 \int_0^{\pi/2} \left[H_1^m \int_{-\psi_0}^{\psi_0} \left(\cos^2\psi + \frac{H_2}{H_1} \sin^2\psi \right)^m d\psi \right] \frac{r}{R} d\Theta d(\frac{r}{R}) \right\}^{-1/m}$$

with $K' = 2(2m+1)\,\Gamma(m+1)/\pi^{3/2}\Gamma\,(m+1.5)$ and ψ_0 as given in Eq. (2-4). This dimensionless quantity is evaluated on a digital computer and is shown as a function of m for various α in Fig. 2-7. The corresponding mean value for the tensile stress at the center of the specimen is

$$\sigma_m = \frac{2p_m}{\pi} (\sin 2\alpha - \alpha). \qquad (2\text{-}10)$$

Experimental Results: The parameters m and σ_0 are evaluated from three-point bending tests to predict behavior in the Brazilian disk test. Alternatively, the parameters could have been obtained from the disk test and used to predict behavior in bending. In testing rectangular beams of span L, height h and thickness b, using fixed supports, an elementary but often neglected source of error is friction at the supports. It may be shown that the maximum stress under load P is

$$\sigma = \frac{3}{2} \frac{PL}{bh^2} \left(1 - \frac{4}{3} \frac{\mu h}{L} \right).$$

The friction coefficient μ is measured and this correction is made in determining parameters from bending test results. An additional aspect, the "wedging stresses" [2-25] due to the localized load may be shown to introduce an error of 0.3% at most and are neglected.

Extensive tests are carried out on granodiorite (a fine to medium grained igneous rock from the Sierra Nevada), and a smaller number of

tests are made on a fine grained limestone, snow-white in color, on a lightly anisotropic greenstone, and on a fine grained basalt.

Bending Tests on Granodiorite: Twelve separate sets of bending tests were made involving a total of 281 specimens. The effects of specimen preparation, cross-sectional size and orientation, friction at the supports and moisture were studied and the results are summarized in Table 2-1. All tests were made using a carefully aligned fixture in an Instron Universal Testing Machine at a cross-head speed of 0.02 inches/min (0.05 cm/min).

The value of m for each set was obtained from the slope of a graphical plot of log log $(\frac{1}{1-G})$ versus log σ. Here G is taken as the mean rank $j/(N+1)$ where j is the number obtained when N specimens are ranked from 1 to N in order of increasing strength.

The first set of specimens prepared was No. 5. These specimens had the smallest cross-sectional dimension of any tested and had a very rough surface finish. Subsequent specimens were finished in as consistent a manner as possible by grinding. For this reason, we ignore Set No. 5 in our subsequent discussion except as evidence that surface finish must be controlled. For specimens which are carefully prepared, it is important to determine whether the strength impairing flaws are distributed throughout the volume or are concentrated on the surface, as in glass. It was shown by Weil and Daniel [2-32] that this can be determined if beams of rectangular cross section are tested in two orientations as with Sets 1 and 2 or Sets 3 and 4. When the long dimension of the cross-section is perpendicular to the neutral axis, the cummulative distribution of stress at fracture should shift to higher stresses if surface flaws are involved.

However, if only a volume distribution of flaws is involved, both orientations should lead to the same distribution. A comparison of Sets 1 and 2 in Fig. 2-8 provides a rather convincing justification of the assumption that a volume distribution of flaws is involved. Sets 3 and 4, which involve fewer and smaller specimens, show the rather puzzling result, in Fig. 2-9, that orientation of the long dimension perpendicular to the neutral axis lowers the strength values. We can argue that since the area at the outer fiber is the smallest for all of the rectangular cross-section specimens tested, some effect due to flaws on the specimen edges may be involved.

To obtain an estimate of m from a large number of tests, we have pooled all of the sets in which rectangular specimens were tested with the long dimension of the cross-section along the neutral axis with the exception of Set 5 (different surface finish) and Set 6 (done wet). Taking the 161 specimens of Sets 1,3,7,8,9,10,11 and normalizing the strengths in each set by their own mean, we obtain from Fig. 2-10 the estimate $m = 12.0$. It is interesting to compare the distribution predicted by this value of m with the data points on linear coordinates as shown in Fig. 2-11. As expected, because of the assumption $\sigma_u = 0$, the data points depart from the predicted curve at the lower stresses.

The value of σ_0 cannot be obtained from such a pooled plot so Set 1, which has the largest number of specimens, was selected. From Fig.2-12 we obtain $\sigma_0 = 1220$ psi (8.41 MN/m^2) before making the correction for friction and $\sigma_0 = 1170$ psi (8.07 MN/m^2) after making this correction for the measured value $\mu = 0.31$.

Excluding Set 5, the m values deduced from the other sets of bending tests show the variability to be expected when estimates are made from small samples (coefficient of variation = 0.097). To show that the shape of the cross-section has no significant effect on the m values, Set 12 is included in the experiments (Fig. 2-13). Set 6 is tested after soaking the specimens in water for five minutes. It indicates that moisture has little effect on the m value, although it does decrease the mean strength, as shown on Fig. 2-14.

Disk Tests on Granodiorite: The dimensions selected for the disks were D = 1.006 inches (2.56 cm), t = 0.205 inches (0.52 cm), and $2\alpha = 18.5^{o}$. Sometimes padding material has to be used in the Brazilian disk test to avoid premature crushing under the loading points but this was not found to be necessary in the present tests. Two series of tests were made on disks and the results are summarized in Table 2-2.

Forty specimens (Set 13) were prepared with a surface finish similar to the bending specimens while 38 specimens (Set 14) had a considerably smoother surface finish obtained by lapping. The predicted value for the mean tensile stress at the center of the disk from Eq. (2-10) and σ_0 = 1170 psi (8.07 MN/m^2), m = 12.0 is 1770 psi (12.20 MN/m^2). This agrees well with the mean of the observed strength values for both sets of tests. A more critical test is to compare the distribution of failure stress or pressure predicted by the Weibull formulation with observed values. This is done in Figs. 2-15 and 2-16 for the two sets of tests. The agreement for the disks with surfaces similar to the bending specimens is very good. For the smoother disks, Set 14, the predicted distribution provides a somewhat less precise fit to the experimental distribution.

Tests on Limestone: A less extensive series of tests was made on a limestone to confirm that the preceding predictions for the Brazilian disk test could be repeated for another material. Since this material is very soft, it is not easy to prepare specimens of rectangular cross-section as the edges tend to crumble. For this reason, Set 15 and Set 16 (Table 2-3) are rejected. Bend tests were made on specimens of circular cross-section (Set 17, Table 2-3). The Weibull parameters deduced from this test, using Fig. 2-17, are m = 10.5 and σ_0 = 420 psi (2.90 MN/m^2). A set of 38 Brazilian disk tests were made using dimensions similar to those for granodiorite except for a decrease in thickness to 0.200 inches (0.508 cm). From Fig. 2-18 the predicted probability distribution is seen to compare very well with experimental results. The mean value observed for the tensile stress at the center of the disk was 690 psi (4.76 MN/m^2) with the predicted value being 668 psi (4.61 MN/m^2).

Tests on Greenstone: Greenstone (amphibolite) is a metamorphosized volcanic rock. It shows schistosity and is randomly intersected with veins of quartz. The bending test data, shown on Fig. 2-19, does not fit a Weibull distribution at all. As discussed by Weibull, the curve is concave upwards and indicates the anisotropy of the material. It is not possible to obtain unique m and σ_0 values to use in the Brazilian disk analysis. Apart from difficulties in estimating the parameters, the disks in diametral compression did not fracture along the loaded diameter; due to insufficient stiffness of the testing machine, disks failed in an explosive manner, completely obscuring the mode of failure. For these reasons, attempts to predict the behavior in one of the tests from the other, using the procedures discussed, would be meaningless.

Tests on Basalt: Similar difficulties arose with basalt as with greenstone. The anisotropy is not strong but the bending test data shown on Fig. 2-20 indicates that there is a high zero strength for basalt. The use of two parameter Weibull formulation can not be justified.

Discussion of the Results: The results obtained here show that if similarly; prepared specimens are compared, the Brazilian disk test may be compared with bending results using Weibull's multiaxial formulation. The predictions are considerably better than can be obtained with other procedures. One approach suggested [2-27] is to compare volumes in which the tensile stress is above 90% of the maximum value. This criterion would predict a mean fracture stress of 1630 psi (11.24 MN/m^2) which is 12% below the experimentally observed values. Another approach would be the maximum strain criteria. But even lower values are predicted for the mean stress at fracture if a maximum strain criterion of fracture is employed since it predicts a reduction in strength in tension-compression quadrant. From Table 2-1 it can be seen that the maximum tensile stress by itself is a completely inadequate fracture criterion.

CHAPTER THREE: UNIAXIAL DYNAMIC LOADING

3.1 Introduction:

Quasistatic fracture and/or dynamic fracture are very often used to denote both the motion of cracks and the type of loading. To avoid any ambiguities the term dynamic loading is used here for external loads that give rise to transient propagating mechanical disturbances (such as impact loads, explosive charges, etc.). There is no need to label the propagation phase. Only rapid (or catastrophic) propagation of cracks will be discussed.

The classic analytical problem of fracture mechanics involves computation of the stress field at the crack tip. This computation has to include the inertia effects for any kind of dynamic loading. Elastodynamic problems often lead to dynamic stresses which are higher than the stresses computed from the corresponding problem of static equilibrium. Reflection of a plane wave from a rigidly-clamped boundary - giving rise to stresses which are twice the original incoming wave magnitude - is a good example of this effect. A comparable effect occurs when a wave is diffracted by a crack. The behavior of the stress intensity factor under short duration pulses is studied in the first part of the chapter under the heading of "crack initiation".

In most instances crack initiation is sufficient for complete failure since the propagation speed of cracks is very high and they can completely traverse a part during conventional loading. Under short duration pulses, however, initiation becomes only a necessary condition for complete fracture, and the propagation phase may be the dominating factor in brittle fracture. In considering the propagation of cracks due to

dynamic loading, we have to admit that even the propagation due to quasistatic loading is not well understood yet. In the second part of the chapter, crack propagation is studied for the case of quasistatic loading.

The last part of the chapter deals with a new theory for brittle failure under dynamic loading. The theory is applied to a practical case - spalling due to energetic electron bursts - in Chapter four.

The phenomena of fracture under short duration stress pulses has drawn attention mainly in relation to back surface spallation of armour plates subject to impact. Recently, the search for efficient tunneling methods in hard rock has required a better understanding of the spallation process. Unlike metals, rocks behave essentially elastically up to the fracture point and do not show strong rate dependence. The plastic flow in metals that accompanies the compressive wave changes the internal structure of the material so that the material which undergoes spallation is quite different from the initial material. Brittle solids being much stronger in compression remain unchanged by the initial compressive wave. This alone makes the brittle solids much easier to analyze. The difficulty with brittle solids, however, arises from strong nonhomogeneity; generally, grain boundaries act as effective cracks and it is very difficult to identify these flaws. As will be discussed later, a knowledge of flaw distribution is very important in predicting dynamic behavior.

3.2 Crack Initation:

We assume that initation of fracture occurs when the stress intensity factor reaches its critical value, called the fracture toughness. The fracture toughness value is assumed to be independent of the loading

rate, which is a reasonable assumption for rocks. The effect of short duration loading on the stress intensity factor is studied in the following problem.

A sharp through crack, of length 2a, is embedded in a homogeneous, isotropic, linear elastic plate of infinite extent loaded by uniaxial tension σ. This geometry corresponds to the simplest problem of quasi-static loading where $K_I = \sigma(\pi a)^{\frac{1}{2}}$. A plane P-wave (tensile) propagates towards the crack, the wavefront being parallel to the plane of the crack. At time $t < 0$, the incident wave is of the form (Fig. 3-1)

$$\sigma_{yy}^{(i)} = \sigma_0 \, H(t-y/c_1)$$

where $H(\tau)$ is the Heaviside function. At $t = 0$, the plane wave strikes the crack. At all subsequent times, there are a reflected plane wave and two diffracted cylindrical waves emanating from each crack tip (Fig. 3-2).

The stress field at the crack tip for this problem was obtained by Thau and Lu [3-1] by considering two hypothetical plane problems:

problem A - plane incident wave $\sigma_{yy}^{(i)} = \sigma_0 \, H(t-y/c_1)$ in infinite domain

problem B - the wave propagation problem defined by the boundary conditions

$$\begin{aligned}
&\sigma_{yy}(x,0,t) = -\sigma_0 \, H(t) && \text{for } 0 < x < 2a \\
&\sigma_{xy}(x,0,t) = 0 && \text{for } -\infty < x < \infty \\
&u_y(x,0,t) = 0 && \text{for } x > 2a,\ x < 0 \\
&u_x = u_y = \dot{u}_x = \dot{u}_y = 0 && \text{for } t \leq 0
\end{aligned}$$

satisfying the field equations of isothermal elasticity.

Super position of problems A and B is the problem of "P-wave striking a

crack". Since the solution of A is trivial (uniform all over), the solution of the main problem reduces to solving problem B, as stated.

Introducing the Lamé potentials $\alpha(x,y,t)$ and $\underset{\sim}{\beta}(x,y,t)$ such that

$$\underset{\sim}{u} = \underset{\sim}{\nabla}\alpha + \underset{\sim}{\nabla} \times \underset{\sim}{\beta}$$

the problem in two dimensions (plane strain, no body forces) reduces to solving the following two wave equations subject to the conditions given in the statement of problem B.

$$\nabla^2\alpha = \frac{1}{C_1^2} \frac{\partial^2\alpha}{\partial t^2}$$

$$\nabla^2\beta_3 = \frac{1}{C_2^2} \frac{\partial^2\beta_3}{\partial t^2}, \quad \beta_1 = \beta_2 = 0$$

where c_1 and c_2 are respectively, dilatational and shear wave speeds. Laplace transform over time and exponential Fourier transform with respect to x-coordinate are applied to the set of governing equations. The resulting equations are solved by the generalized Wiener-Hopf technique.

The analytical solution for the stress intensity factor obtained by Thau and Lu [3-1] is shown on Fig. 3-3. The ratio of the stress intensity factor under dynamic loading to the stress intensity factor under static loading (K_{Id}/K_I) increases as $(\text{time})^{\frac{1}{2}}$ until the scattered S-wave from opposite crack tip hits the tip in question (i.e. $t \leq 2a/c_2$). The rise is accelerated with the arrival of the S-wave, and the maximum occurs right at the moment when the scattered Rayleigh wave reaches the tip. This maximum is about 30% higher than the corresponding static case.

The results are valid only for times $t \leq 4a/c_1$. That is, denoting

the tip in question by 1 and the other by 2, only $P_1, S_1, P_2P_1, P_2S_1, S_2P_1$, S_2S_1-waves are considered (No. $P_1P_2P_1, P_1P_2S_1$ etc.). Hence it is not possible to claim that the peak values quoted are indeed the maximum ones for all subsequent time. However, decaying responses with time are expected since scattered waves propagating outward to infinity continuously remove energy from the vicinity of the obstacle.

Further study of dynamic loading: For a step pulse $\sigma = \sigma_0 H(t)$, each crack will reach the same maximum ratio of K_{Id}/K_I, no matter what the size of the crack is. The larger cracks will take longer time than the small ones to reach that maximum. Since the static stress intensity factor, K_I, itself is proportional to $a^{\frac{1}{2}}$, the maximum K_{Id} will increase as the crack size increases. The variation of K_{Id} with time is shown on Fig. 3-4 for various crack lengths. Thus, for small times K_{Id} is independent of crack size. All cracks, larger than some minimum value, will reach a particular value of K_{Id} at the same time*; hence, all the "active cracks" (cracks which will start propagating for the given stress pulse) will have the same delay time t_0. Since the crack size is immaterial, we can replace the crack of length 2a by a semi-infinite crack. The problem becomes much easier without higher order diffractions at the second tip, and Freund [3-2] obtained a closed form expression for delay time as

---

*Because of the peculiar cusp shape of the last portion of dynamic stress intensity factor curve (Fig. 3-4), a limited number of cracks will reach the critical value of the stress intensity factor K_{Ic} at slightly lower times. These are the cracks with sizes very close to that of minimum active crack.

$$t_0 = \frac{\pi \quad (1-\nu)^2 \; K_{Ic}^2}{2 \; (1-2\nu) \; \sigma_0^2 \; c_1}$$

where K_{Ic} = fracture toughness and ν = Poisson's ratio of the material. It follows that there is always a finite time between the wave striking the crack and the crack starting to propagate, no matter how large the stress. Crack propagation at an instantaneous velocity, i.e. $t_0 = 0$, occurs only if the stress has a square-root singularity at the wavefront of the incident wave; that is, if $\sigma(t) \sim t^{-\frac{1}{2}} H(t)$ (Achenbach and Nuismer [3-3]).

Interaction of a finite pulse with a crack of length 2a is much harder to analyze rigorously. Superimposing two step inputs $\sigma_0 H(t)$ and $-\sigma_0 H(t-\tau)$ would yield the behavior of the finite pulse of duration τ, if it can be shown that the crack does not close under the loading $-\sigma_0 H(t-\tau)$. Motivated by the fact that the crack is already open when the compressive step function is applied, the assumption is made that the crack opening will not increase for $t > \tau$ and hence, K_{Id} will reach its maximum value at $t = \tau$. Consequently, for a given pulse (σ,τ), cracks larger than $c_R \tau$ (c_R being the Rayleigh wave speed) will not reach a 30% overshoot in K_{Id} over K_I since the unloading pulse will be due before the Rayleigh wave reaches the tip. The variation of maximum stress intensity factor reached within $(0,\tau)$ is as shown on Fig. 3-5. Thus, the fracture criteria for cracks smaller than $c_R \tau$ is just the Griffith type; there is only an additional factor of 1.3 to raise K_I due to dynamic effects. Larger cracks, however, are insensitive

to crack size. This is a peculiar behavior associated with dynamic loading.

If no fracture occurs, increasing the pulse length λ will increase the stress intensity factor reached by large cracks, thereby increasing the probability of failure. Above a certain threshold λ, however, all pulses will have the same effect as far as initiation is concerned.

Generalizing Thau and Lu's work led to the conclusion that K_{Id} reaches the maximum value for crack lengths equal to $c_R \tau$. Hence, for fracture

$$K_{Ic} \leq K_{Id} \cong 1.3 \ \sigma \sqrt{\pi a} \lesssim 1.3 \sqrt{\pi}\sigma \left(\frac{\tau c_R}{2}\right)^{\frac{1}{2}}$$

$$\sigma^2 \lambda \geq C K_{Ic}^2$$

where C is a function of Poisson's ratio and is of the order one. This is a necessary condition for fracture to initiate. In order to be also sufficient, the material should contain at least one crack of length $c_R \tau$.

The left hand side of the last equation is proportional to the energy of the stress pulse. To crack a given material, either a long pulse with low stress profile or a short pulse with high stress profile can be used. Among pulses of the same energy content, the short ones will be more destructive than the long pulses, since the short pulses will have a greater range of cracks to affect, as shown on Fig. 3-6.

It is more realistic to consider penny-shaped cracks rather than two-dimensional cracks. The diffraction problem of a step function input has not been solved for penny-shaped crack geometry. But, harmonic

incident waves, diffracted at Griffith - as well as penny-shaped cracks are considered by Mal [3-4, 3-5]. The maximum overshoot of dynamic stress intensity factor is 30% in the former, 45% in the latter case. This maximum occurs for incident waves where the wavelength is roughly 4 to 6 times the crack length. This compares favorably with rectangular pulse solution, where maximum occurs at pulse lengths roughly 2 times the crack length (Table 3-1). By analogy, it is expected that $K_{Id} \sim 1.45\ K_I$ for a penny-shaped crack struck by a rectangular pulse.

3.3 Crack Propagation

In the propagation phase of cracks the main concern is how far cracks can travel before the pulse is over. Questions about the path of the cracks and instabilities such as forking will be avoided here. The assumption is made that all cracks will continue growing in their own plane, on a straight line.

Not much progress has been made on propagation theories in the last decade. Still, formulations based on static stress fields are used. Mott [3-6] was the first to extend Griffith's energy balance to dynamic cases by including the kinetic energy term into the balance equation. Using the potential energy term as given by Griffith, deriving the kinetic energy term on dimensional grounds and making the simplifying assumption $\partial c/\partial a = 0$ initially (where c = crack speed, a = crack half length), he came up with the expression:

$$c = \sqrt{\frac{2\pi}{K}}\sqrt{\frac{E}{\rho}}\left(1 - \frac{a_0}{a}\right)^{\frac{1}{2}} \qquad (3\text{-}1)$$

where E is the Young's modulus, ρ is the density, a_0 is the initial

crack half length and K' is the constant to be evaluated from the displacement field of the problem. Roberts and Wells [3-7] evaluated it in 1953 for Poisson's ratio 0.25 and obtained the expression

$$c = 0.38\sqrt{\frac{E}{\rho}}\left(1 - \frac{a_0}{a}\right)^{\frac{1}{2}}. \tag{3-2}$$

Dulaney and Brace [3-8] recognized that for early periods of propagation the assumption $\partial c/\partial a = 0$ is not correct and solved the energy balance equation of Mott by using the initial condition $c = 0$ when $a = a_0$. They obtained the following expression

$$c = 0.38\sqrt{\frac{E}{\rho}}\left(1 - \frac{a_0}{a}\right) \tag{3-3}$$

Berry [3-9] extended this last formulation by differentiating between the applied stress σ and the critical stress σ_c and came up with

$$c = 0.38\sqrt{\frac{E}{\rho}}\left(1 - \frac{a_0}{a}\right)^{\frac{1}{2}}\left[1 - (2n^2-1)\frac{a_0}{a}\right]^{\frac{1}{2}} \tag{3-4}$$

where $n = \sigma_c/\sigma < 1$. In all these cases, the limiting crack speed is predicted to be $0.38\sqrt{E/\rho}$ or $0.6\ c_2$ for $\nu = 0.25$.

All of the foregoing formulations are known to be incomplete since they are based on static solutions of crack geometry. Tsai [3-10] recently computed the stress distribution around the tip of a running crack. As shown on Fig. 3-7, the correction factor is appreciable at large speeds; not only the magnitude but also the plane at which the maximum circumferential stress acts is changing at crack speeds above $0.7\ c_2$.

It has been shown first by Broberg [3-11] that the terminal crack speed is the Rayleigh wave speed c_R, i.e. $0.92\ c_2$ for $\nu = 0.25$, rather

than the predicted value of 0.6 c_2, where c_2 is the shear wave speed. Experimental results on steel, polymers and glass show, however, a closer agreement with the value 0.6 c_2. Only in limited cases, such as tungsten single crystals, have high terminal velocities up to 0.82 c_2 been observed. A possible explanation can be given by considering the behavior of the stress intensity factor with increasing crack speeds. For semi-infinite cracks, Freund [3-12] found that the stress intensity factor K_I decreases sharply at high crack speeds and reaches zero at $c = c_R$. This clearly shows that the Rayleigh speed is the absolute maximum for conventional crack propagation, which occurs through energy transfer from the surrounding stress field to the tip. It also indicates that this speed can be approached only asymptotically. Since all engineering materials will have a finite fracture toughness value, terminal velocities will be considerably lower than c_R (Figs. 3-8).

There is no reason a prior to assume the energy absorbtion behavior constant at all crack velocities, as is done in the early propgation theories. In fact, the contrary might be expected. At low crack velocities and crack tip strain rates, yield strength increase may decrease the localized yield zone, thereby decreasing the energy absorbed. At high crack velocities, the tendency to form small cracks in front of the crack tip increases, thereby increasing the energy absorbed. Experiment on plexiglas (Bergkvist [3-13]) show that the surface energy increases at an increasing rate as crack velocity increases. Assuming that the critical energy release rate g_c can be determined experimentally, the crack speed can be calculated by using the available solutions for energy release rate, as shown in the following.

The rigorous solution for a finite crack extending at a nonuniform rate due to Mode I loading has to include diffractions at each crack tip and therefore is expected to be very complicated. "Semiinfinite crack extending at a nonuniform rate" and "finite crack extending at a uniform rate" are easier problems although less descriptive of the physical situation. Freund [3-12] and Broberg [3-14] considered these two cases and obtained solutions for the energy release rate g. The solutions are complicated. However, on examination it can be seen in both cases that the ratio of the energy release rate at some velocity c to that at initiation, i.e. at $c = 0$, can be approximated for equivalent crack lengths by:

$$g = \frac{g(c)}{g(0)} \cong 1 - c/c_R \tag{3-5}$$

Tsai [3-15] investigated the dynamic stress intensity factor for a brittle crack extending at a constant speed and at a constant acceleration. The results for these two cases are identical at $c = 0$ and $c = c_R$ and do not deviate from each other more than 5% over the entire range of crack speeds. (It is worth noting here, however, that the stress intensity factor and the energy release rate for a propagating crack are no longer related by $K_I^2(1-\nu^2)/E = g$ but by $K_I^2(c)\ A(c)\ (1-\nu^2)/E = g(c)$, where $A(c)$ is a function of crack speed and elastic constants. When c is zero, $A = 1$; and when c approaches the Rayleigh wave speed, A becomes unbounded (Freund [3-12]).

A crack under time independent loading starts to propagate when the energy release rate g reaches its critical value g_c. The subsequent motion is such that g remains equal to g_c. Hence, considering

the simplest case, a crack of length 2a in an infinite plate subject to uniform traction σ at infinity, we have:

initially: $$g_c(0) = g(0) = \frac{\pi a_0 \sigma_0^2}{E}$$

later: $$g_c(c) = g(c) = g \frac{a}{a_0} \frac{\sigma^2}{\sigma_0^2} \frac{\pi a_0 \sigma_0^2}{E}$$

$$g_c(c) = g \frac{a}{a_0} \frac{\sigma^2}{\sigma_0^2} g_c(0) \ .$$

Using the approximate expression for g as given in Eq. (3-5), we can rearrange the last equation,

$$c \cong c_R \left(1 - \frac{a_0}{a} \frac{g_c(c)}{g_c(0)} \frac{\sigma_0^2}{\sigma^2} \right) . \qquad (3\text{-}6)$$

This relationship of crack speed and crack size is similar to the early formulations given in Eqs. (3-1) - (3-4). A comparison of Eqs.(3-2), (3-4) and (3-6) is made on Fig. 3-9. The two extreme cases, $g_c(c)/g_c(0) = 1$ and $g_c(c)/g_c(0) \to \infty$, are shown by dashed lines; a real solid is expected to lie in between. Without an experimental knowledge of $g_c(c)/g_c(0)$ variation with crack speed, Berry's curve seems to be the best available at this stage.

Increasing the applied stress over the critical stress does not effect the terminal velocity, but decreases the period of acceleration. The trend is similar in both Berry's analysis and the analysis based on g_c-variation with crack tip speed. As shown on Fig. 3-9, among pulses with the same energy content, i.e. $\sigma^2\tau$ = constant, long pulse lengths will be more destructive than high stress amplitudes.

3.4 A New Theory of Dynamic Fracture

A study of the last two sections leads to the conclusions that under impulsive loading cracks will be activated at stress levels 30-45% lower than quasi-static loading and that they will travel at velocities considerably lower than the Rayleigh wave speed. It is also found experimentally that the strength level of brittle solids increases sharply as the loading time is decreased. Hence, fracture under short duration pulses must be governed by propagation of cracks as opposed to initiation, which is the governing factor in quasi-static loading. And this is not surprising at all. Due to the limited time available large cracks cannot propagate far enough to meet the free surface or each other; many smaller cracks have to be initiated. Thus, much higher stresses are necessary for failure. Clearly, a weakest link or series type anlysis (like that of Weibull's treatment (Chapter II) where the structure as a whole is only as strong as its weakest link) will not hold anymore; a model requiring the failure of many elements in parallel may be more appropriate. Not only the size but also the density of cracks will be vital.

Research in the area of short duration loading has consisted primarily of experimental determination of conditions necessary to produce spall. Analysis has been confined to empirical relationships. The spall criterion proposed by Tuler and Butcher [3-16] for metals

$$\int_0^{\tau} (\sigma-\sigma_0)^{\lambda} dt = K$$

has been applied most widely. (In this equation σ_0 corresponds to

fracture stress at long times, λ and K are constants.) It seems to fit the experimental evidence well but lacks any theoretical basis. The constants λ and K have to be determined from a series of spall experiments which requires sophisticated equipment and experimentation. Available limited data show that λ is around 2. If its value can be obtained more precisely by theoretical analysis or extensive experimental work, the usefulness of this criterion can be increased greatly.

Shockey et al. [3-17] attempt to determine the flaw distribution in rocks by counting and measuring the flaw traces on a particular plane. Cumulative distribution per unit volume is then obtained by means of a statistical transformation. Failure is assumed when cracked volume reaches a certain percentage of total volume. The criterion is arbitrary and the procedure of counting crack traces is less likely to be successful in most rocks than in novaculite, the material they tested.

In the light of these developments, a new theory is proposed to predict failure in brittle solids due to dynamic loading: Consider a plane, rectangular stress wave of magnitude σ and duration τ such as one generated by impacting a thin propjectile plate against a stationary target plate. It can cause failure only if (i) the energy delivered to the solid is large enough to initiate crack propagation, and (ii) the duration of the stress is long enough for active cracks to coalesce. Thus, the time to failure τ can be written as the sum of initiation and propagation time

$$\tau = \tau_i + \tau_p \ .$$

From Freund's [3-2] solution for the delay time of a semi-infinite

crack, we know

$$\tau_i = \frac{\pi(1-\nu)^2 K_{Ic}^2}{2\ (1-2\nu)\ \sigma^2\ c_1} \tag{3-7}$$

where K_{Ic} is the fracture toughness, c_1 is the dilatational wave speed and ν Poisson's ratio.

A similar expression for propagation time τ_p is much harder to obtain. A global energy balance including the kinetic energy term is not useful since the fresh surface area created is very hard to estimate. The cumulative distribution of crack sizes is crucial at this point.

Distribution of flaws. We will assume that in a brittle solid the number of flaws per volume having a strength equal or less than σ is Poisson distributed. In the face of a large number of similar phenomena obeying a Poisson probability law - such as the number of misprints per page, spontaneous decomposition of radioactive atomic nuclei, occurrence of breakdown or accidents - the assumption is expected to be reasonably close to reality. Denoting the expected number of cracks per volume having a strength $\leq \sigma$ by n, we can write the probability of finding zero flaws in volume V having a strength $\leq \sigma$ by

$$p = \frac{e^{-nV}\ (nV)^0}{0!} .$$

Or, the probability of finding at least one flaw as

$$1-p = 1 - e^{-nV} .$$

From static tests we know the distribution of failure stresses (i.e., the probability of finding at least one flaw in volume V having a strength

$\leq \sigma$) obeys Weibull's distribution closely. Hence

$$G = 1 - e^{-\left(\frac{\sigma - \sigma_u}{\sigma_0}\right)^m V} = 1 - e^{-nV}$$

and

$$nV = N(\sigma) = \left(\frac{\sigma - \sigma_u}{\sigma_0}\right)^m V \ . \tag{3-8}$$

Static tests give the distribution of the largest cracks since brittle solids in such tests always fail due to the most severely loaded flaw. Thus, the above expression is strictly valid only within the experimental range. It does not give information, e.g., about the number of very small cracks since very large failure stresses can be obtained only in very very small specimens which are neither suited for experiments nor justified in terms of their modified microstructure. But, after recognizing this limitation, we assume that brittle strength will continue to obey the Weibull distribution beyond the range justified by experiments and extrapolate Eq. (3-8) to vanishing crack lengths.

<u>A simple criterion</u>: All cracks are assumed to lie parallel to each other and perpendicular to the applied loading. They are also assumed to propagate in their own plane in a straight line. (These simplifications are discussed later in the chapter.) A mean path 2d is defined as the distance an average crack propagates before coalescing with another crack. If all cracks are the same size and on the same level, $d = \frac{1}{2}(A/N)^{\frac{1}{2}}$ where A is the area subjected to tension and N is the number of cracks that are active at or below a stress σ. To assume that all cracks lie on the same level is too much of a simplification. Instead, we can assume that they are distributed uniformly to ℓ different levels such that any

two cracks in one layer have to merge if they grow long enough. Thus,

$$d = \frac{1}{2}(A\ell/N)^{\frac{1}{2}} = \frac{1}{2}\left[\frac{A\ \sigma_0^m\ \ell}{(\sigma - \sigma_u)^m V}\right]^{\frac{1}{2}}$$

since $V = A \cdot h = A \cdot \Delta h \cdot \ell$, where Δh is the thickness of a single layer

$$d = \frac{1}{2}\left[\frac{\sigma_0^m\ \ell}{(\sigma-\sigma_u)^m h}\right]^{\frac{1}{2}} = \frac{1}{2}\ \frac{\sigma_0^{m/2}}{(\sigma-\sigma_u)^{m/2}}\left(\frac{1}{\Delta h}\right)^{\frac{1}{2}}.$$

In the face of all the assumptions and approximations involved, it is not justified to use a complicated propagation law such as mentioned in Section 3.3. Neglecting both the initial crack size and the period of acceleration, we can write

$$\tau_p \cong \frac{d}{c} = \frac{1}{2c}\ \frac{\sigma_0^{m/2}}{(\sigma-\sigma_u)^{m/2}}\left(\frac{1}{\Delta h}\right)^{\frac{1}{2}}$$

where c is the crack velocity.

The number of layers ℓ in the direction of wave propagation (z-axis) is ambiguous; since the wave travels down all along the z-axis, there is no immediate dimension corresponding to the depth of stressed volume. The layer thickness Δh is sensitive to applied stress level σ; the stress field at the tip of a crack will reach farther for larger σ. The maximum opening δ_{max} of crack of length 2a subject to a stress σ at infinity may be shown to be $\delta_{max} = 4a\ \sigma/E$. This suggests an approximate estimate of Δh as

$$\Delta h \cong 2\delta_{max} = 8\ a\frac{\sigma}{E}$$

giving

$$\tau_p = \frac{1}{2c} \frac{\sigma_0^{m/2}}{(\sigma-\sigma_u)^{m/2}} \frac{1}{\sigma^{\frac{1}{2}}} \left(\frac{E}{8a}\right)^{\frac{1}{2}} \tag{3-9}$$

The crack size a is unknown in the above expression. Hence, we leave it and the other constants as parameters to be determined from one dynamic test and write Eq. (3-9) as

$$\tau_p = \frac{K}{\sigma^{\frac{1}{2}} (\sigma-\sigma_u)^{m/2}} \tag{3-10}$$

For most practical purposes, $\tau_i << \tau_p$ and $\tau \approx \tau_p$, and

$$\tau \ \sigma^{\frac{1}{2}} (\sigma-\sigma_u)^{m/2} = K.$$

If σ is applied for a time Δt less than τ,

$$\Delta t \ \sigma^{\frac{1}{2}} (\sigma-\sigma_u)^{m/2} = \left(\frac{\Delta t}{\tau}\right) K .$$

Successive application of constant stress pulses of duration Δt_i each gives

$$\sum_{i=1}^{k} \Delta t_i \ \sigma_i^{\frac{1}{2}} \ (\sigma_i - \sigma_u)^{m/2} = K$$

where $\sum_{i=1}^{k} \Delta t_i = \tau$. In the limit,

$$\int_0^{\tau} \sigma^{\frac{1}{2}} (\sigma - \sigma_u)^{m/2} \, dt = K. \tag{3-11}$$

This last equation is very similar to the empirical relationship proposed by Tuler and Butcher, except that the material properties m and σ_u can be found by static pure bending tests; a single dynamic fracture test is sufficient to determine the constant K.

Discussion: In developing a simple dynamic fracture model, we assumed the cracks to lie parallel to each other and to propagate in their own plane. These assumptions are motivated by following arguments. We know a crack oriented at some angle Θ to the applied tensile stress will extend in such a way as to maximize the stress intensity factor at its tip; i.e., it will turn perpendicular to the applied tensile stress. Besides that, Freund [3-18] has shown recently that the delay time is a strong function of the orientation and increases sharply for cracks which make large angles with the plane perpendicular to the applied tensile stress. Thus, it is reasonable to disregard such cracks and treat the rest as being on planes perpendicular to tension.

CHAPTER FOUR: ANALYSIS OF ELECTRON BEAM TESTS

4.1 Introduction

Several novel techniques have been introduced recently in the areas of tunneling and drilling. Use of intense submicrosecond electron bursts, which will be studied here, has the particular advantage of leading to tensile loading of rocks and hence exploiting their relative weakness in tension. A detailed picture of the investigation is presented in [4-1] and especially in [4-2].

Energetic electrons delivered from a pulsed electron accelerator penetrate the rock to a finite depth and deposite most of their energy. The heated region cannot expand freely due to the surrounding rock at ambient temperature and large thermal stresses are created. The knowledge of these thermal stresses is essential to any failure prediction. The situation can be formulated as follows:

Given homogeneous, isotropic, linear-elastic half space, $z \geq 0$ (Fig. 4-1), find the stress field $\sigma_{ij}(x,t)$ satisfying the equations of isothermal elasticity:

$$\begin{aligned} \sigma_{ij,j} &= \rho\, \ddot{u}_i \\ \sigma_{ij} &= 2\mu\, \varepsilon_{ij} + \lambda \delta_{ij} \varepsilon_{kk} - (3\lambda + 2\mu)\, \alpha\, T\, \delta_{ij} \\ \varepsilon_{ij} &= \frac{1}{2}(u_{i,j} + u_{j,i}) \end{aligned} \tag{4-1}$$

subject to boundary conditions

$$\begin{aligned} \sigma_{zz} = \sigma_{zr} &= 0 \qquad \text{at } z = 0 \text{ for } t \geq 0 \\ \sigma_{\theta} \equiv \sigma_{\theta} &\equiv 0 \qquad \text{everywhere} \end{aligned}$$

and to initial conditions $u_r = u_z = \dot{u}_r = \dot{u}_z = 0$

where $T = T(r,z,t)$ is the temperature rise, λ and μ the Lame constants, and α the coefficient of linear thermal expansion.

There are two distinct regions of interest depending on the application of the heat source. If the electron deposition is fast enough such that there is practically no heat transfer to the surroundings and slow enough not to have any wave phenomena (i.e. subsecond duration pulses), the mechanism is called "thermal crater" fracture. If the electron deposition is almost instantaneous (i.e. submicrosecond pulses), the fracture is by "spalling" due to the tension wave.

4.2 Thermal Crater Analysis

The stress field for the "thermal crater" problem can be solved, at least in principle, using Eq. 4-1 after replacing the equations of motion by the equations of equilibrium. Instead, a finite element code [4-3] with quadrilateral elements is used. The input energy is converted to temperature rises at nodal points, from which the strains and stresses at those nodal points are calculated. The probable fracture paths are shown on Fig. 4-2. The lines represent the planes on which maximum tensile stresses act, and the symbols are proportional to the magnitude of the stresses. Considering that brittle materials fail under tension, this is expected to be a close approximation of the actual cracking pattern. These fracture paths do not intersect the free surface; hence, "thermal crater" mechanism is not expected to cause removal of material but only damage and weakening of the rock.

Not only the direction but also the magnitude of the maximum principal stress is unfavorable for fracture. Since the depth versus dose curve is truncated-bell shaped, the induced thermal gradient and tensile

stresses are low. For the temperature rise profile shown on Fig. 4-2, with a peak value of $100^{o}C$, the maximum principal stress is approximately 4.83 MN/m^2. It is 1/2 to 1/3 of the static strength of granite. A short duration pulse giving the same temperature rise creates a tensile stress wave of approximately 27.6 MN/m^2 peak value. Although the strength of rocks under dynamic loading is much higher than their static strength, "spallation" mechanism still appears to be much more promising than "thermal crater" fracture.

4.3 Shock Spalling Analysis

When the temperature rise due to intense electron bursts is too short for the stress wave to advance any appreciable distance, we can assume the temperature change a step function in time. The experiments discussed here have bombardment times of the order of 10^{-7} seconds. The stress wave within this time cannot propagate more than 0.5 mm. Even for sets #1 and #2 (Table 4-1), where the wavelengths are shortest, the error in maximum tensile stress due to assuming instantaneous energy deposition is less than 5% [4-4].

The fate of the initial compressive pulse can theoretically be determined using Eq. 4-1 with the given boundary and initial conditions, and taking $T = T_0 f(r,z) H(t)$ where $H(t)$ is the Heaviside function. Since we are mainly interested in an estimate of the dynamic strength, we will approximate the conditions by one-dimensional plane wave propagating in the half space $z \geq 0$, and avoid the complicated 3-dimensional problem of elastodynamics. The electron beam diameter is large compared to the electron penetration depth and the plane wave approximation is expected to give good results.

Since thermal expansion causes only dilatation and no distortion, the initially stressed region can be thought to create two P-waves of equal magnitude and of opposite directions. The P-wave travelling in the $-\hat{z}$ direction is reflected from the free surface as a P-wave only since the incidence angle is 90°. The resulting P-wave is unchanged except that the direction of propagation and amplitude are reversed. The rear going tensile wave can now cause brittle failure if the magnitude is high enough. The wave profile is non-uniform and the maximum tension builds up first at a depth of approximately 1/3 of the maximum penetration depth (Fig. 4-3).

There are five series of tests which lend themselves to dynamic analysis. The data accompanying experiments earlier than these last five series is not sufficient to determine the stress fields accurately enough to use in the analysis. These five series of experiments are summarized in Table 4-1 which is a modified version of Table III in Ref. [4-2]. Each series includes 30-40 shots, half of which are calorimetric readings. Most of the remaining shots are made on wet rocks since wet rock closely approximates conditions in a tunnel and shows much lower strength levels under short duration pulses. The fracture mechanism involved in wet rocks is, however, quite different than that of dry rocks. Water, and subsequently steam, in the pores play an important role. Only fracture in dry rocks is analyzed here.

Five different kinds of rock are used. Granodiorite, limestone and greenstone are described in Chapter II. Besides these, basalt and sandstone were tested. Basalt is very fine grained, gray-black in color and is obtained from Napa, California. The sandstone, known as

Lyons Sandstone, originates in Colorado. It is ferruginous sandstone, rust in color, with medium to fine grains. No attempt is made to analyze tests on greenstone since it is extremely anisotropic and very few data are available. Only the experimental results are shown on Fig. 4-10 for the sake of completeness. Density, coefficient of thermal expansion, modulus of elasticity, and Poisson's ratio for these rocks are obtained from Ref. [4-5].

The energy delivered per unit area is obtained from several calorimetric readings with identical conditions. The deposition of energy with depth is not determined for each case separately. Calorimetric short #2386 and #2364 have been analyzed in detail; resulting depth versus dose curves are very close to Spencer's predictions. All depth vs. dose curves are then taken to be of the same shape as shot #2386 (Fig. 4-4).

Combining depth versus dose and energy per unit area curves, the energy/volume variation with radius is determined for each shot used in the analysis (Fig. 4-5). Specific heat for most rocks varies sharply with temperature. Hence, the heat input per unit volume is converted to temperature rise by using the heat contents of the minerals which make up the rock. The data on heat content and heat capacity of various minerals is compiled by Kelly [4-6] and the procedure is described in [4-7].

The threshold stresses are determined using temperature rise at the rim of the spalled area. These threshold stresses - i.e., dynamic strengths - are shown by vertical bars in Figs. 4-6 through 4-10 as a function of the pulse duration, together with predictions. The theoretical analysis is based on the model developed in Section 3.3. The

stress pulse is idealized as uniformly distributed in depth and the analysis is carried out using Eq. (3-10). Weibull parameters m, σ_0, σ_u for granodiorite and basalt are determined from pure bending tests directly. For limestone and sandstone three-point bending results of Section 2.2 are used in conjunction with Weibull's uniaxial theory to obtain m, σ_0 and σ_u. Limestone does not show a marked zero strength (Fig. 2-17 is close to a straight line). It is difficult to determine a unique σ_u. Therefore, two sets of properties are used in predictions. Fracture toughness values are determined by three-point bend of notched specimens (50.8 mm × 12.7 mm × 6.4 mm) as specified in ASTM standards. Sharp cracks are introduced at the tip of 0.5 mm wide notches using ultrasonic cutting technique. Eight tests are done on basalt, 15 on granodiorite and four on limestone. The results are summarized together with other material properties on Table 4-2.

The parameter K in Eq. (3-10) is evaluated for each material using the shot of longest duration. The predictions for dynamic strength with changing pulse duration are shown for granodiorite on Fig. 4-6, for limestone on Fig. 4-7, for basalt on Fig. 4-8, for sandstone on Fig. 4-9. For all cases, except sandstone, the initiation phase, as given by Eq. (3-7), is included in the predictions; its effect is rather small. The experimental data points for wet rock are also included for comparison purposes. The static strength of brittle solids is a function of the volume; hence, it is shown as a band rather than a line.

The predictions agree very well with the data points. It is surprising that such a crude analysis can provide so close an estimate. The data of Carlson and Kerley [4-9] on shoal granite and Rinehart on

granite [4-10] also coincide well with the predictions. Carlson and Kerley found that for a pulse of 0.07 μsec duration dynamic strength is 224 MN/m^2. Rinehart's results are less clear; he shows a threshold stress of 40 MN/m^2 for a pulse roughly 2-3 μsec long.

Discussion of the Results: The results of this chapter show clearly that there is no unique dynamic strength of a material that we can tabulate. It can be estimated if we know the duration of stress application and the strength corresponding to some known pulse. Unfortunately, there are not many ways to obtain that one strength value. Experiments are virtually limited to flyer plate and electron deposition techniques. Hopkinson bar type experiments require long wavelengths compared to bar diameter to avoid higher modes which are dispersive. But using very slender bars made of rock is not reasonable since grain sizes are quite large. Besides, a small cross section would not lend itself to a typical coalescence phenomena.

The experimental scatter is quite large as can be seen by the length of vertical bars in Figs. 4-6 to 4-10. The intrinsic variation of rock strength is probably the most important factor. Static behavior from this point of view is discussed in detail in Chapter II. Besides material properties, calorimetric readings, delivered power, and location of threshold show quite large variations.

The velocity of the spalled particles is given by $\dot{u} = 2\ \sigma/\rho c_1$ for a one dimensional plane wave. These theoretical predictions are compared on Table 4-3 with observed values which are determined from high speed movie frames. The values compare favorably for dry granite; wet granite shows much higher spall velocities. The chunky spall debris of dry

granite indicates that there is appreciable amount of crack propagation before spalling; wet granite debris, on the other hand, is in the form of fine sand and indicates that there is hardly any crack propagation involved in the failure process. This agrees well with the fact that the data points for wet rocks are clustered close to the initiation curve rather than the fracture curve.

Theoretically, volume removed by a plane wave by spalling will increase as the length of the pulse increases since the depth at which tensile stress builds up shifts deeper. However, increasing the depth of deposition leads to large deviations from a plane wave; energy will be lost by outgoing waves in radial direction. Besides that, as the electron deposition depth increases, the cracks may arrest before reaching the free surface since they initiate at a plane too far from the free surface; damage will be extensive, but no spalling will occur. Prediction of the optimum deposition depth seems to be a rather difficult job; the wave propagation problem stated at the beginning of this chapter has to be solved for deposition depths comparable to electron beam diameters.

The transverse stresses due to the one-dimensional plane wave are compressive but roughly of the same magnitude as the longitudinal tensile stress. From the study of brittle solids under multiaxial loading we know that such a stress state will give very similar results to that of uniaxial loading as far as initiation is concerned. Thus neglecting the transverse stresses is justified. The effect of these transverse stresses on the propagation phase is unknown. It does not appear that they would alter the stress field at the tip of a running crack to such an extent as to change the general conclusions that have been reached.

CHAPTER FIVE: CONCLUSIONS

It has been pointed out that the Weibull multiaxial treatment of brittle strength is applicable only to materials with sharp cracks. The Weibull treatment does not take into consideration the effect of the stresses in the plane of the cracks, hence the analysis is not expected to be valid for materials with spherical flaws. It is demonstrated, however, that the theory is applicable even to porous materials if uniaxial stress states are considered.

Weibull's multiaxial formulation is applied in analyzing the results of diametral compression of solid disks. Based on the three-point bending tests done on rectangular and round beams, the behavior of disks is predicted successfully in terms of both the mean value of pressure at fracture and the distribution of pressure at fracture for granodiorite and limestone. Tests on greenstone and basalt showed that two parameter multiaxial Weibull formulation is incapable of predicting the behavior of materials which are highly anisotropic and have large threshold stress levels below which no failure occurs.

Brittle solids behave very differently under dynamic loading and in static loading. Unstable crack growth does not lead to catastrophic failure. Failure is due to coalescence of many small cracks. A simple formulation is developed to predict this coalescence process. The fracture is assumed to be complete when a crack reaches the walls of its "cell", where the size of the "cell" is determined by the applied stress and the crack population. The predictions of this new theory agree well with rock shattering experiments using intense bursts of energetic electrons.

It would be desirable to develop a dynamic fracture model which includes the arbitrary orientation of cracks and a more realistic propagation law. Such a model gives the fraction of volume damaged as a function of time, but is not self-sufficient since it is not clear what volume fraction will lead to total fracture. A probabilistic study of the percentage of cracked grains or grain boundaries required for total fracture has been provided by Lindborg [5-1]. It was hoped to build upon his work. Unfortunately, on examination it is seen to have serious errors. A discussion of the features that could be incorporated in a more complete model and Lindborg's work is contained in the Appendix.

REFERENCES

1-1 Avery, R. T., et. al. "Shattering of rock with intense bursts of energetic electrons" IEEE Transactions on Nuclear Science, V. NS-20, No. 3 pp. 1010-1014.

2-1 Weibull, W. "A statistical theory of the strength of materials" Ingvetenskakad. Handl. No. 151, Stockholm (1939) p.1-45.

2-2 Oh, H. L. and I. Finnie "On the location of fracture in brittle solids-I. Due to static loading" Int. J. Fracture Mech., 6 (1970) p. 287-300.

2-3 Oh, K. P. L. and I. Finnie "On the location of fracture in brittle solids - II. Due to wave propagation in a slender rod", Int. J. Fracture Mech., 6 (1970) p. 333-339.

2-4 Salmassy, O. K., E. G. Bodine, W. H. Duckworth and G. K. Manning, "Behavior of brittle-state materials", WADC Technical Report 53-50, Part II (1955) p. 46.

2-5 Davidenkov, N., E. Shevandin and F. Witman "The influence of size on the brittle strength of steel" J. Appl. Mech., 14 (1947) p. 63-67.

2-6 Manson, S. S. Thermal stress and low-cycle fatigue, McGraw-Hill Book Co. (1966) p. 295.

2-7 Weibull, W. "The phenomenon of rupture in solids" Ingvetenskakad. Handl., No. 153, Stockholm (1939) p. 3-54.

2-8 Broutman, L. J. and R. H. Cornish "Effect of polyaxial stress states on failure strengths of alumina ceramics" J. Am. Ceramic Soc., 48 (1965) p. 519-524.

2-9 Ely, R. E. "Combined stress strength results for Titania" U. S. Army Missile Comm. Report, No. RR-TR-70-23 (1970).

2-10 Priddle, E. K., "Effect of multiaxial stresses on the fracture strength of silicon carbide" J. Strain Analysis, 4 (1969) p. 81-87.

2-11 Mair, W. M. "Fracture criteria for cast iron under biaxial stresses" Gr. Britain, Nat. Eng. Lab Report No. 261 (1966).

2-12 Oh, K. P. L., Ö. Vardar and I. Finnie "Failure of brittle solids under biaxial stresses" Int. J. of Fracture, 9 (1973) p. 372-375.

2-13 Babel, H. W. and G. Sines "A biaxial fracture criterion for porous brittle materials" J. Basic Engineering, 90 (1968) p. 285-291.

2-14 Ref. [2-4] p. 53.

2-15 Inglis, C. E. "Stresses in a plate due to the presence of cracks and sharp corners" Transactions of the Institute of Naval Architecture, Vol. 55, Part I (1913) p. 219-230.

2-16 Whittaker, E. T. "A Treatise on the Analytical Dynamics of Particles and Rigid Bodies" Dover publications, New York (1944) p. 8.

2-17 McClintock, F. A. "Statistics of brittle fracture" Fracture Mechanics of Ceramics, V.1 (R. C. Bradt et al. editors) Plenum Press New York (1974).

2-18 Batdorf, S. B. and J. G. Crose "A statistical theory for the fracture of brittle structures subjected to nonuniform polyaxial stresses" J. Appl. Mech. 41 (1974) pp. 459-464.

2-19 Batdorf, S. B. "Fracture statistics of isotropic brittle materials with surface flaws" Aerospace Report No. TR-0074 (4450-76)-2 (1973).

2-20 Oh, K. P. L. "On the statistical nature of brittle fracture" Ph. D. Thesis, University of California, Berkeley (1970).

2-21 Dukes, W. H. "Handbook of Brittle Material Design Technology" AGARDograph 152, North Atlantic Treaty Organization (1971).

2-22 Fairhurst, C. and M. P. Hardy "Fracture in rocks and engineering implications "Proceedings of the 3rd International Congress on Fracture, München, W. Germany.

2-23 Hardy, M. P. "Fracture mechanics applied to rock" Ph. D. Thesis, University of Minnesota (1973).

2-24 Hudson, J. A. "A critical examination of indirect tensile strength test for brittle rocks" Ph. D. Thesis, University of Minnesota (1970).

2-25 Marschall, C. W. and A. Rudnick "Conventional strength testing of ceramics" in Fracture Mechanics of Ceramics" to be published by Plenum Press.

2-26 Carniero, F. L. L. B. and A. Barcellos "Concrete tensile strength" Union of Testing and Research Laboratories for Materials and Structures, No. 13 (1953).

2-27 Shaw, M. C., P. M. Braiden and G. J. DeSalvo "The disk test for brittle materials", ASME Paper No. 73-WA/Prod-17.

2-28 Mellor, M. and I. Hawkes "Measurement of tensile strength by diametral compression of disc and annuli" Eng. Geol., 5 (1971) pp. 173-225.

2-29 Rudnick, A., A. R. Hunter and F. C. Holden "An analysis of the diametral-compression test" Mater. Res. Std., 3 (1963) pp. 283-289.

2-30 Berenbaum, R. and I. Brodie "Measurement of the tensile strength of brittle materials" Brit. J. Appl. Phys., 10 (1959) pp. 281-287.

2-31 Hondros, G. "The evaluation of Poisson's ratio and the modulus of materials of a low tensile resistance by the Brazilian test with particular reference to concrete" Australian Journal of Applied Science, 10 (1959) pp. 267-268.

2-32 Weil, N. A. and I. M. Daniel, "The influence of stress gradient on the strength of brittle materials", ASME paper 63-WA-228.

3-1 Thau, S. A. and T. H. Lu "Transient stress intensity factors for a finite crack in an elastic solid caused by a dilatational wave" Int. J. Solids Structures, 7(1971), p. 731-750.

3-2 Freund, L. B., "Crack propagation in an elastic solid subjected to general loading - III. Stress wave loading", J. Mech. Phys. Solids, 21, (1973) p. 47-61.

3-3 Achenbach, J. D. and R. Nuismer "Fracture generated by a dilatational wave", Int. J. Fracture Mechanics, 7 (1971), p. 77-88.

3-4 Mal, A. K. "Interaction of elastic waves with a Griffith crack", Int. J. Engng. Sci., 8, (1970), p. 763-776.

3-5 Mal, A. I. "Interaction of elastic waves with a penny-shaped crack" Int. J. Engng. Sci., 8, (1970), p. 381-388.

3-6 Mott, N. F. "Brittle fracture in mild steel plates", Engineering, 165 (1948) p. 16-18.

3-7 Roberts, D. K. and A. A. Wells, "The velocity of brittle fracture", Engineering, 178 (1954) p. 820-821.

3-8 Dulaney, E. N. and W. F. Brace, "Velocity behavior of a growing crack", J. Appl. Phys., 31 (1960), p. 2233-2236.

3-9 Berry, J. P. "Some kinetic considerations of the Griffith criteria for fracture" J. Mech. Phys. Solids, 8, (1960) p. 194-216.

3-10 Tsai, Y. M. "Dynamic stress distribution around the tip of a running crack" Engng. Fracture Mechanics, 6, (1974) p. 509-522.

3-11 Broberg, K. B. "The propagation of a brittle crack" Arkiv. für Fysik, 18 (1960) p. 159-192.

3-12 Freund, L. B. "Crack propagation in an elastic solid subjected to general loading - II. Non-uniform rate of extension", J. Mech. Phys. Solids, 20, (1972), p. 141-152.

3-13 Bergkvist, H., "The motion of a brittle crack", J. Mech. Phys. Solids, 21 (1973) p. 229-239.

3-14 Broberg, K. B. "Discussion of fracture from the energy point of view" Recent Progress in Applied Mechanics (edited by Broberg, Hult, Fritthoif) p. 125-151 Almquist and Wiksell, Stockholm.

3-15 Tsai, Y. M. "Propagation of a brittle crack at constant and accelerating speeds", Int. J. Solids Structures, 9, (1973) p. 625-642.

3-16 Tuler, R. F. and B. M. Butcher, "A criterion for the time dependence of dynamic fracture", Int. J. Fracture Mechanics, 4 (1968) p. 431-437.

3-17 Shockey, D. A. et al., "Fragmentation of rock under dynamic loads" Int. J. Rock Mech. Sci. and Geomech. Abst. V.11 (1974) p. 303-317.

3-18 Freund, L. B. "Crack propagation in an elastic solid subjected to general loading - N. Obliquely incident stress pulse" J. Mech. Phys. Solids, 22 (1974), p. 137-146.

4-1 Avery, R. T., D. Keefe, T. L. Brekke and I. Finnie, "Use of intense sub-microsecond electron bursts to produce rock shattering" Advances in Rock Mechanics, Proc. of 3rd Congress of Int. Soc. of Rock Mechanics, Denver, Colo., V.II (1974) p. 1415-1420.

4-2 Avery, R. T. "Study of rock shattering by intense bursts of energetic electrons", D. Eng. Thesis, University of California, Berkeley (1974).

4-3 Doherty, W., E. Wilson, R. Taylor, "Stress analysis of axisymmetric solids utilizing higher-order quadrilateral finite elements"

University of California, Berkeley, Structural Engineering Lab Report No. 69-3.

4-4 Keefe, D. "Stress wave propagation following energy deposition by a monoenergetic electron beam - one dimensional case" (1973) (unpublished research).

4-5 Korbin, G. E. and T. L. Brekke "Summary of rock property data for the study of rock shattering by intense bursts of energetic electrons" University of California, Berkeley, College of Engineering Internal Report UCX-2437 (1972).

4-6 Kelly, K. K., "Contributions to the Data on Theoretical Metallurgy XIII" U. S. Bureau of Mines Bulletin 584.

4-7 Somerton, W. H. "Some thermal characteristics of porous rocks" J. Petroleum Technology (1958) p. 61-64.

4-8 Pankow, D. (Unpublished research).

4-9 Carlson, G. A. and T. M. Kerley "Dynamic response of geological materials to pulsed electron beam deposition" Sandia Laboratories Report, SLA-74-0248 (1974).

4-10 Rinehart, J. S. "Dynamic fracture of rocks" Proceedings of the 7th symposium on rock mechanics, V.1 (1965) p. 205-208.

5-1 Lindborg, U. "A statistical model for the linking of microcracks" Acta Metallurgica, 17 (1969) pp. 521-526.

Table 2.1. Bending Tests on Granodiorite Beams. All Stress Values are Corrected for Friction.

Set no.	No. of sp's tested	Size (in.)	Cross section	Parameters m	σ_0[psi]	Mean Stress [psi]	Comments
#1	35	$1\frac{3}{4}\times\frac{3}{16}\times\frac{5}{16}$		m=12.4;	σ_0=1170	2150	identical specimens
#2	36	$1\frac{3}{4}\times\frac{5}{16}\times\frac{3}{16}$		m=12.1;	σ_0=1140	2147	
#3	17	$1\frac{3}{4}\times\frac{5}{32}\times\frac{5}{16}$		m=12.7;	σ_0=1230	2290	identical specimens
#4	16	$1\frac{3}{4}\times\frac{5}{16}\times\frac{5}{32}$		m=12. ;	σ_0=1160	2164	
#5	26	$1\frac{3}{4}\times\frac{1}{8}\times\frac{3}{8}$		m=8 ;	σ_0= 930	2000	very rough
#6	26	$1\frac{3}{4}\times\frac{3}{16}\times\frac{5}{16}$		m=10.4;	σ_0=1015	2050	wet
#7	26	$1\frac{3}{4}\times\frac{3}{16}\times\frac{5}{16}$		m=10.5;	σ_0=1100	2211	rough supports μ =.31
#8	34	$1\frac{3}{4}\times\frac{3}{16}\times\frac{5}{16}$		m=10.9;	σ_0=1130	2215	smooth supports μ =.20
#9	22	$1\frac{3}{4}\times\frac{5}{32}\times\frac{5}{16}$		m= 9.8;	σ_0=1030	2160	rough surf., smooth sup.
#10	15	$1\frac{3}{4}\times\frac{3}{16}\times\frac{5}{16}$		m= 9.5;	σ_0=1020	2151	rough surf., rough sup.
#11	12	$1\frac{3}{4}\times\frac{3}{16}\times\frac{5}{16}$		m=11 ;	σ_0=1125	2200	smooth surf., smooth sup.
#12	16	L=2.5 D=.416		m=11.1;	σ_0=1230	2330	

(1 in. = 2.540 cm. ; 1000 psi = 6.895 MN/m^2)

Table 2-2 Disk Tests on Granodiorite

Set no.	Number of Specimens	Surface Condition	Predicted Mean Stress psi Eq.(2-10) σ_0=1170 psi m=12.0	Observed Mean Stress at Fracture psi	% Error
#13	40	Similar to Bending Specimens	1770 psi	1850 psi	4.3
#14	38	Smoother than Bending Specimens	1770 psi	1856 psi	4.6

Table 2-3 Bending Tests on Limestone Beams

Set no.	Number of Specimens Tested	Size (in.)	Cross section	Parameters m	σ_0 (psi)
#15	49	1.75 × 0.188 × 0.313		9.6	270
#16	22	2.5 × 0.3 × 0.4	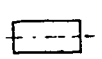	10.6	260
#17	30	L=2.5 D=0.413		10.5	420

(1 in.= 2.540 cm. ; 1000 psi = 6.895 MN/m^2)

Table 3-1 Increase in dynamic stress intensity factor for different input pulses

Incident Wave		Griffith crack	Penny-shaped crack
Rectangular Pulse	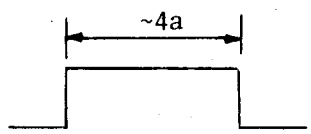	30% overshoot (analytic soln.)	~45% overshoot by analogy
Harmonic	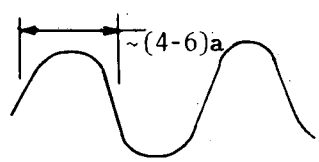	30% overshoot (analytic soln.)	45% overshoot (analytic soln.)

a - crack half length

% - overshoot is given as $\frac{(K_{Id}-K_I)}{K_I} \times 100$

Table 4-1 Typical parameters of electron accelerators used (from Ref. 4-2)

Set no.	Accelerator used	Beam Voltage [MV] mean	max.	Approximate beam diameter [cm]	Approx. penetration depth for granite [cm]	Approx. pulse length for granite [μsec]
1	Pulserad 422 Run I	1.0	1.3	4.8 - 3.1	0.18	0.38
2	Pulserad 422 Run II	1.1	1.4	6.3 - 3.8	0.20	0.42
3	Pulserad 422 Run III	2.0	3.1	3.6	0.37	0.78
4	PI 1140	4.0	5.0	3.5	0.87	1.8
5	Hermes II	9	12.5	9.0	1.82	3.8

Table 4-2 *The data from 3 point bending tests is converted to simple tension data using Weibull's 2 parameter formulation which in turn is plotted to get m, σ_u, σ_0.

Rock type	m —	σ_0 MN/m^2 (psi)	σ_u MN/m^2 (psi)	K_{Ic} $MN/m^{3/2}$	($lb/in.^{3/2}$)	Source
Granodiorite	4.4	1.93 (280)	7.60 (1100)	0.87	(780)	Pankow [4-8]
Basalt	2.9	1.12 (175)	19.50 (2800)	1.38	(1240)	Experiments
Limestone	3	0.69 (100)	2.07 (300)	0.26	(235)	m, σ_0, σ_u using Weibull*
	4	0.83 (120)	1.79 (260)			K_{Ic} by experiments
Sandstone	2	0.48 (70)	1.72 (250)	—	—	m, σ_0, σ_u using Weibull*

Table 4-3 Observed & predicted spall velocities for granite

Shot no.	Target		Observed max. spall velocity [m/sec]	Predicted max. spall velc. [m/sec]
2065	Dry block		35	50
2381	Dry slab of 1 cm	F:	150	90
		B:	55	
3641	Dry slab of 1.1cm	F:	60	45
		B:	13	
2064	Wet block		100	50
2071	Wet slab of 1 cm	F:	> 80	100
		B:	22	
2072	Wet slab of 0.5cm	F:	> 150	100
		B:	22	
2377	Wet slab of 1.1cm	F:	550	90
		B:	80	
2382	Wet slab of 1.7cm	F:	> 150	90
		B:	40	
3633	Wet slab of 1cm	F:	245	45
		B:		
3635	Wet slab of 0.9cm	F:	68	25
		B:	—	

F: Front face, B: Back face

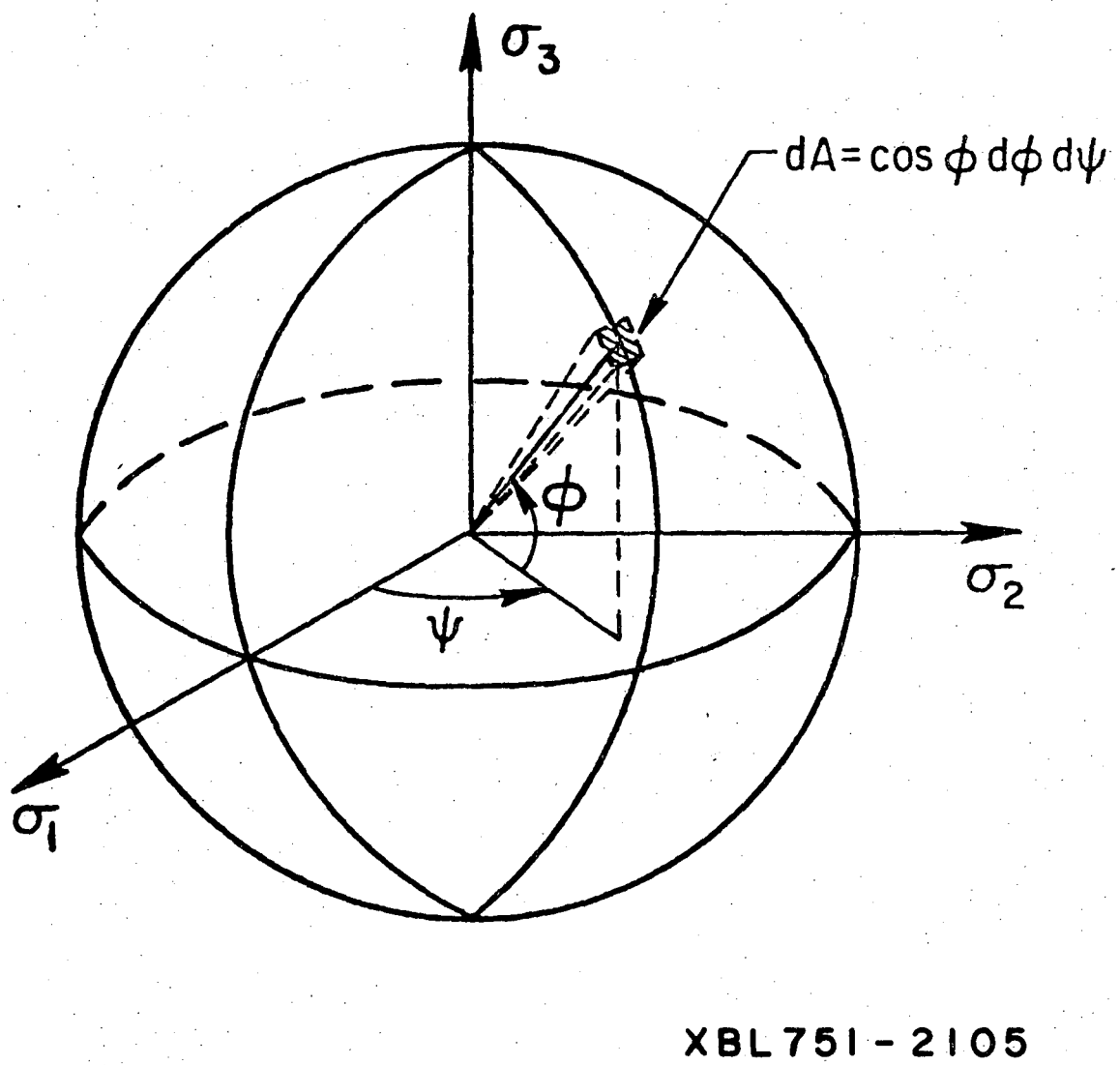

Fig. 2-1. Geometric variables used to describe location on a unit sphere.

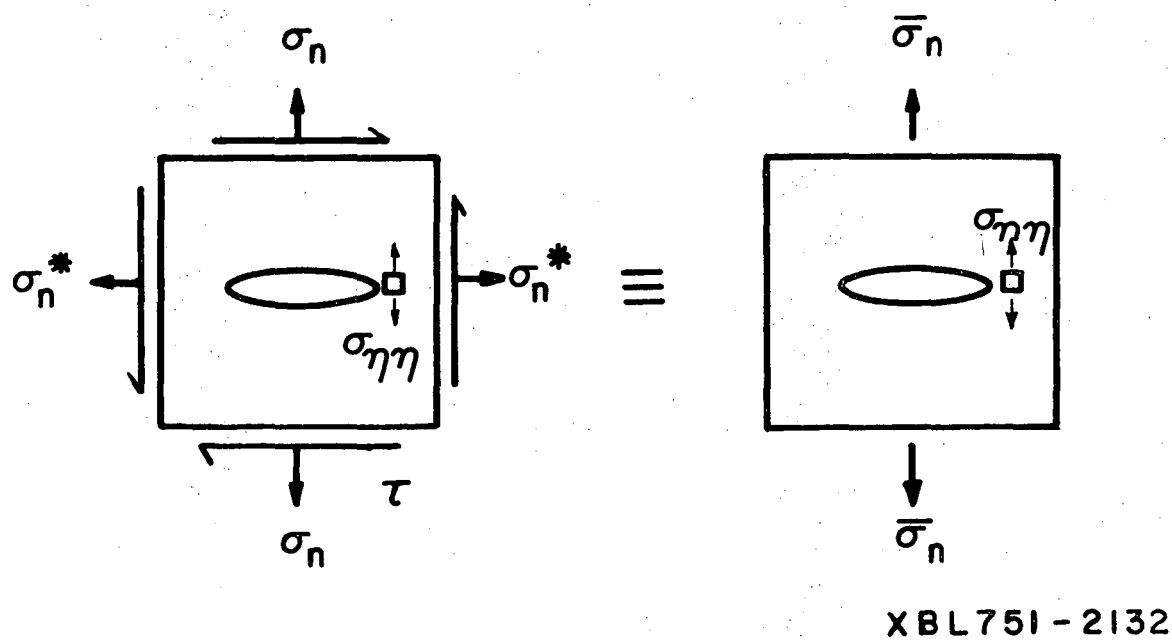

Fig. 2-2. Reducing the stresses acting on a crack to an equivalent stress.

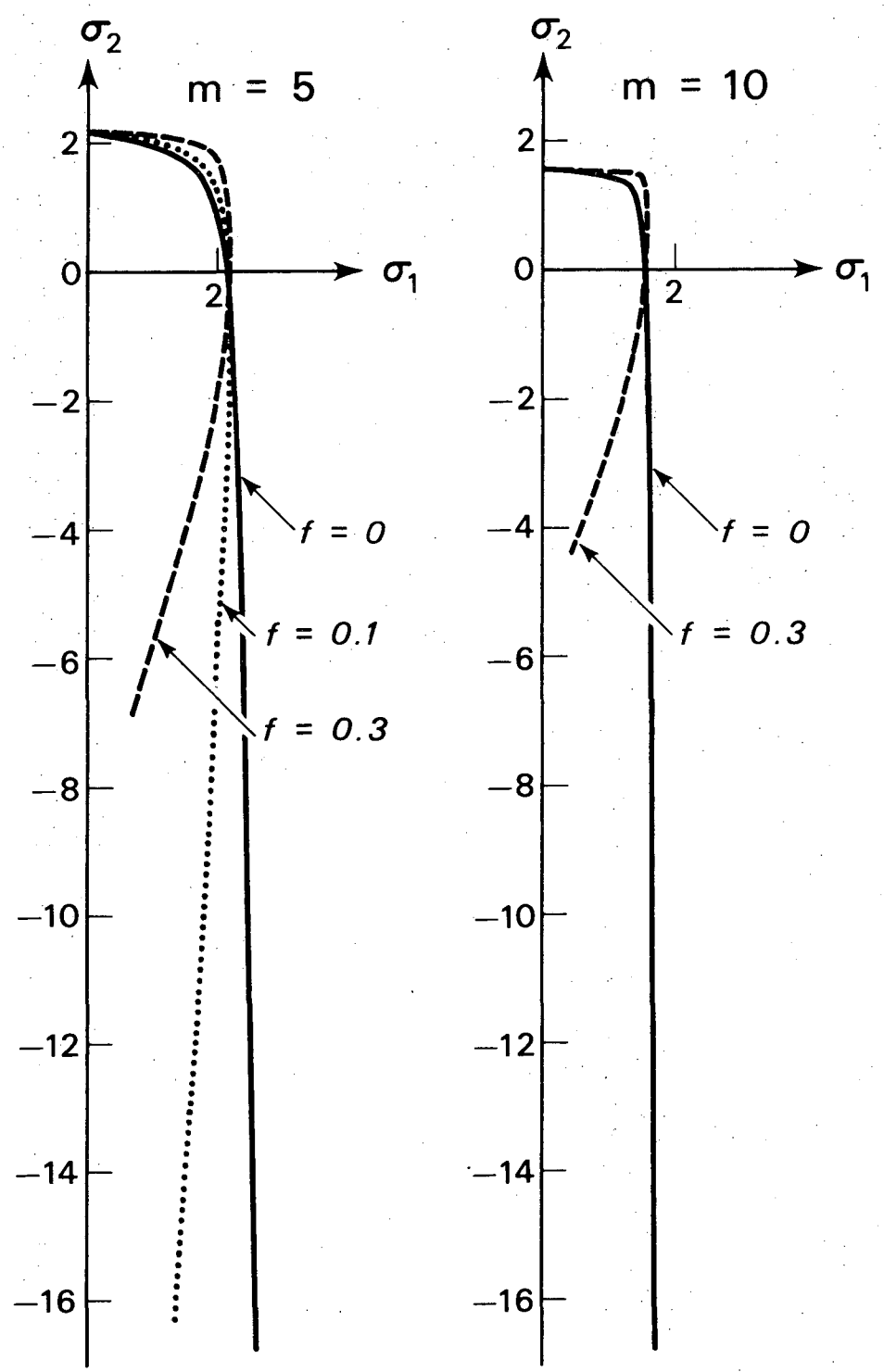

XBL 752-4678

Fig. 2-3. Fracture envelope for $\sigma_{1\ \mathrm{mean}}\ (VK)^{1/m}\ /\ \Gamma(1+\frac{1}{m})$.

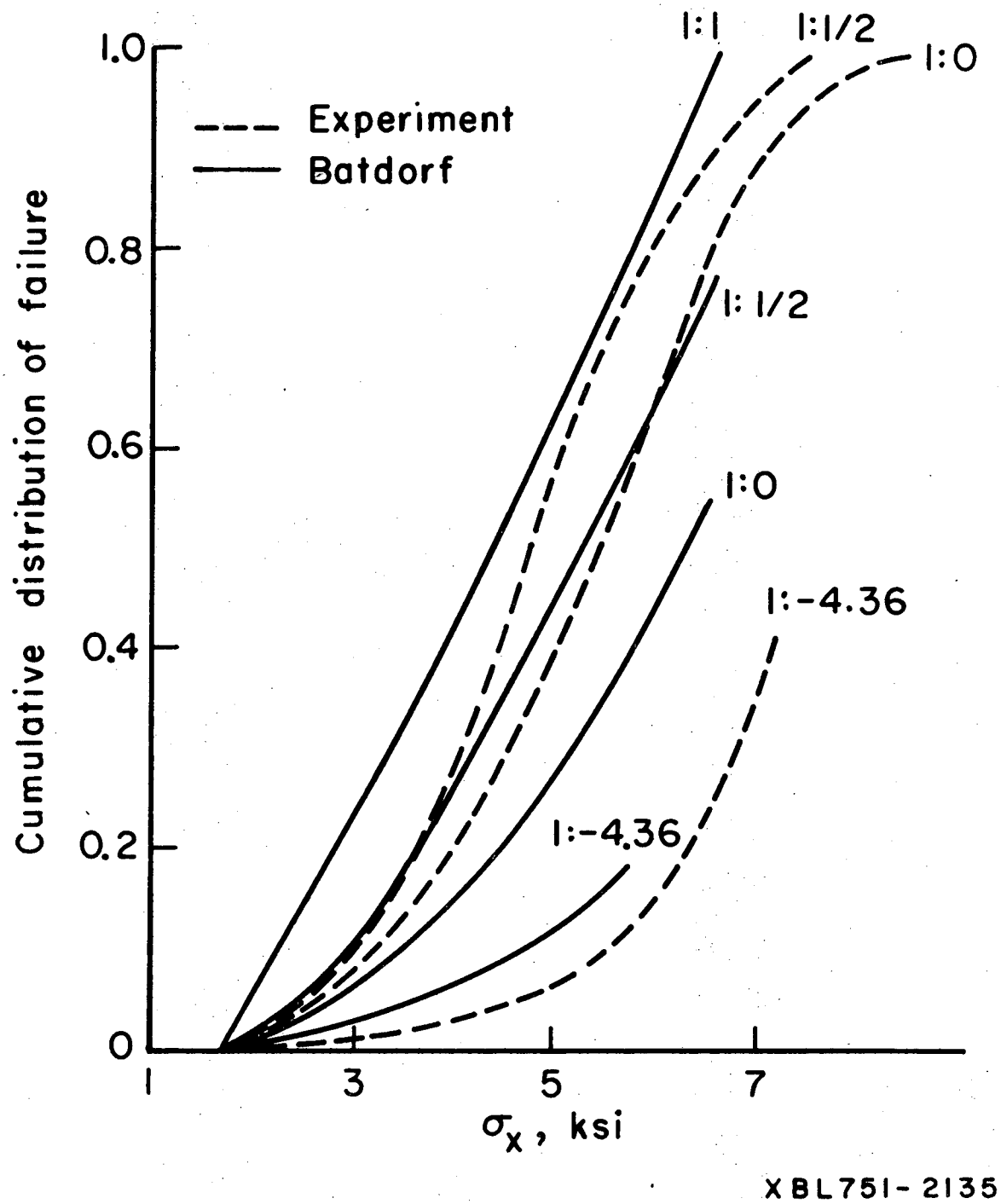

Fig. 2-4. Predictions of Batdorf (fitted to 1:1 data) compared with experimental data from Ref. [2-20] (1 ksi = 1000 psi = 6.895 MN/m^2).

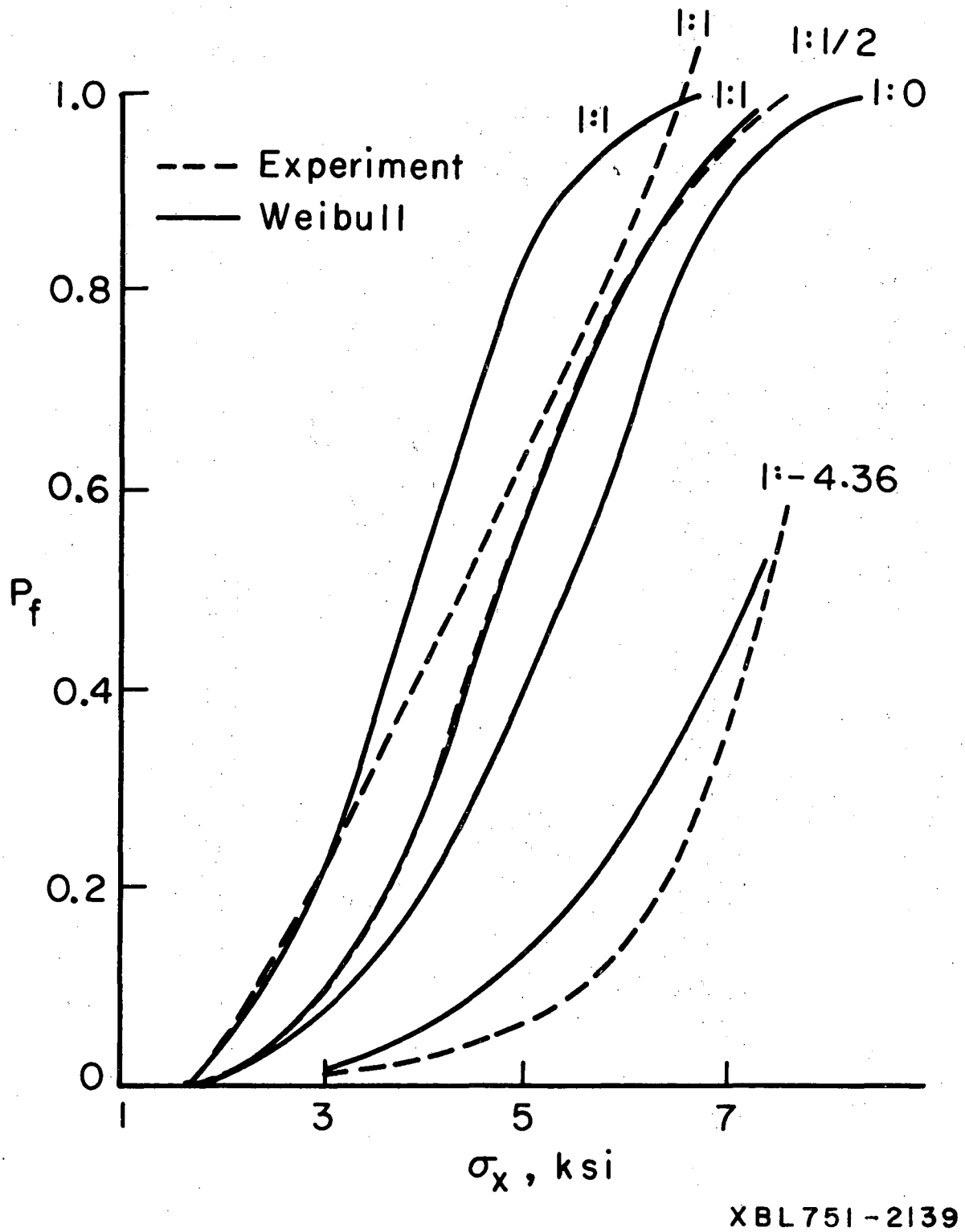

Fig. 2-5. Predictions of the 2 parameter Weibull theory (fitted to 1:0 data) compared with experimental data from Ref. [2-20] (1 ksi = 1000 psi = 6.895 MN/m^2).

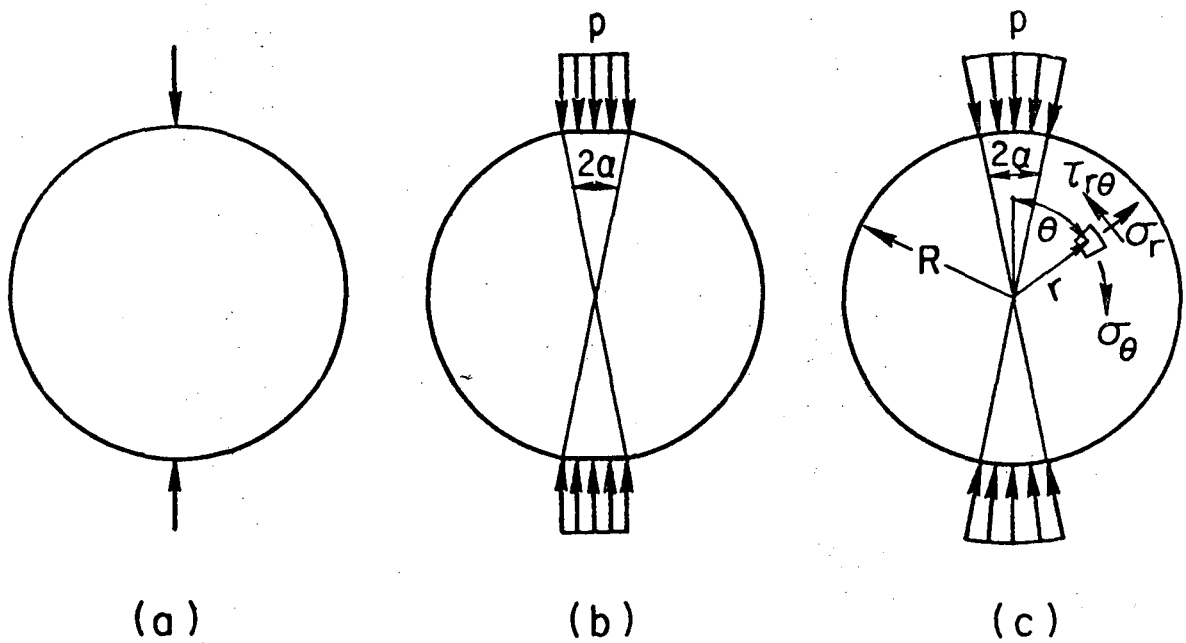

XBL751-2120

Fig. 2-6. (a) Idealized diametral compression test under point loads.

(b) Specimen with small flats used for tests,

(c) Geometry for which an analytical solution is available [2-31].

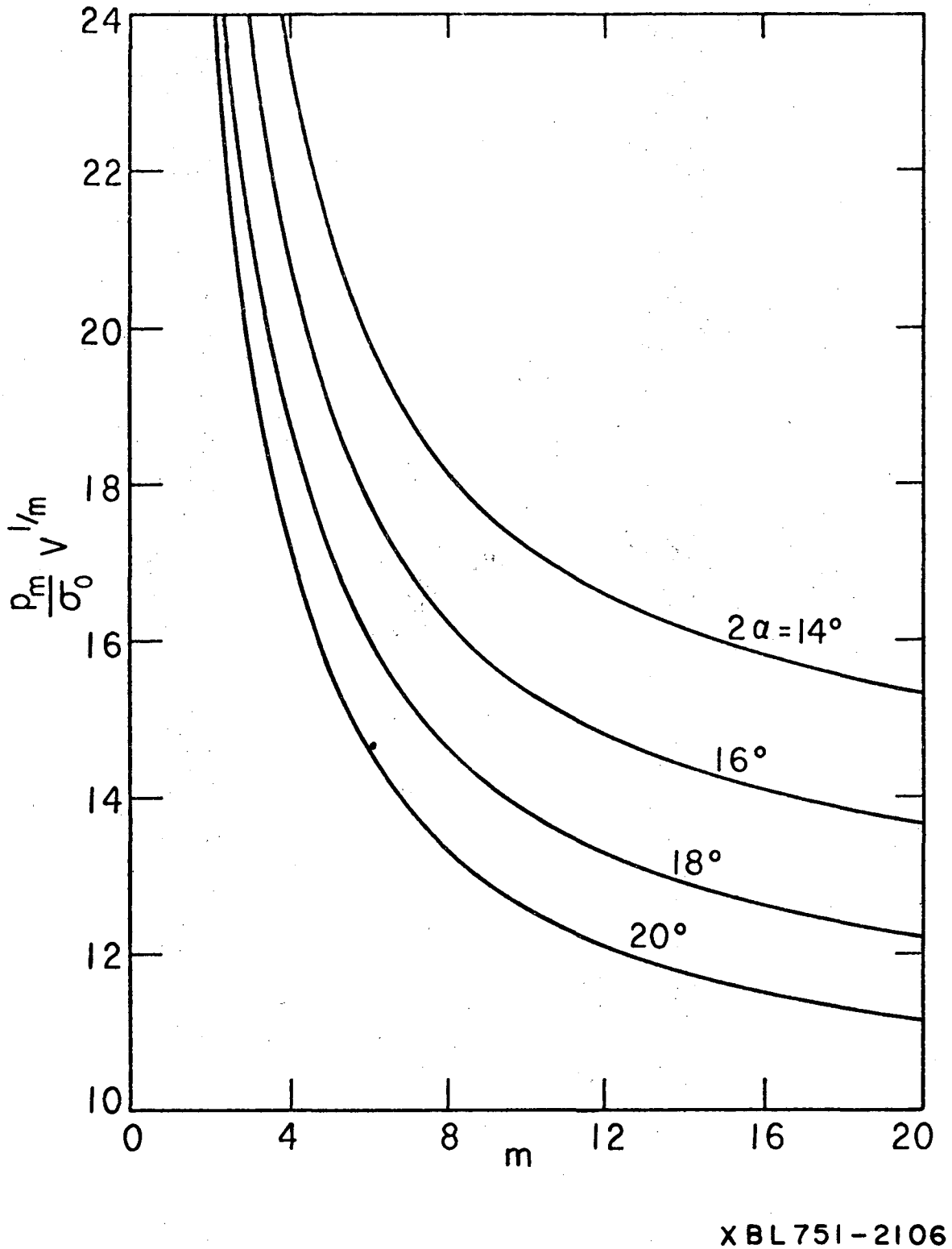

Fig. 2-7. Mean value of pressure at fracture for given values of V, σ_0, m and α.

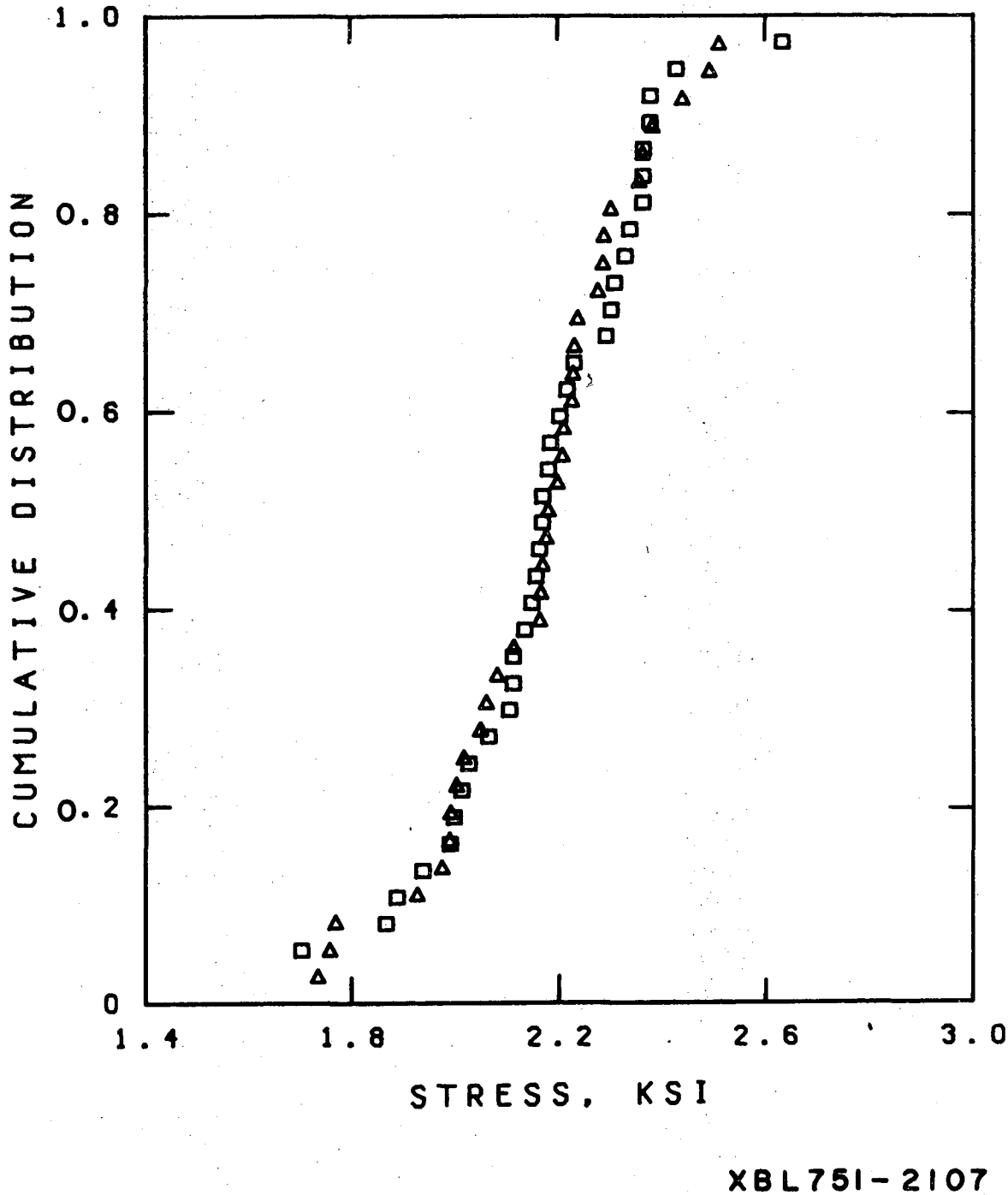

Fig. 2-8. A comparison of bending specimens with different orientations of the cross-section, (set 1 Δ, set 2□) (1 ksi = 1000 psi = 6.895 MN/m^2).

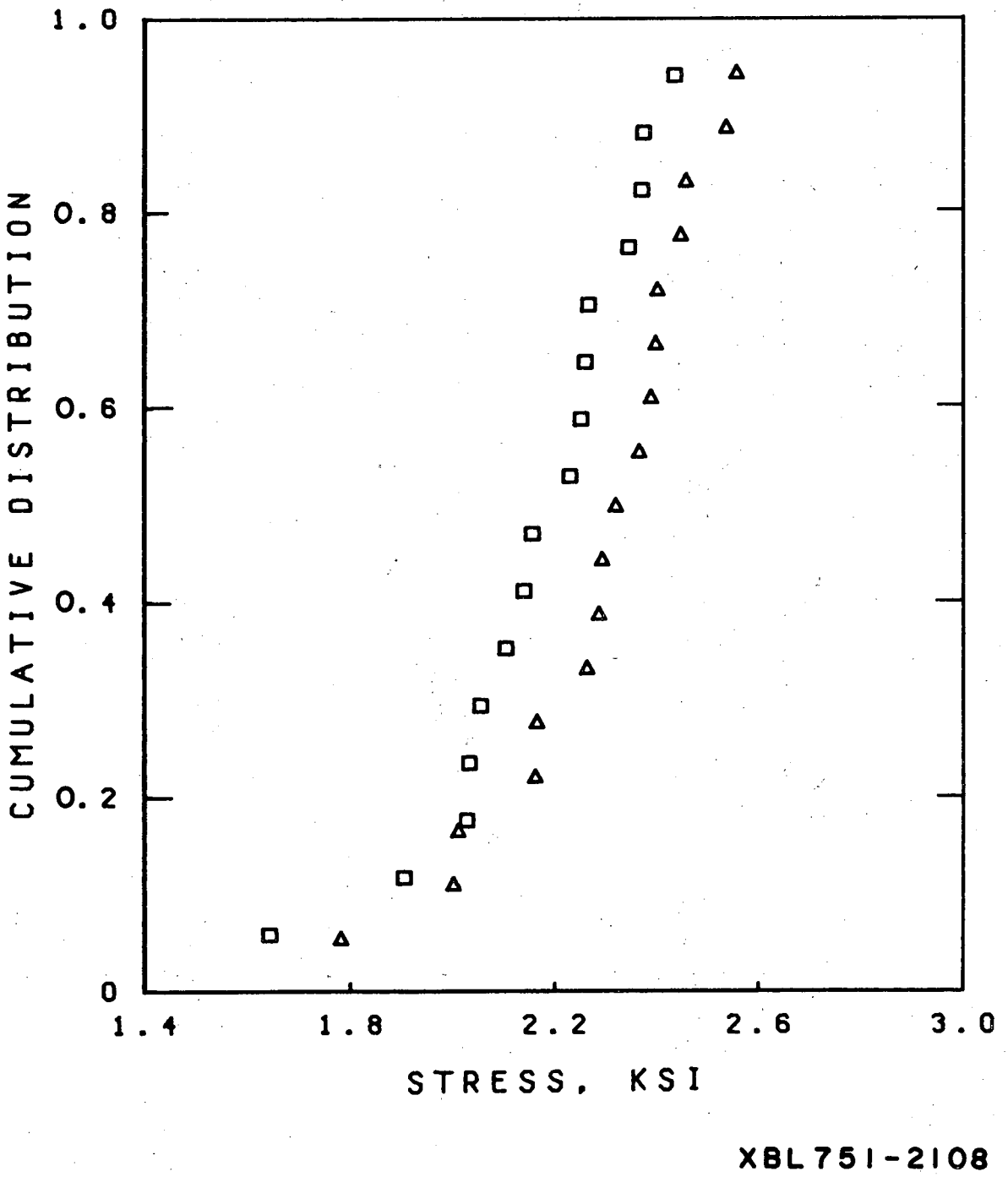

Fig. 2-9. A comparison of bending specimens with different orientatations of the cross-section, (set 3 Δ, set 4 □) (1 ksi = 1000 psi = 6.895 MN/m^2).

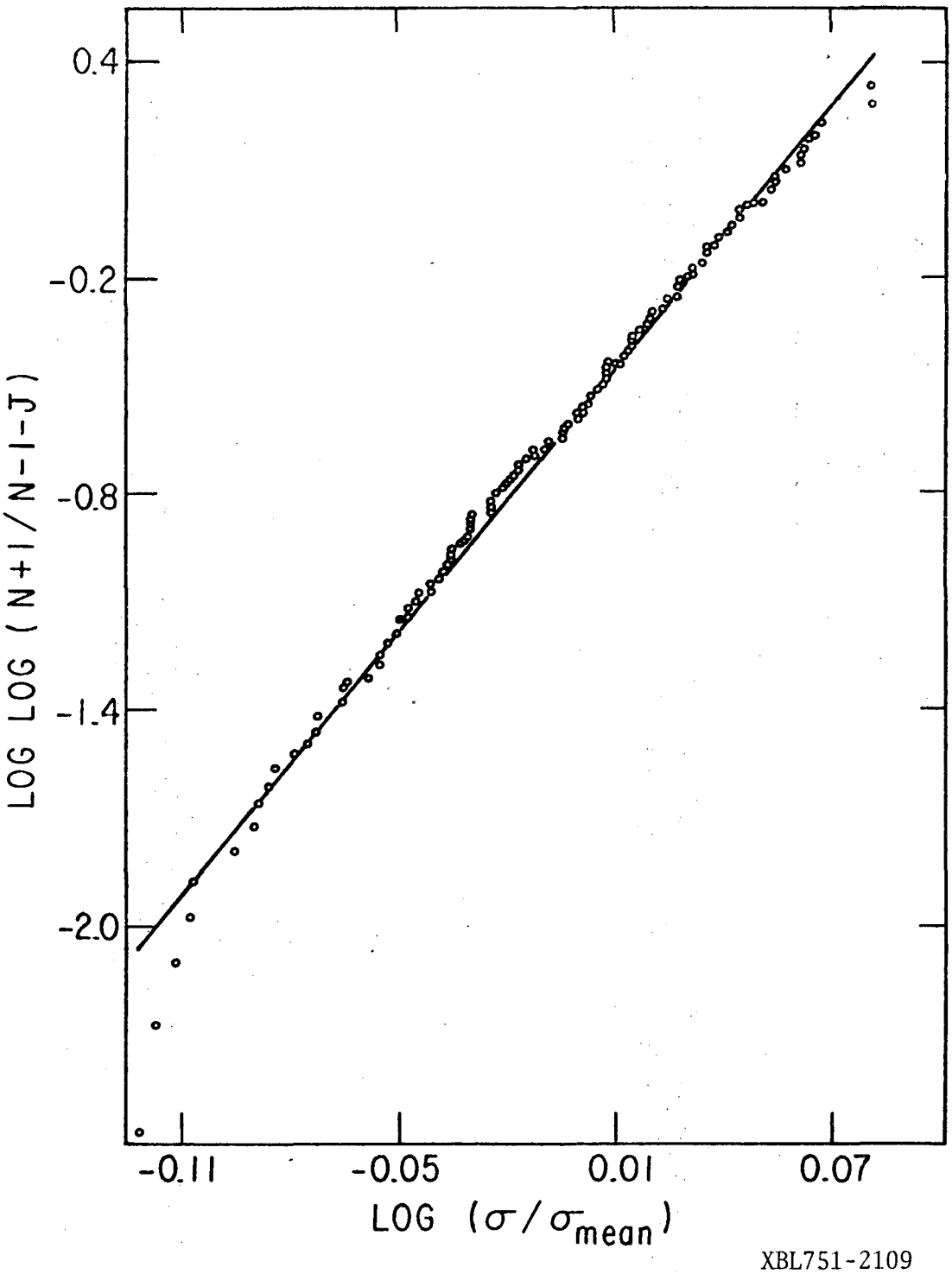

Fig. 2-10. Plot of pooled bending strength values normalized by mean for each set to obtain an estimate of m. Ordinate is log log $(\frac{1}{1-G})$ where G = j/(N+1). Some of the 161 data points coincide and these values are not shown.

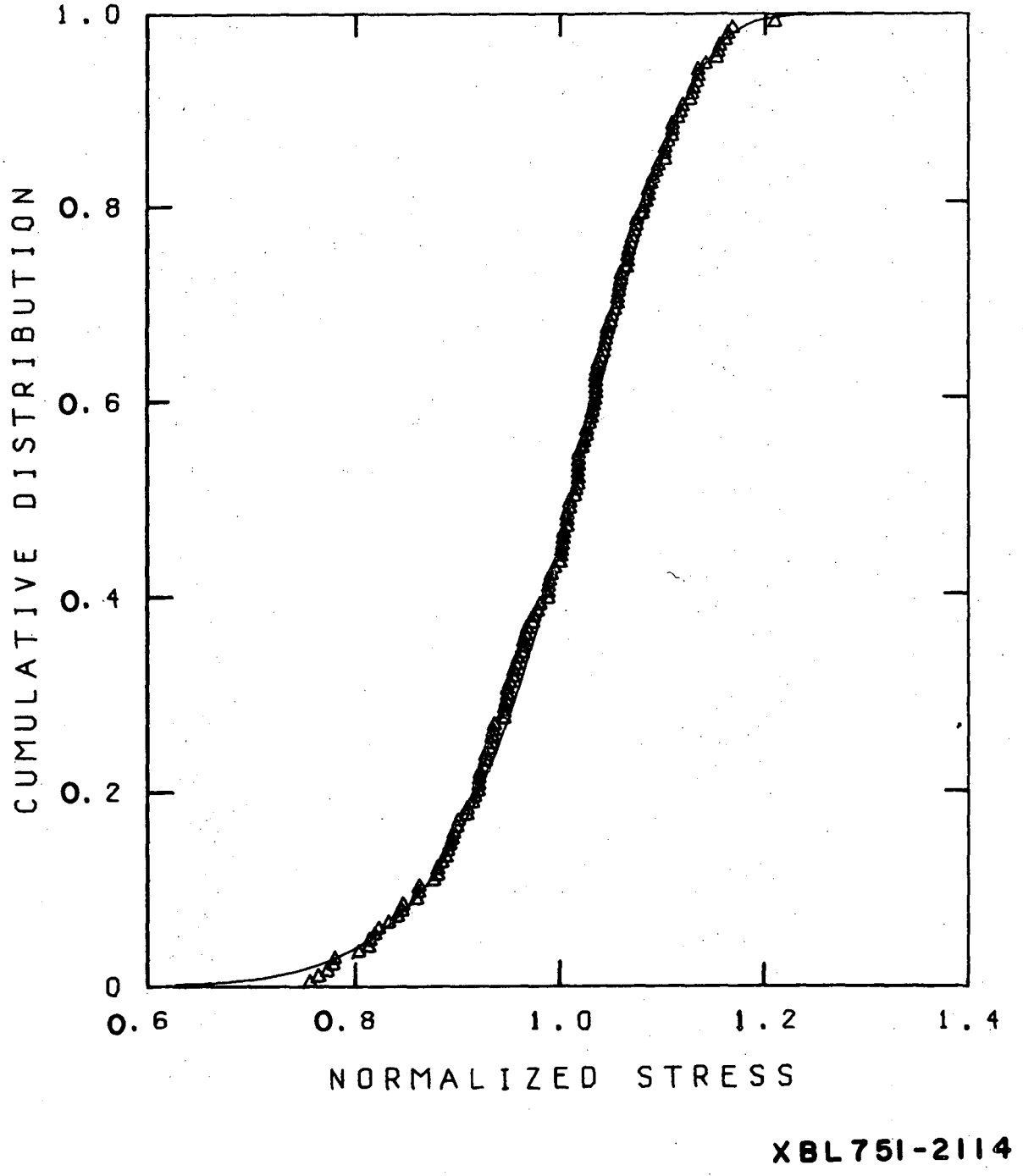

Fig. 2-11. Replot of Fig. 2-10 on linear coordinates.

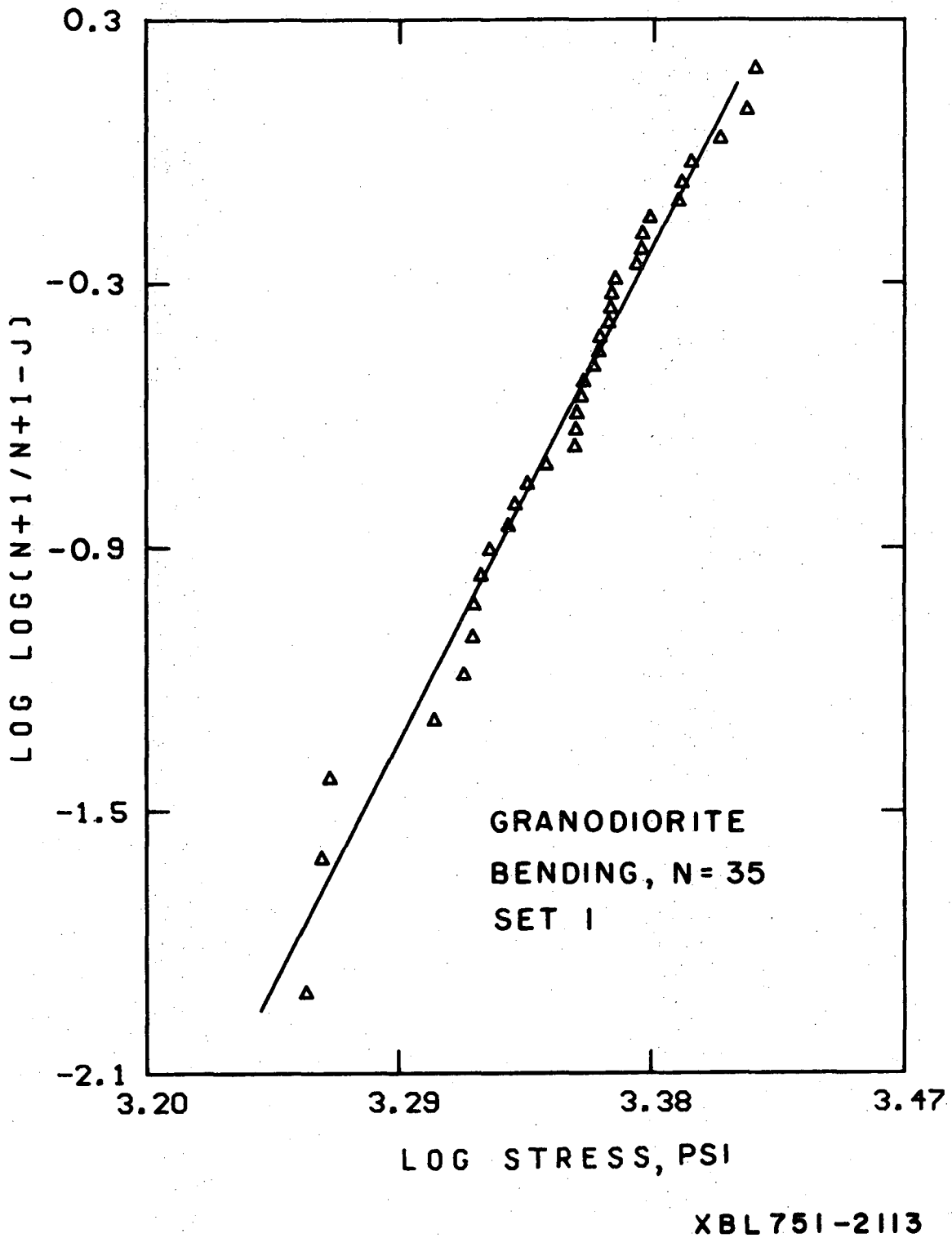

Fig. 2-12. Strength values from set 1 plotted to estimate the parameter σ_0 (1000 psi = 6.895 MN/m^2).

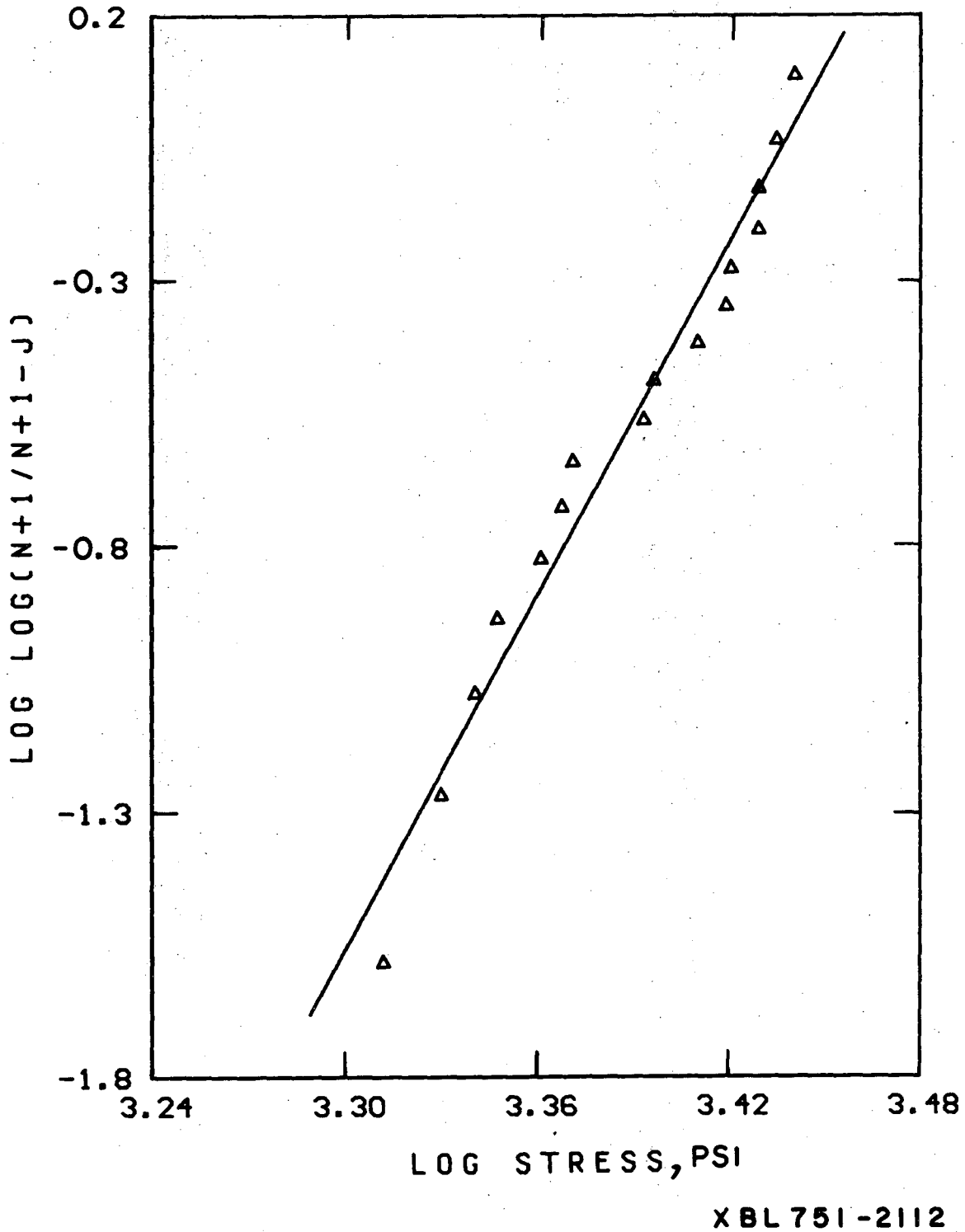

Fig. 2-13. Strength values from set 12 plotted to estimate the parameters σ_0 and m (1000 psi = 6.895 MN/m^2).

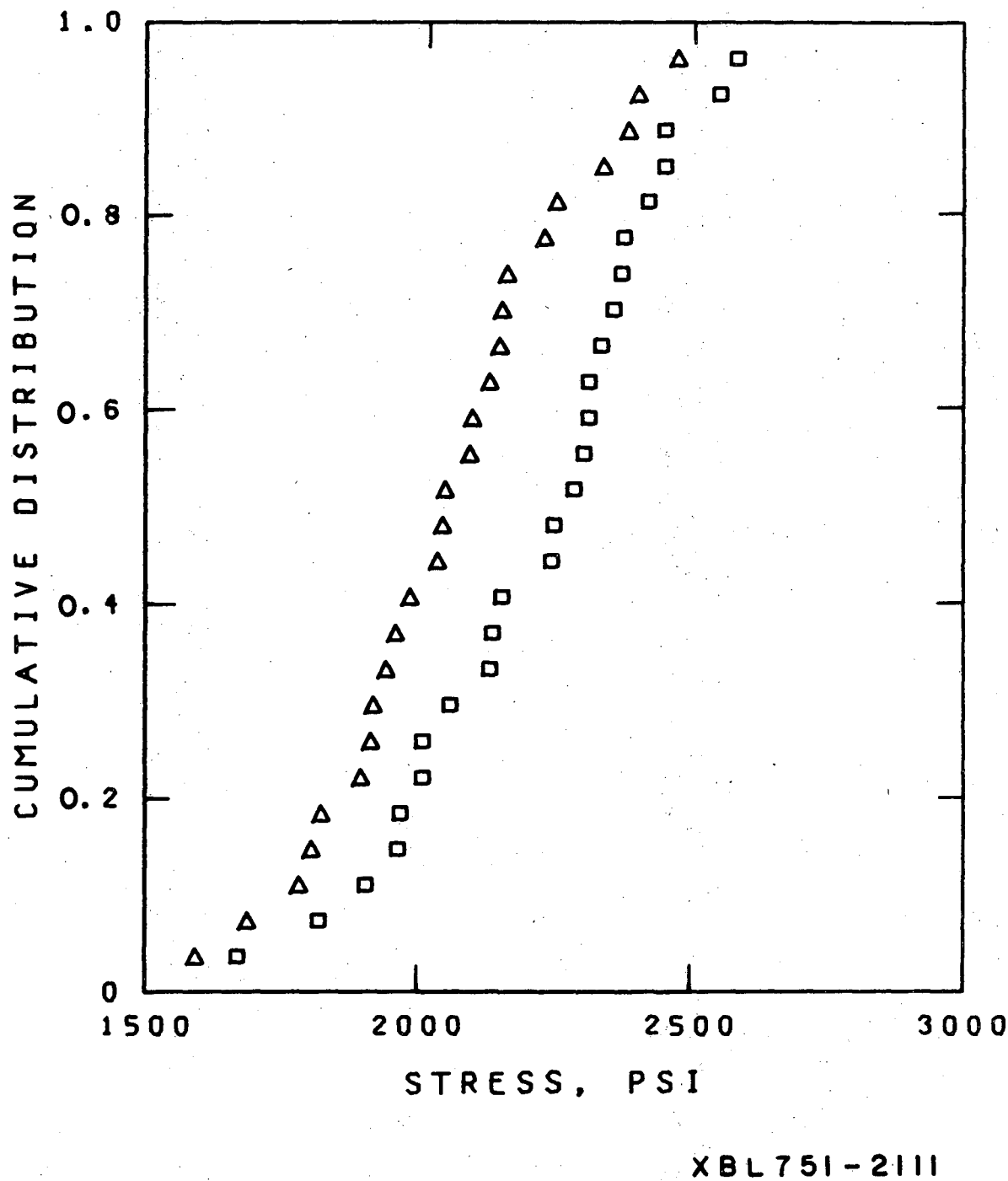

Fig. 2-14. Effect of water on strength, Δ set 6 (wet), □ set 7 (dry) (1000 psi = 6.895 MN/m^2).

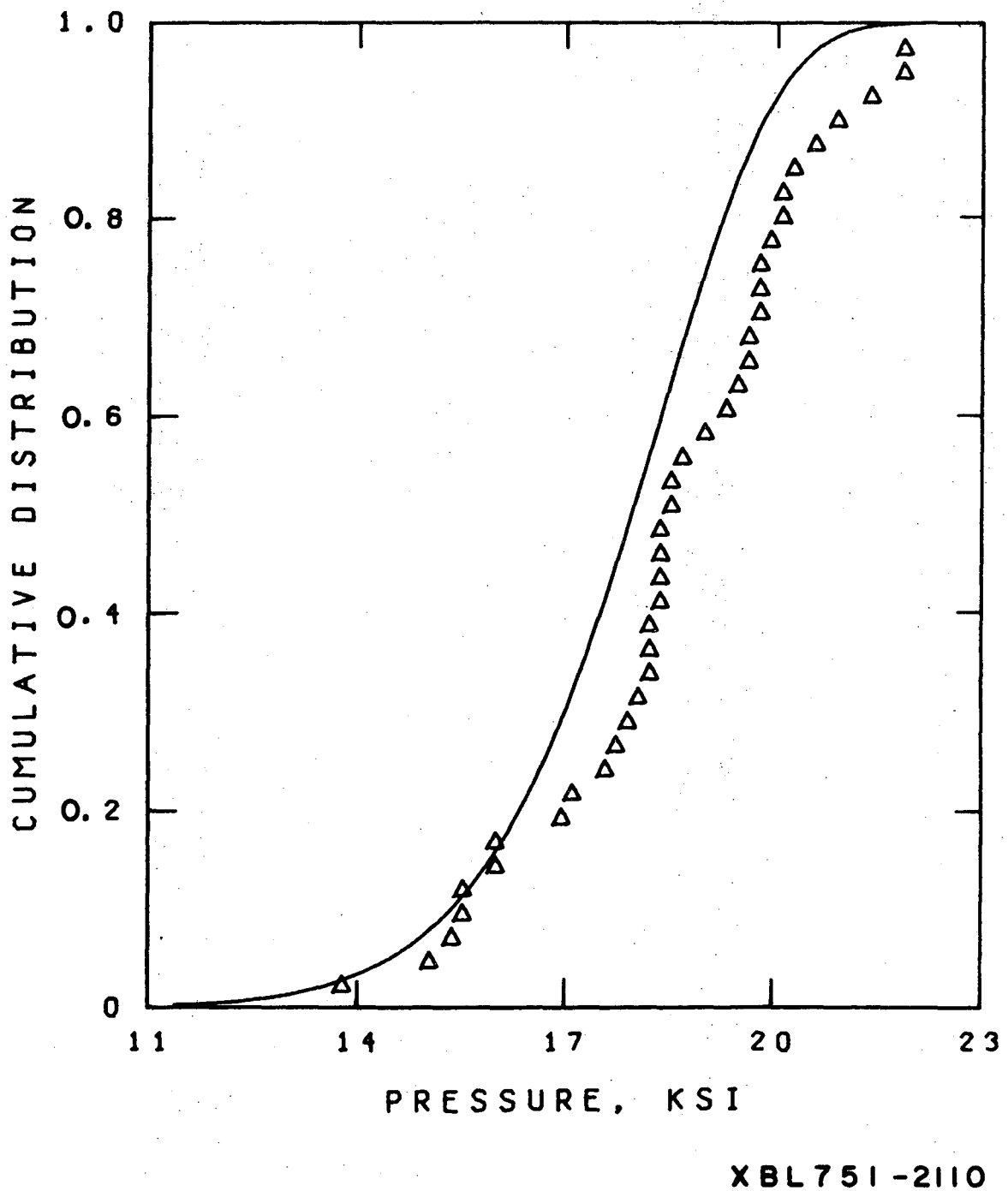

Fig. 2-15. A comparison of Brazilian disk tests on granodiorite, set 13, with predictions based on bending data (1 ksi = 1000 psi = 6.895 MN/m^2).

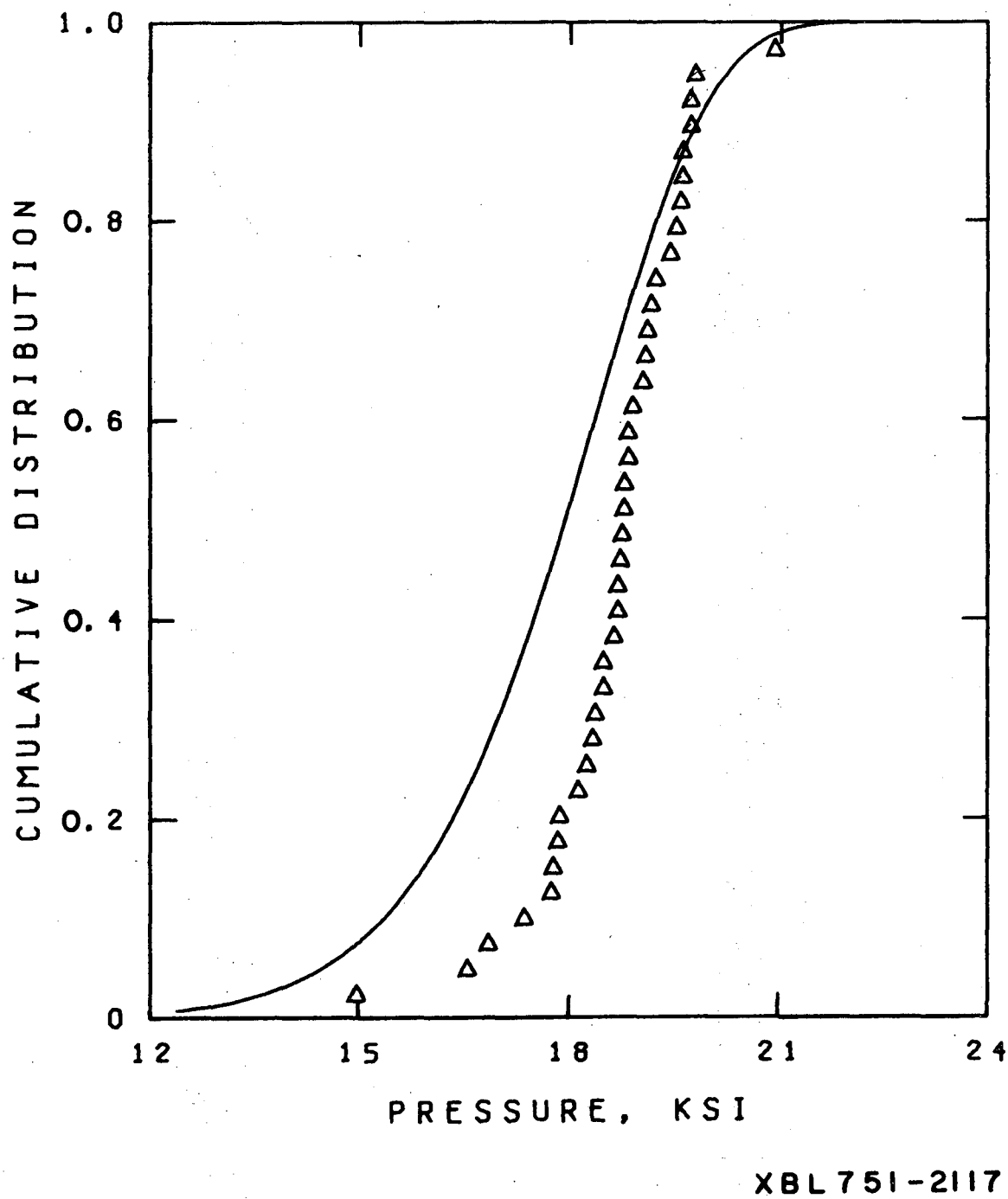

Fig. 2-16. A comparison of Brazilian disk tests on granodiorite, set 14, with predictions based on bending data (1 ksi = 1000 psi = 6.895 MN/m^2).

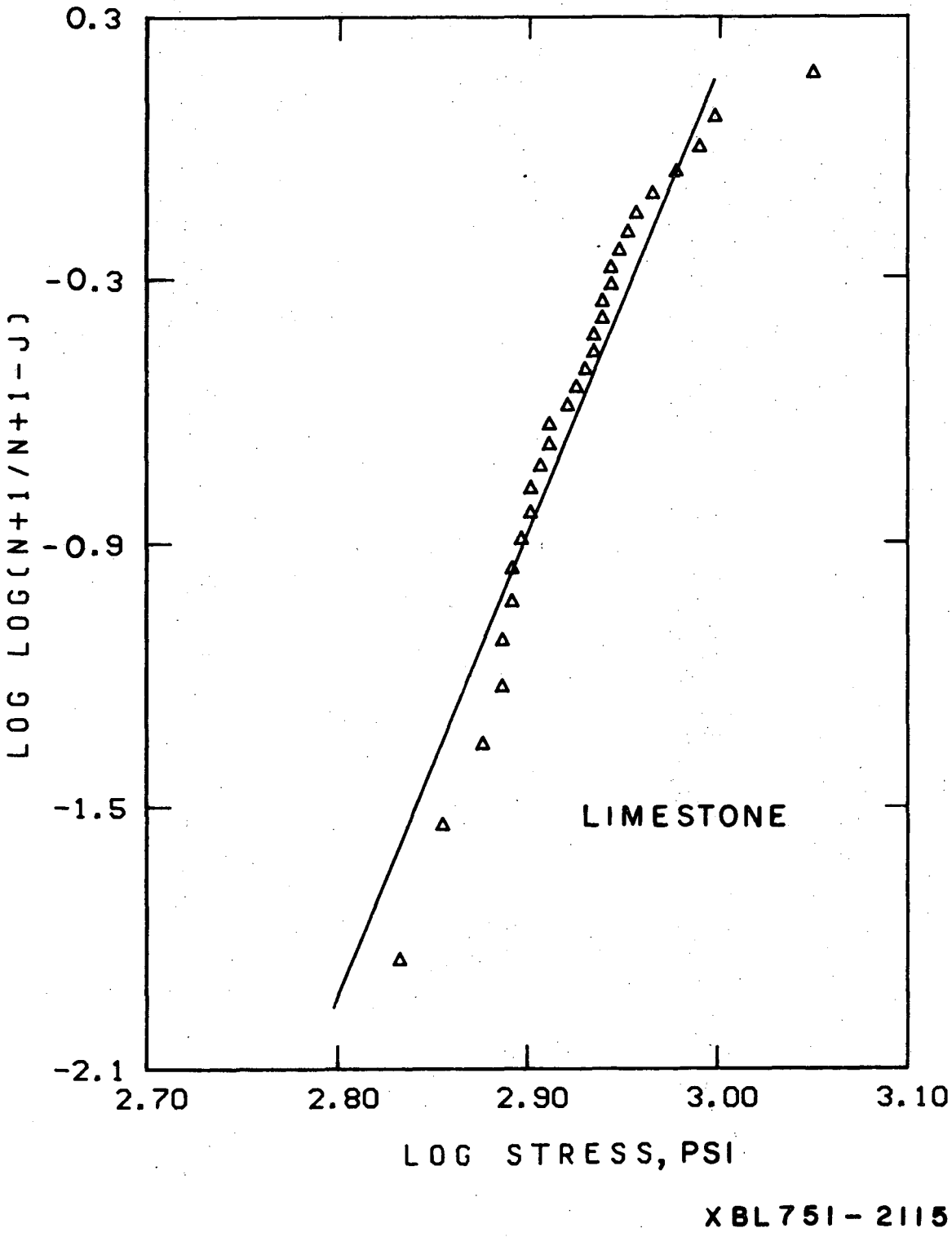

Fig. 2-17. Strength values from set 17 plotted to estimate the parameters σ_0 and m (1000 psi = 6.895 MN/m^2).

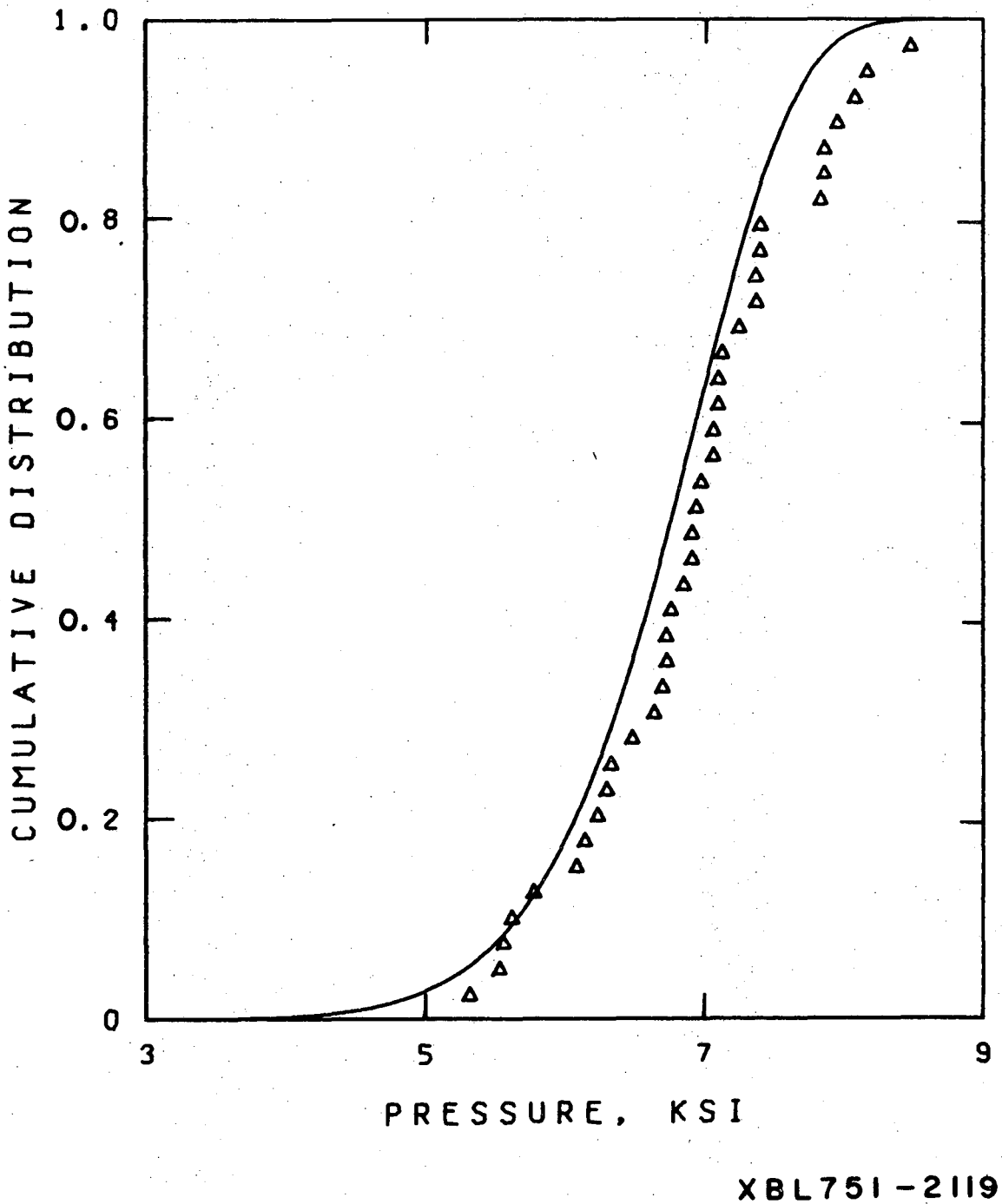

Fig. 2-18. A comparison of Brazilian disk tests on limestone with predictions based on bending data (1 ksi = 1000 psi = 6.895 MN/m^2).

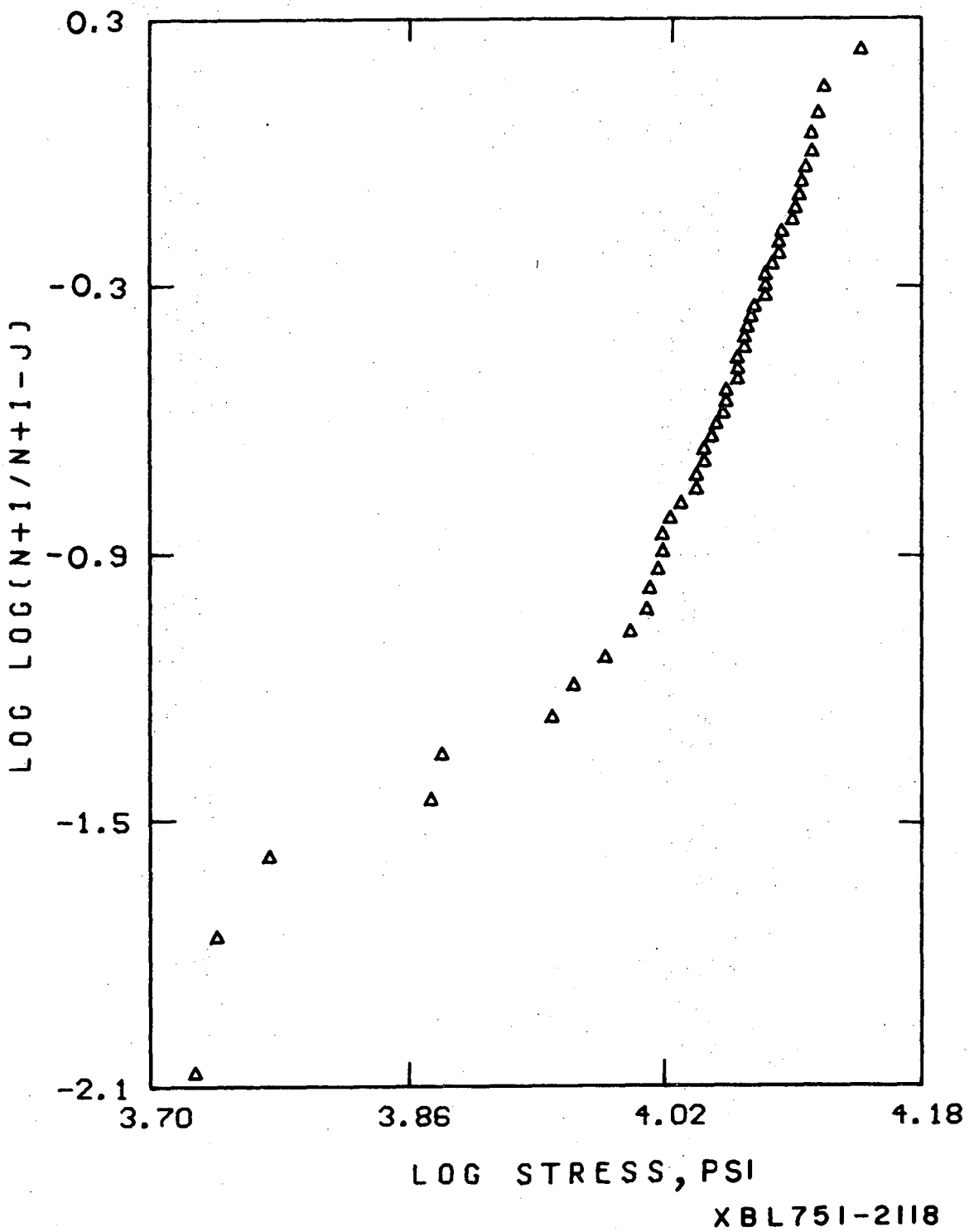

Fig. 2-19. Strength values from three point bending of greenstone beams (1000 psi = 6.895 MN/m^2).

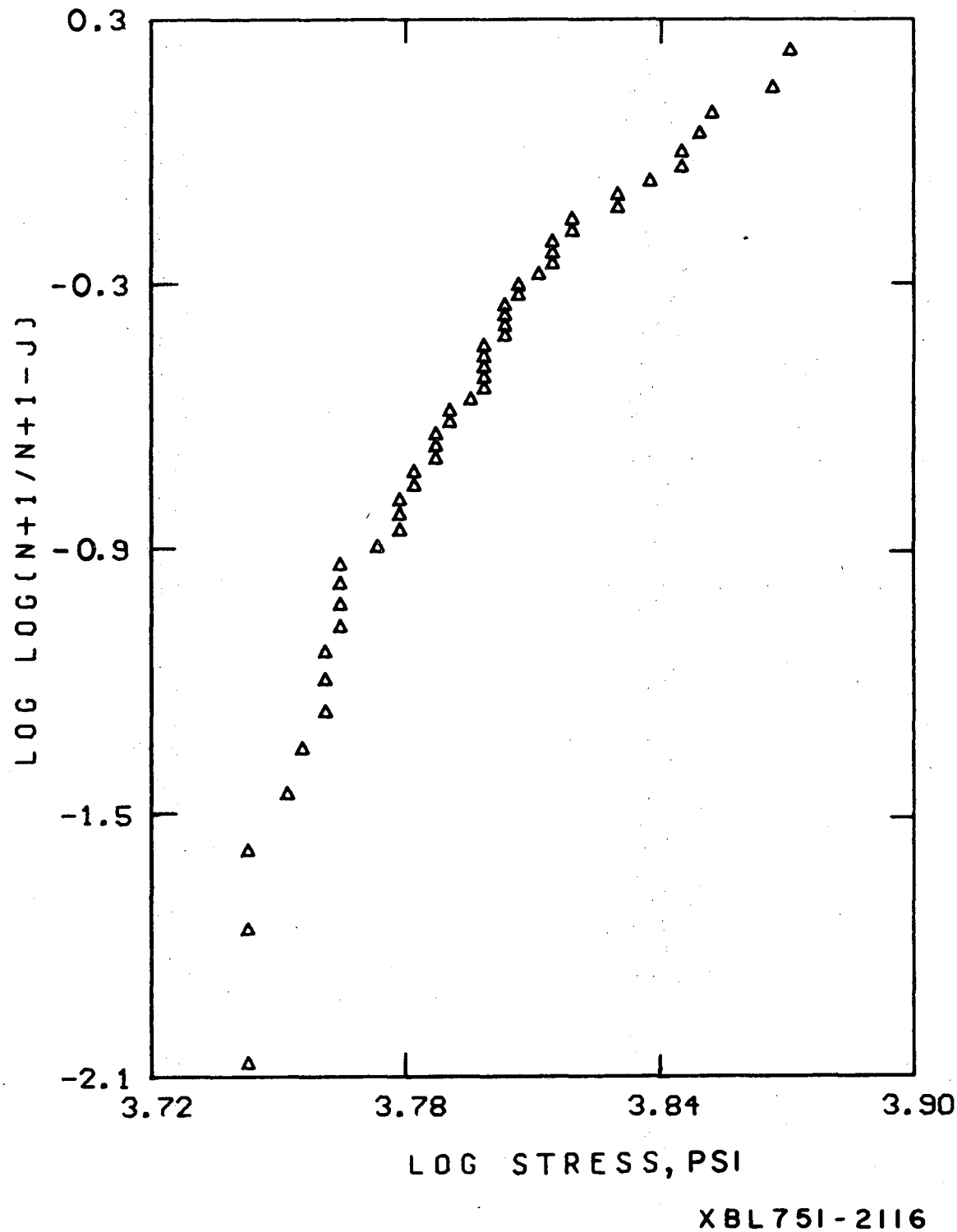

Fig. 2-20. Strength values from three point bending of basalt beams (1000 psi = 6.895 MN/m^2).

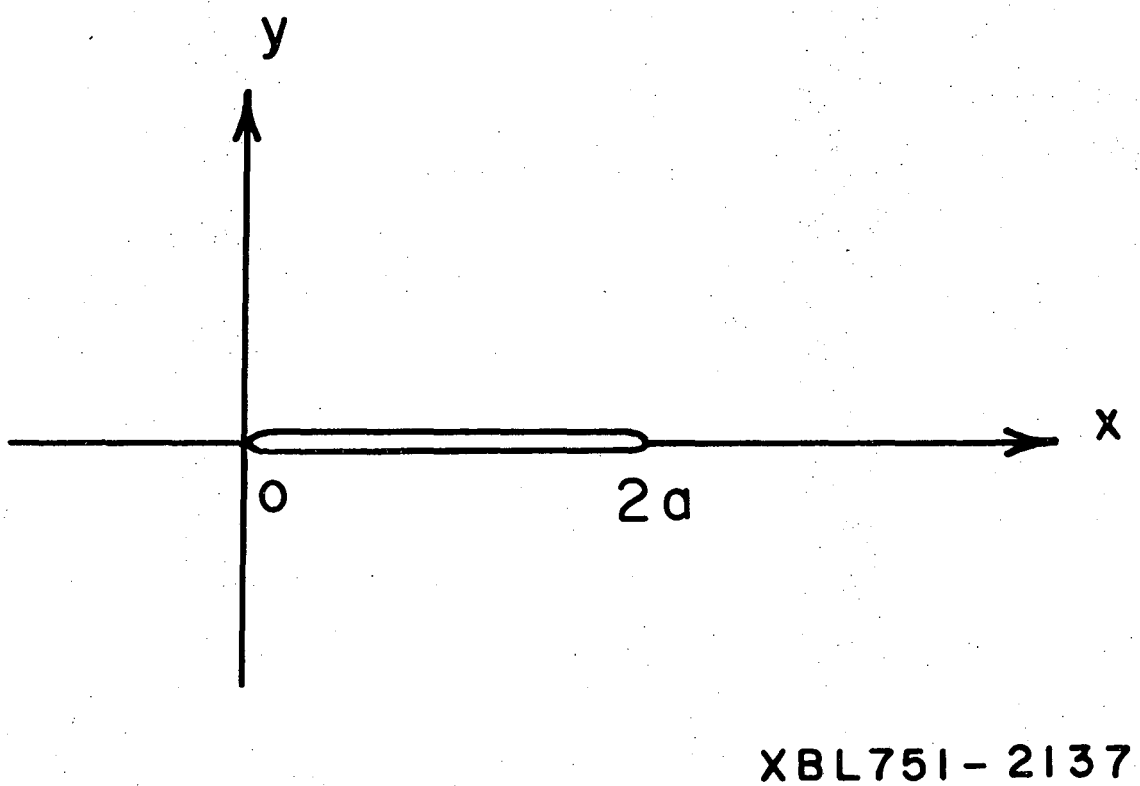

Fig. 3.1. Crack geometry.

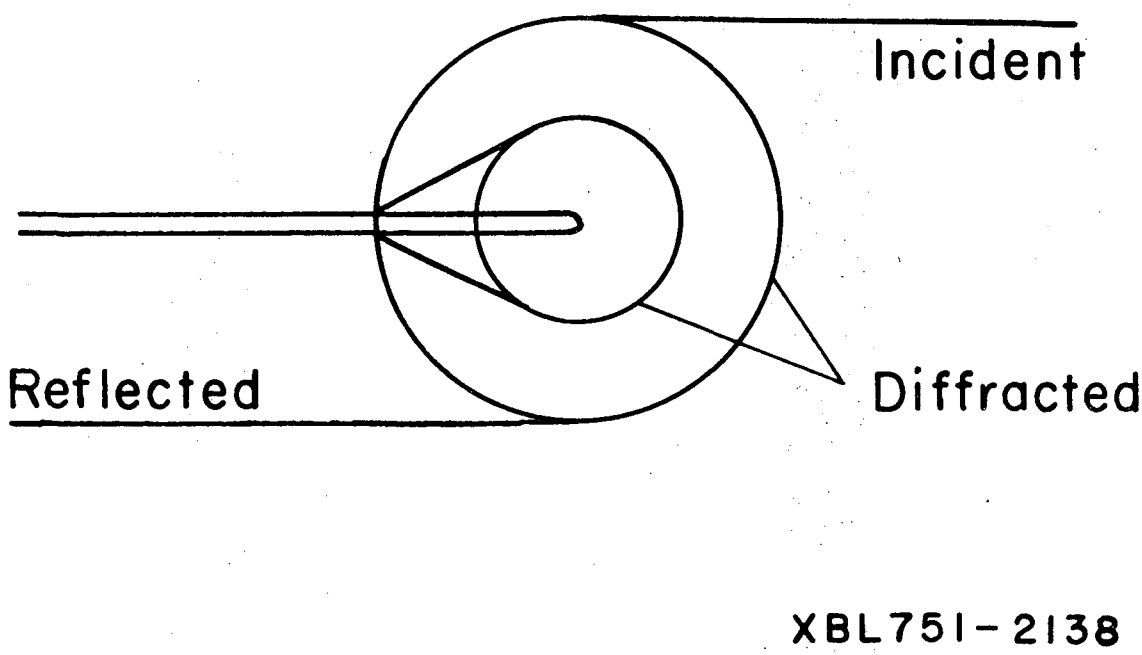

Fig. 3-2. The pattern of wavefronts for t larger than zero.

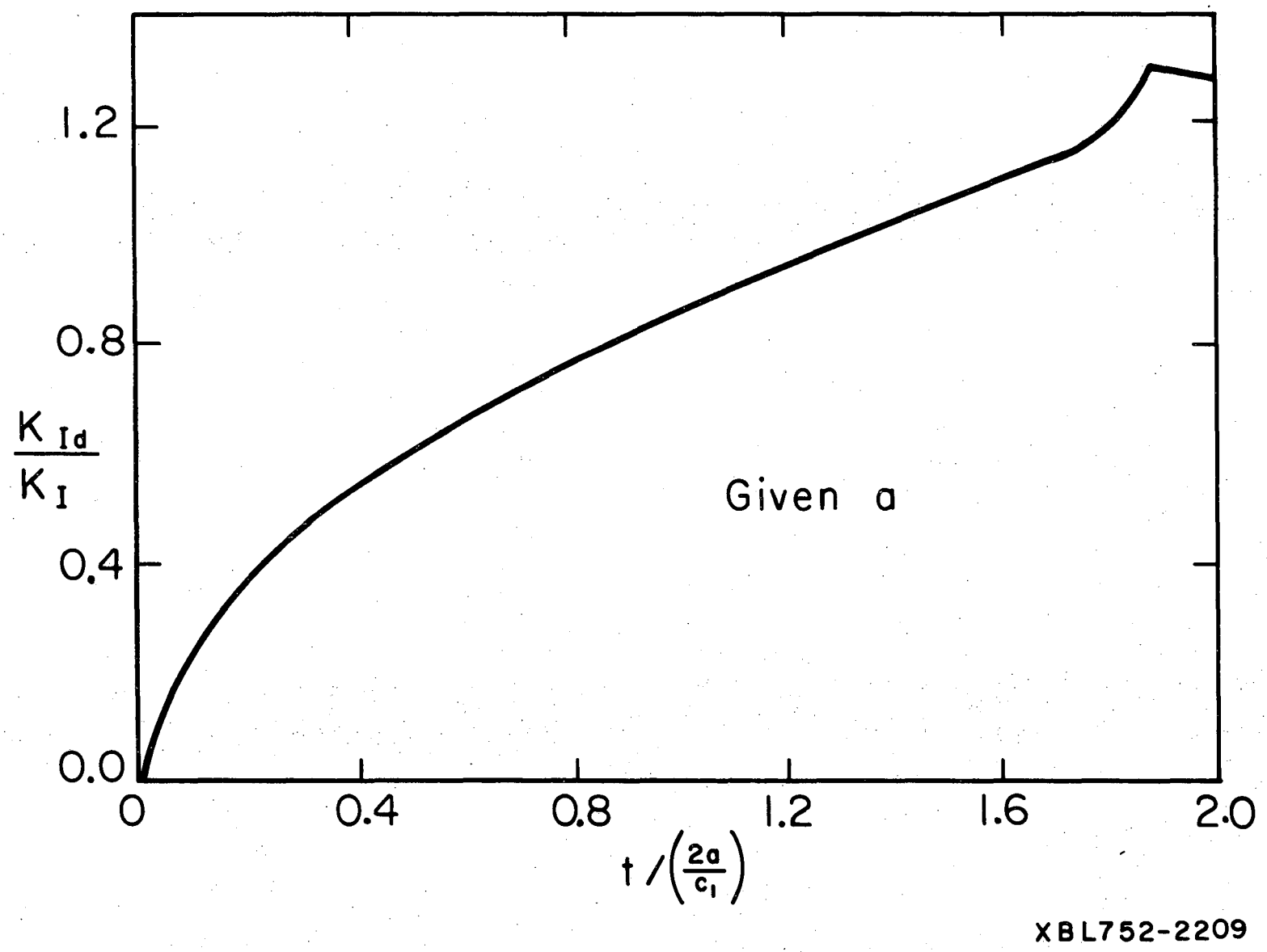

Fig. 3-3. Time variation of stress intensity factor (Thau & Lu [3-1]).

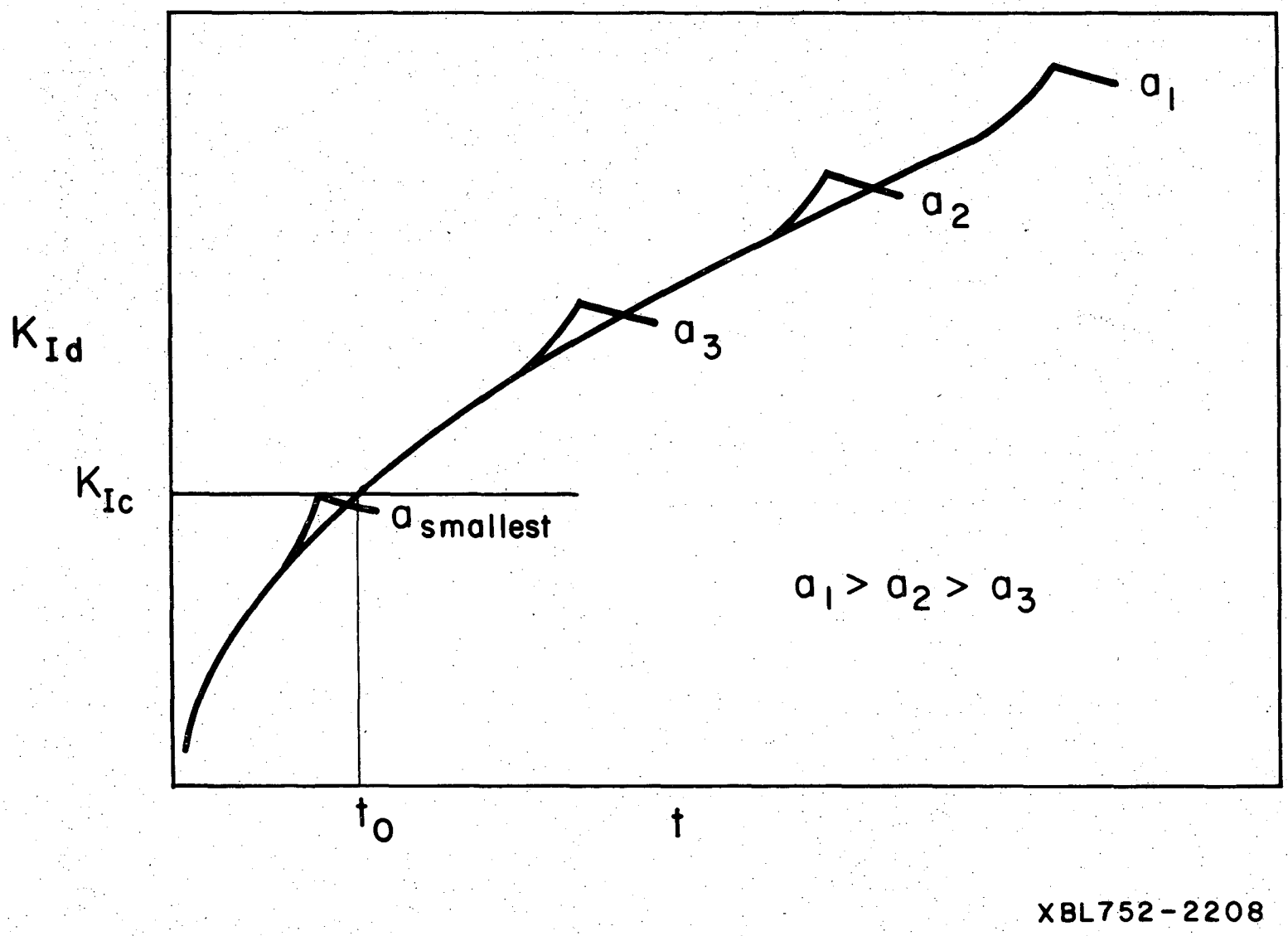

Fig. 3-4. Time variation of stress intensity factor.

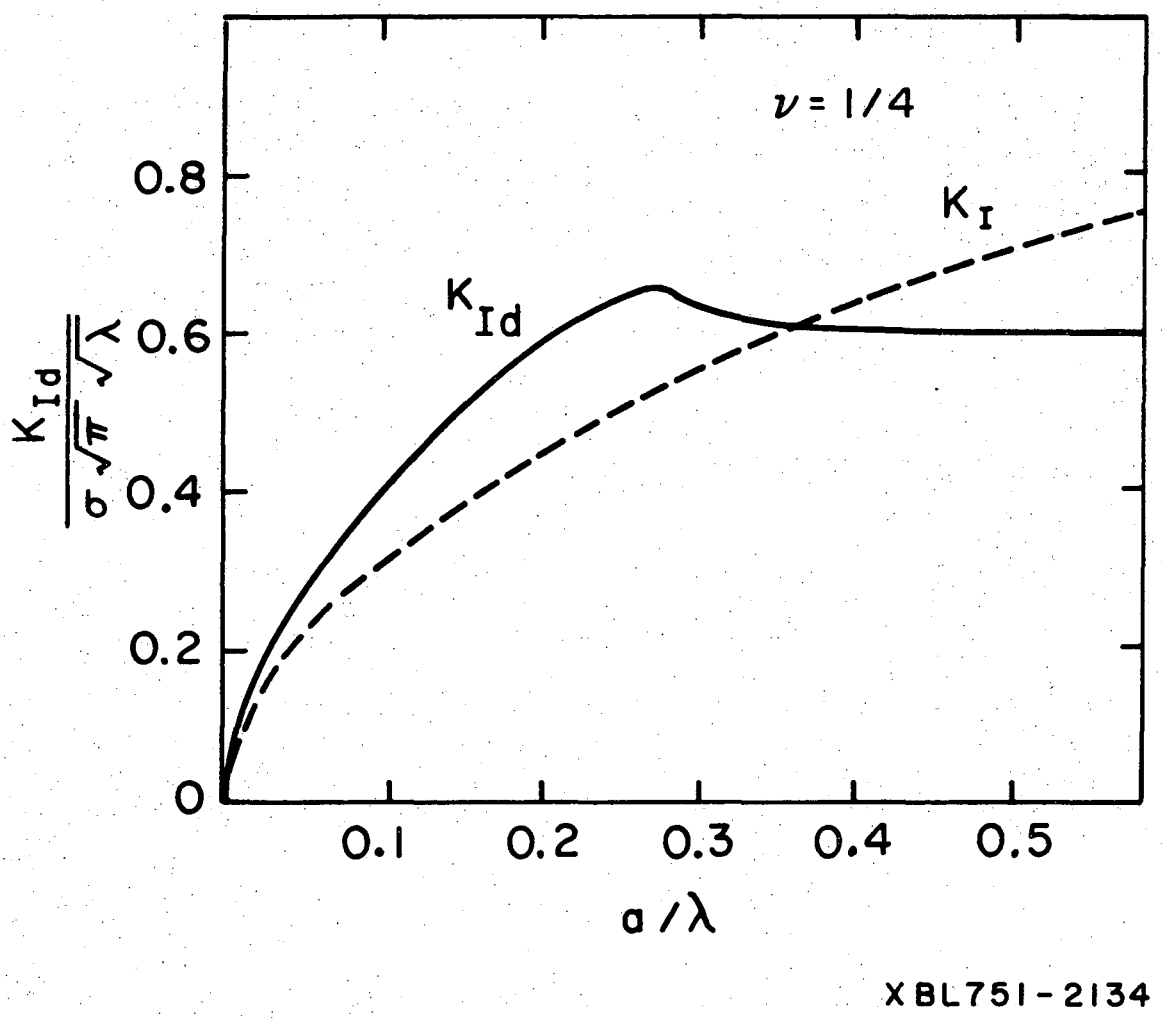

Fig. 3-5. Maximum K_I for a given pulse (σ,λ) as a function of crack length $(\lambda = c_1\tau)$.

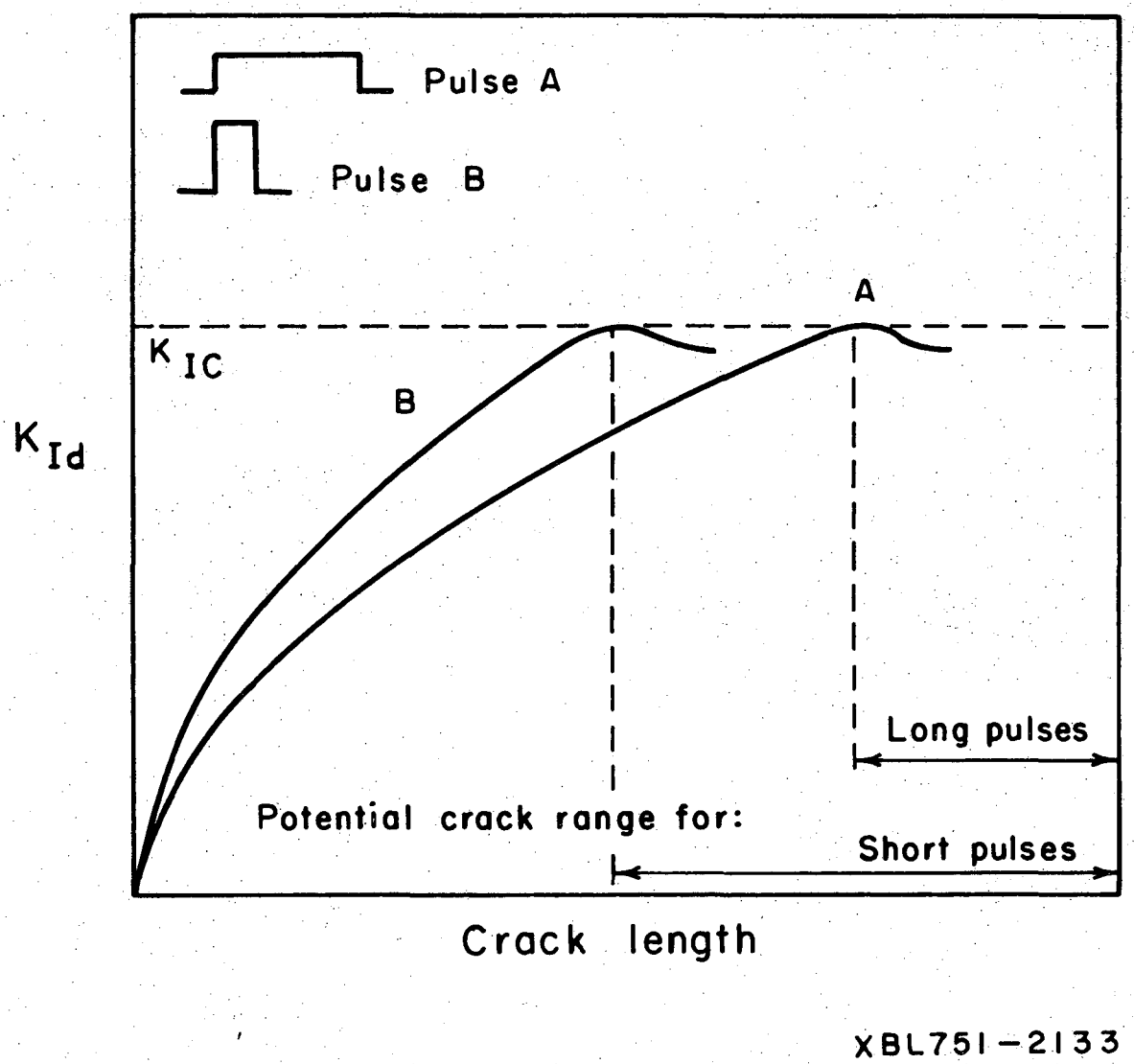

Fig. 3-6. Comparison of pulses with equal energy content.

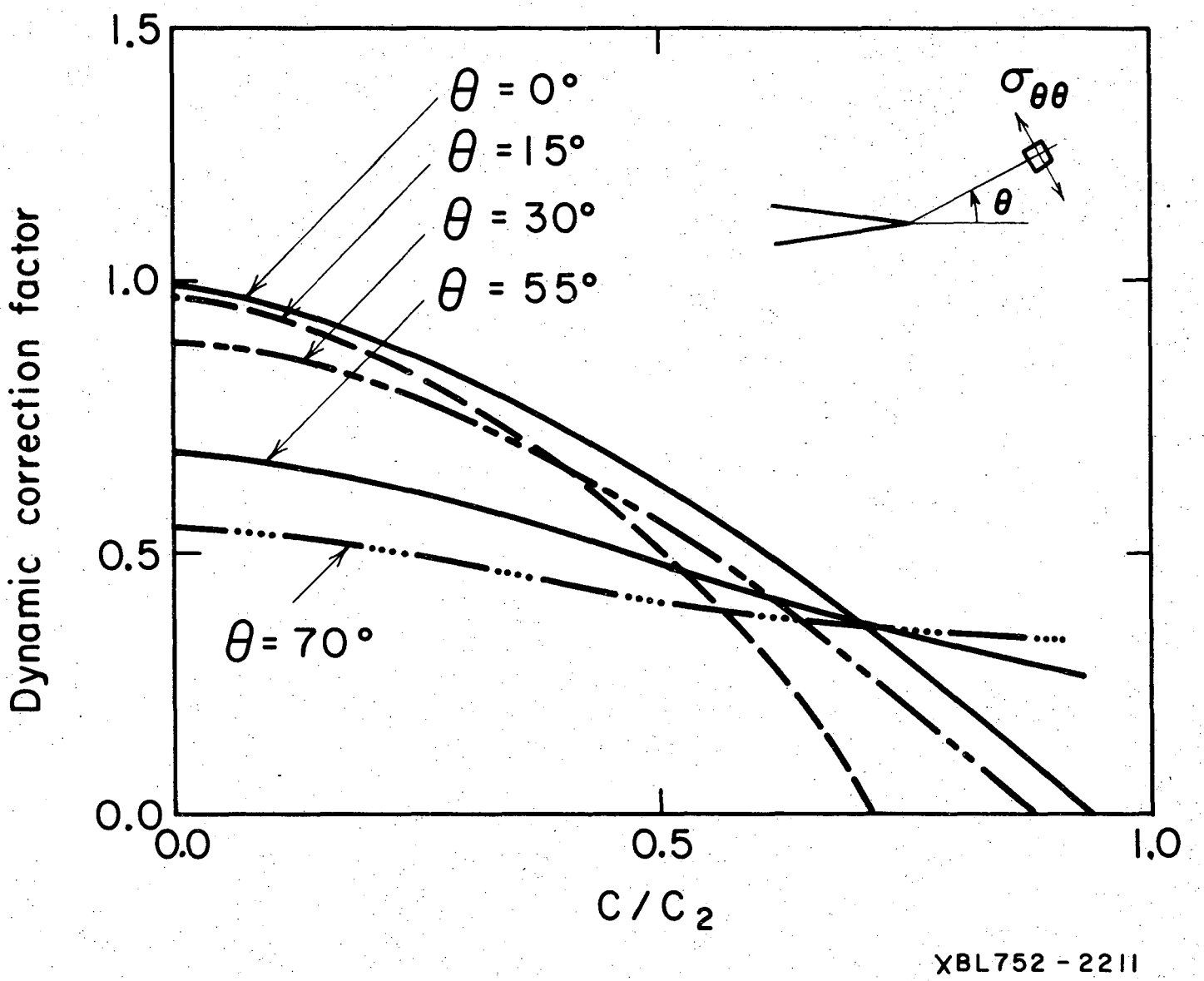

Fig. 3-7. Dynamic correction factor for circumferential stress $\sigma_{\theta\theta}$.

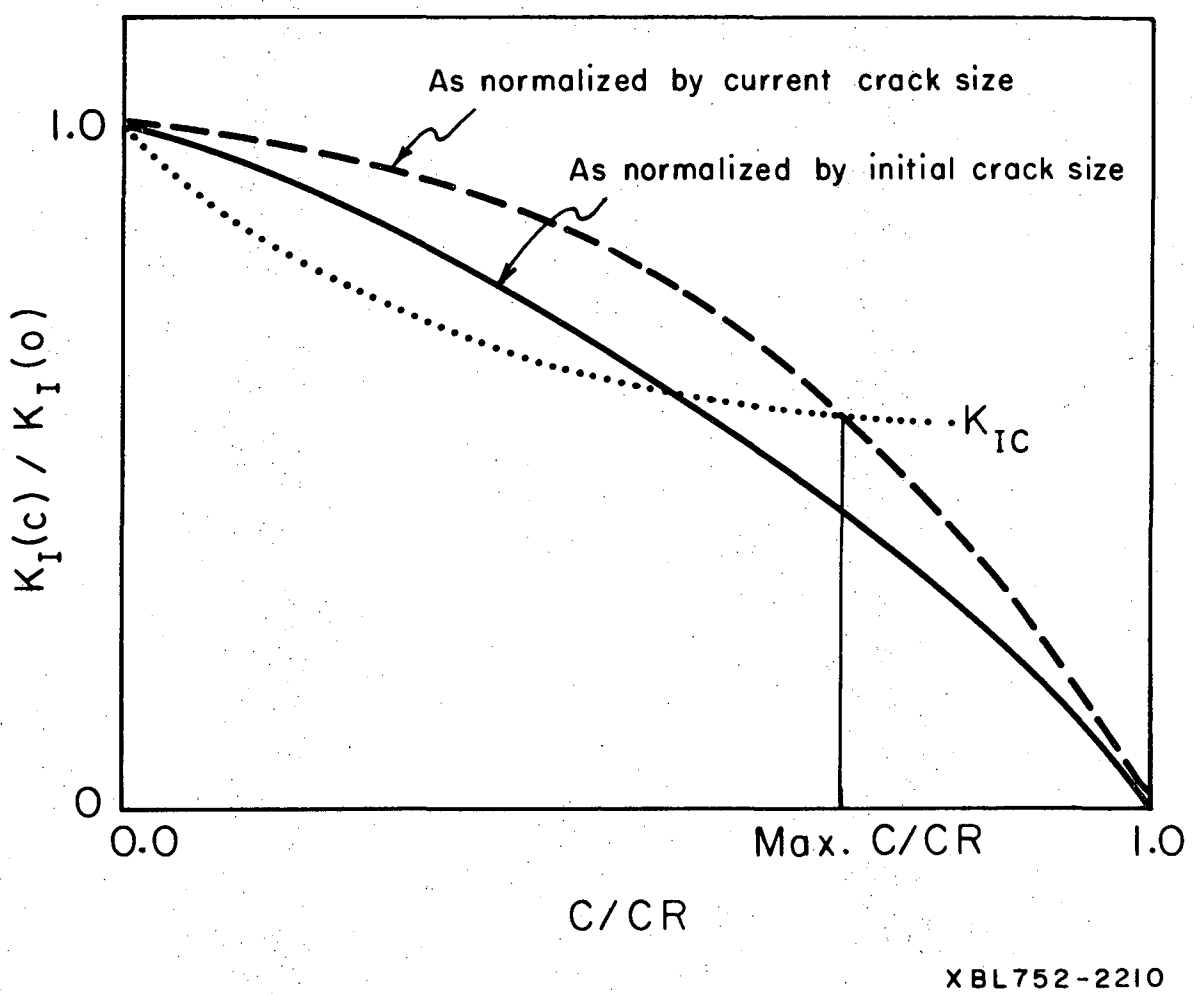

Fig. 3-8. Variation of K_I with crack tip speed.

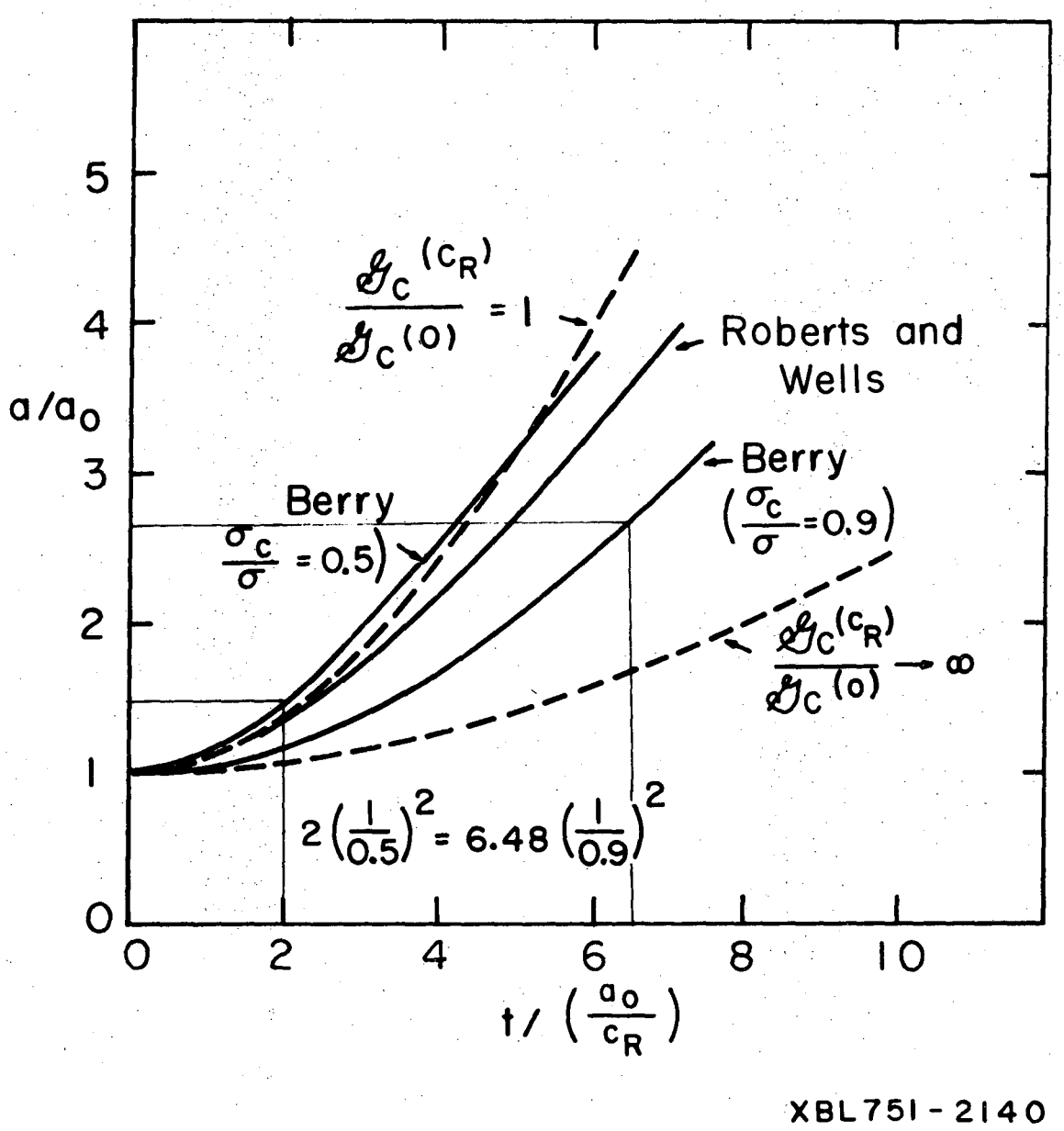

Fig. 3-9. Comparison of propagation theories (crack size vs. time).

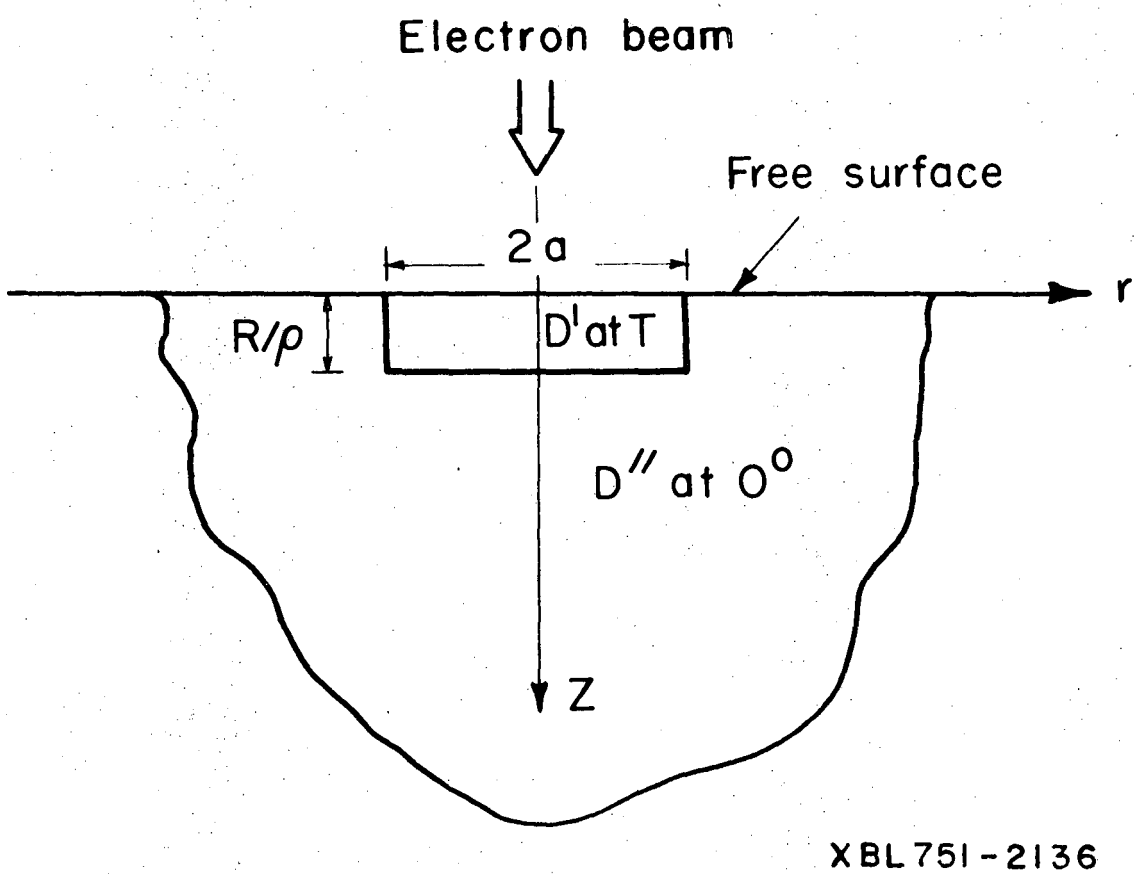

Fig. 4-1. Geometry of electron beam tests.

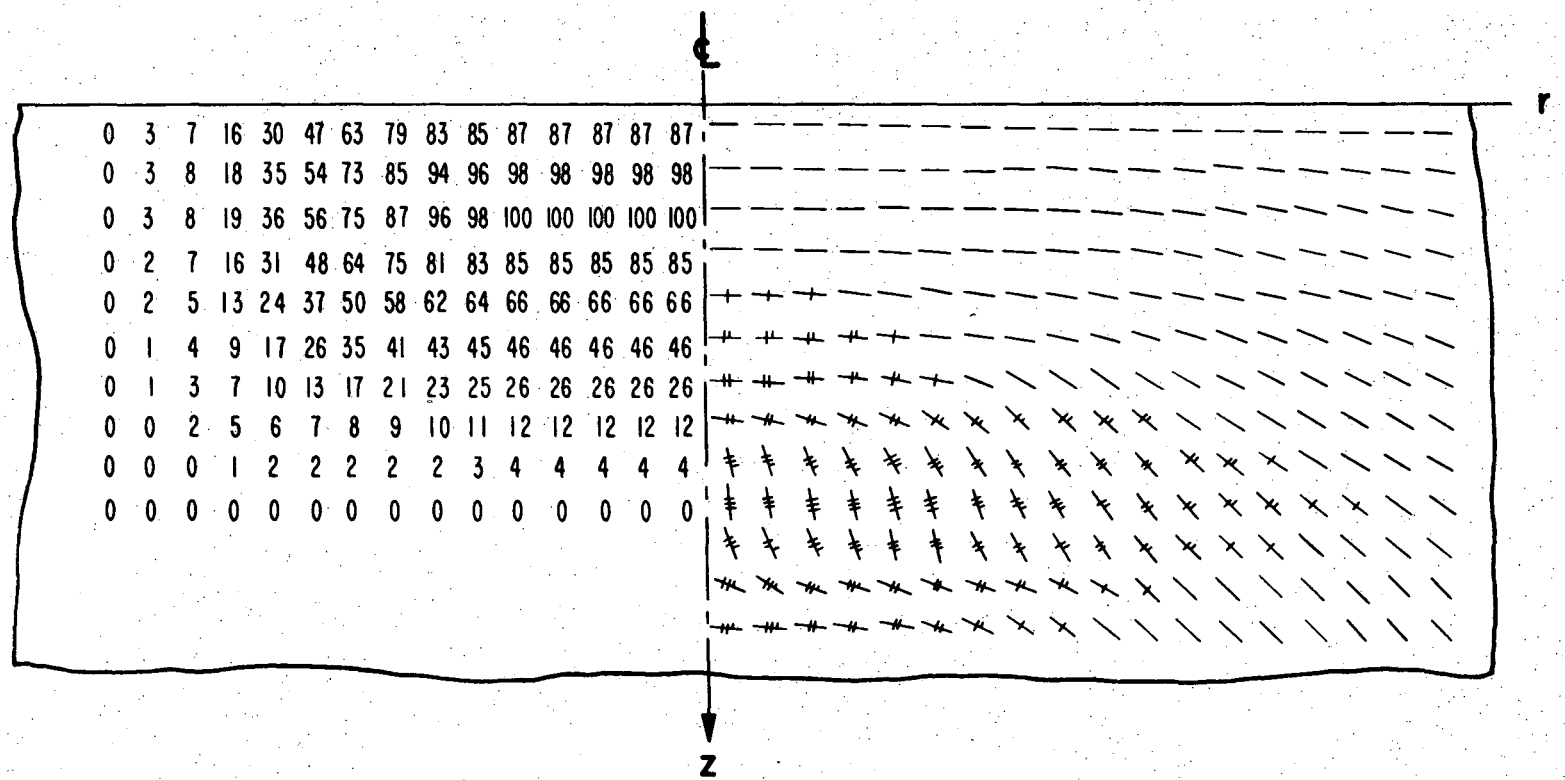

XBL752-2207

Fig. 4-2. Expected cracking pattern (right) for a specific temperature distribution (left) (temperature in ^{o}C; each full bar corresponds to 1.75 MN/m^2).

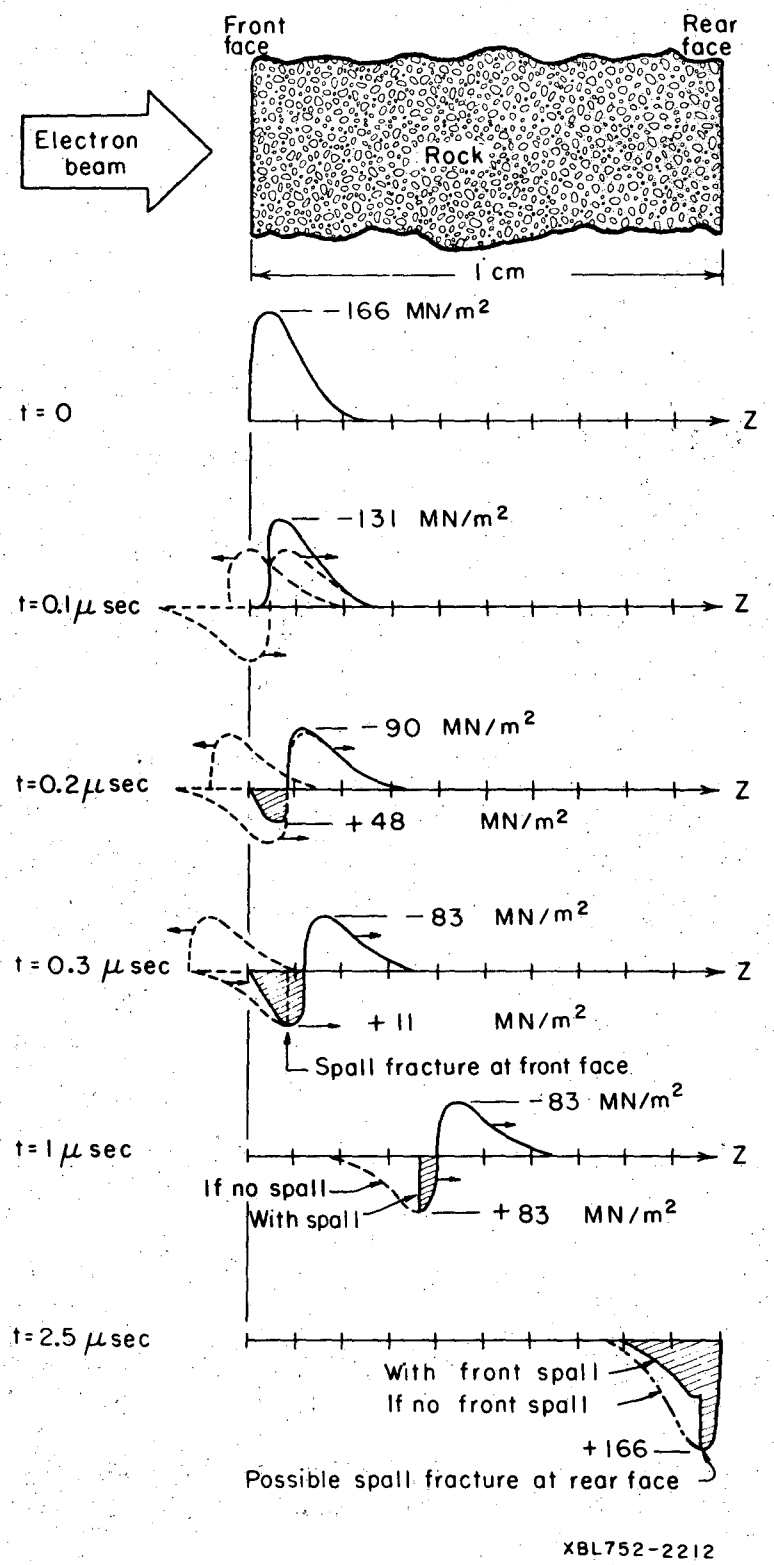

Fig. 4-3. Propagation of a plane wave in a 1-cm thick slab (c = 4000 m/sec, peak stress = 166 MN/m^2) (from Ref. [4-2].

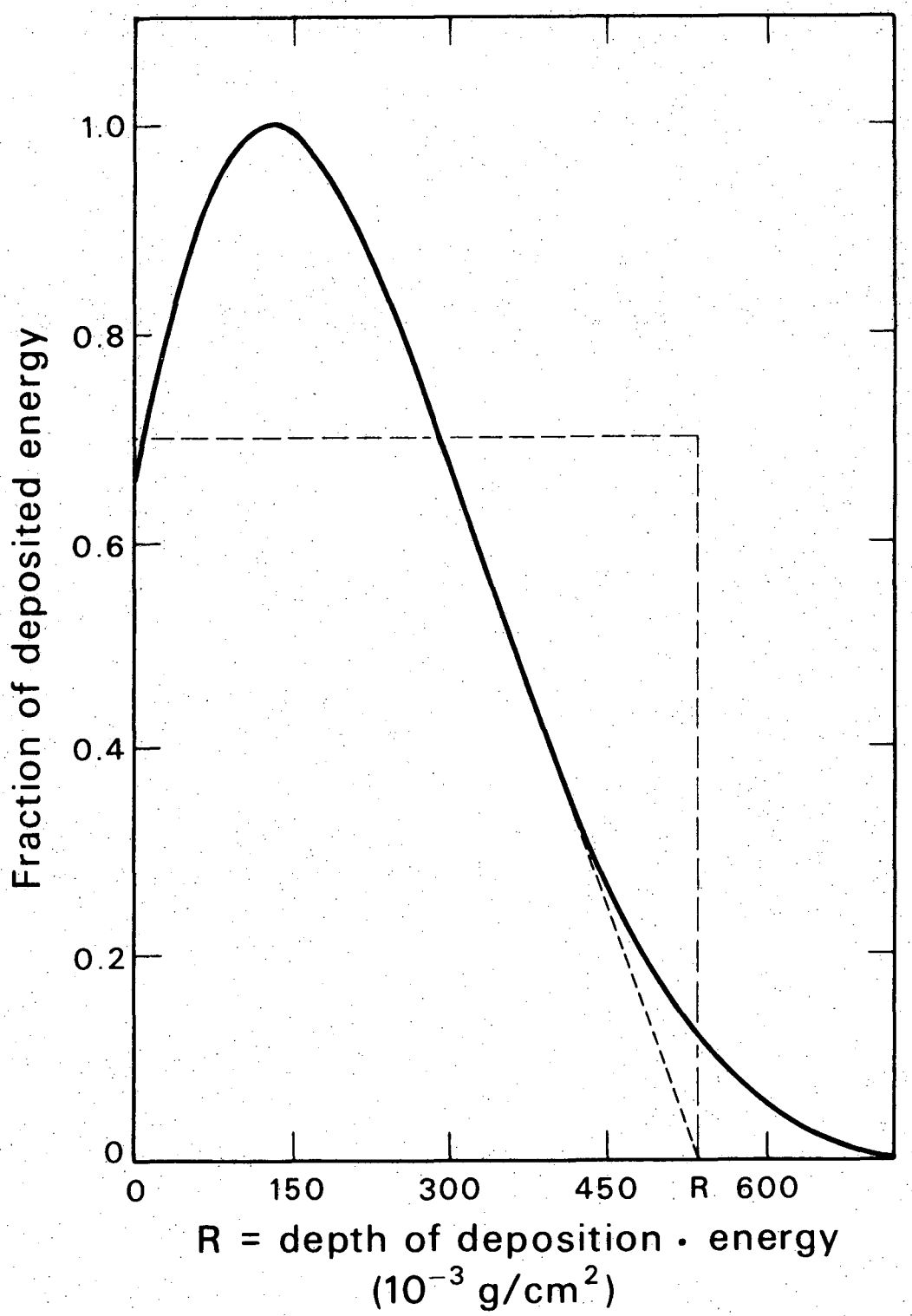

XBL 752-4677

Fig. 4-4. Depth vs. dose curve for shot # 2386.

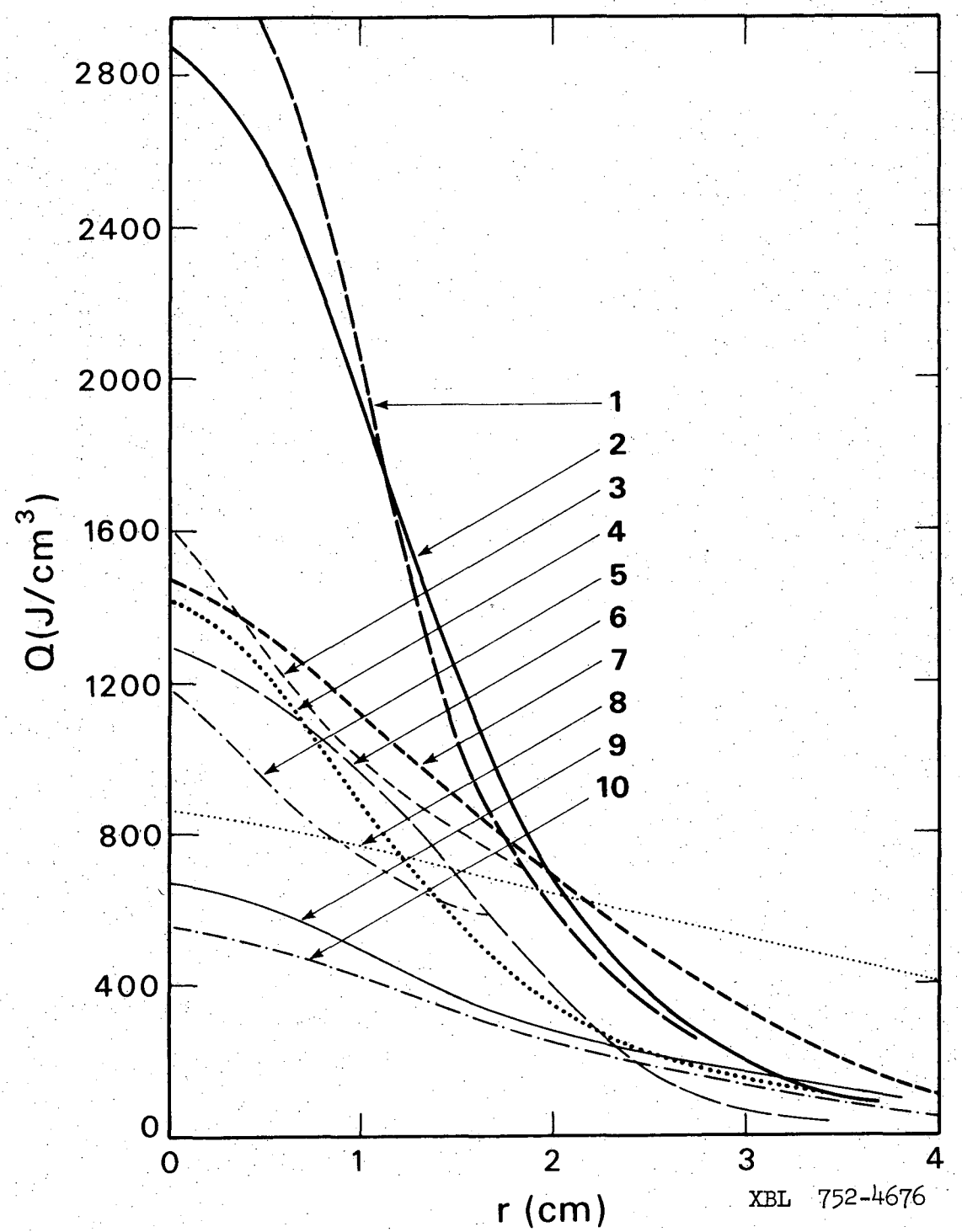

Fig. 4-5. Energy/volume variation with radius.
1) pulserad 422 Run I using 2076; 2) pulserad 422 Run II using 2364, 2372, 2386; 3) pulserad 422 Run I using 2058; 4) PI 1140 using 18094, 96, 99; 5) pulserad 422 Run I using 2060; 6) pulserad 422 Run III using 3630, 3643; 7) pulserad 422 Run I using 2075; 8) Hermes II using 9150, 57, 61; 9) PI 1140 using 18072, 73, 77; 10) pulserad 422 Run III using 3638.

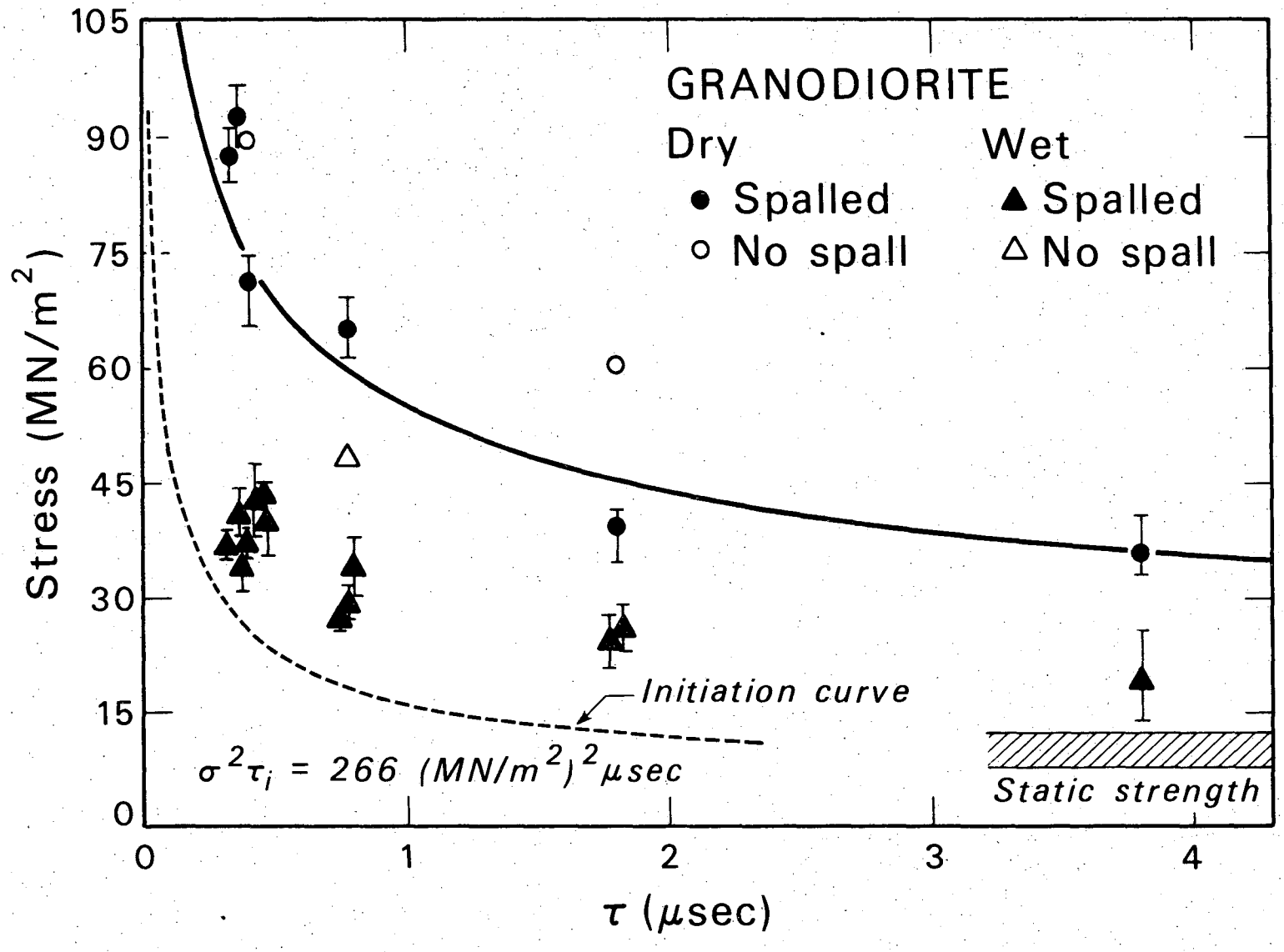

XBL 752-4673

Fig. 4-6. Predicted failure curve and the experimental data for granodiorite.

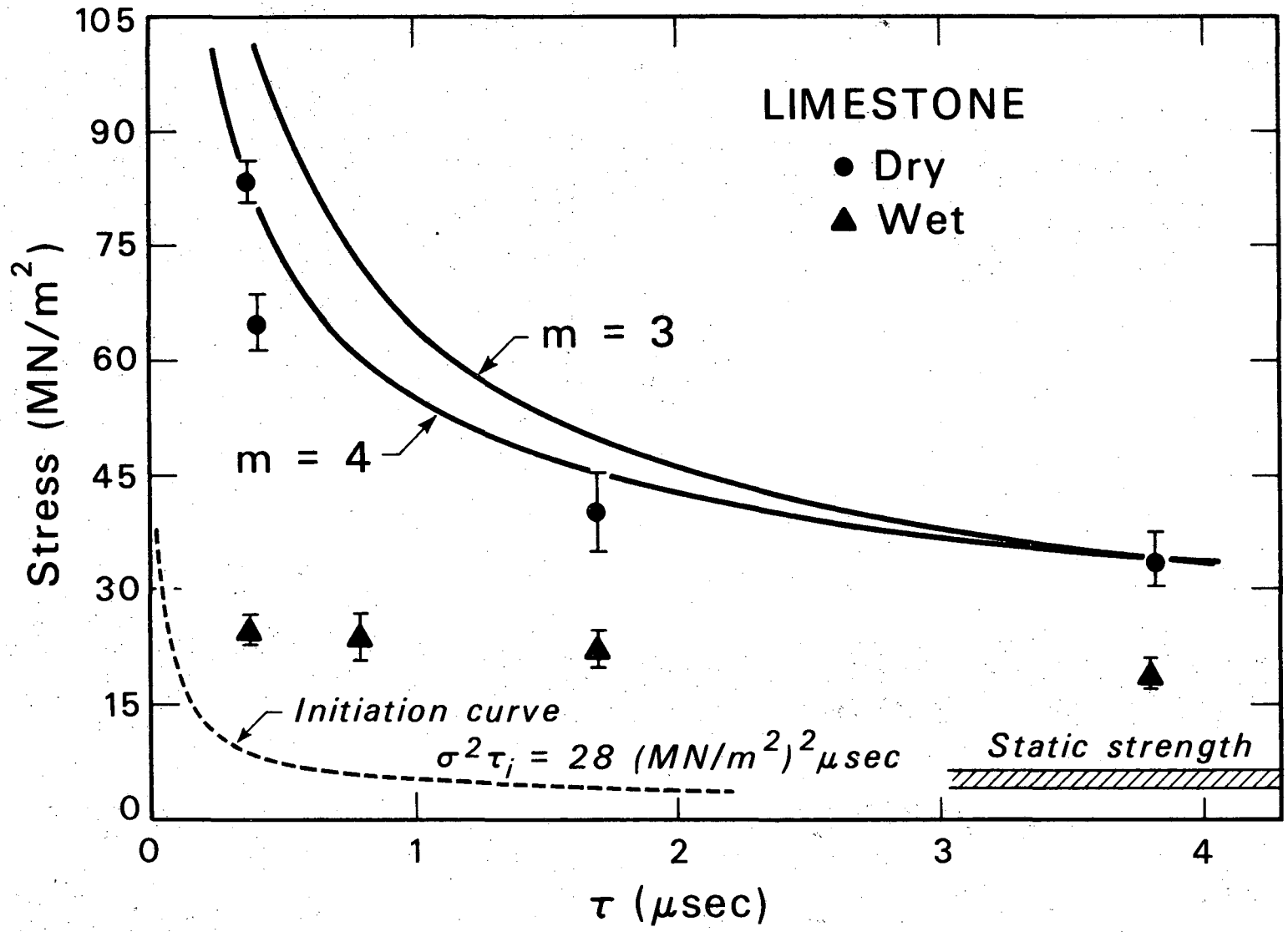

XBL 752-4671

Fig. 4-7. Predicted failure curve and the experimental data for limestone.

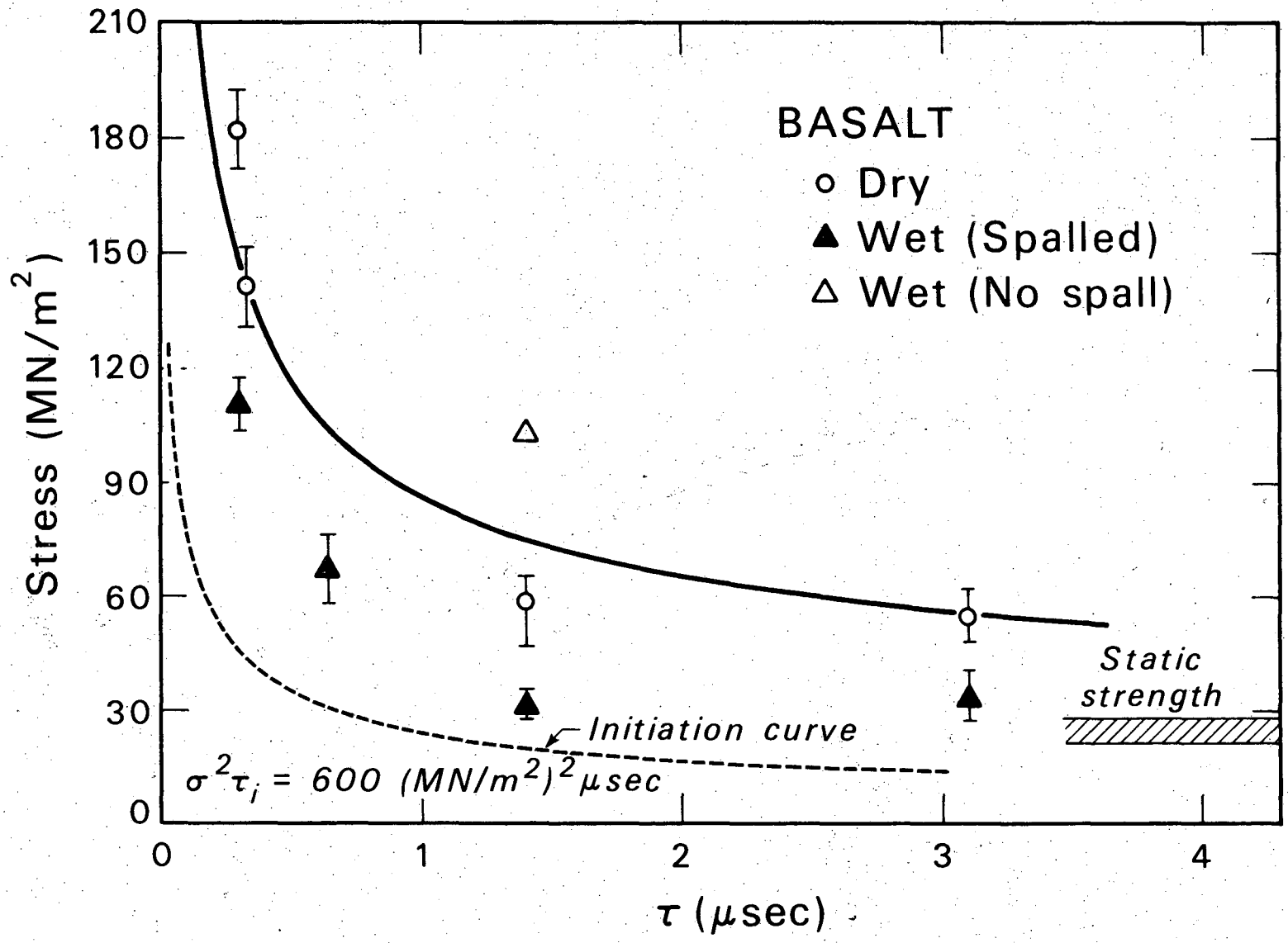

XBL 752-4672

Fig. 4-8. Predicted curve and the experimental data for basalt.

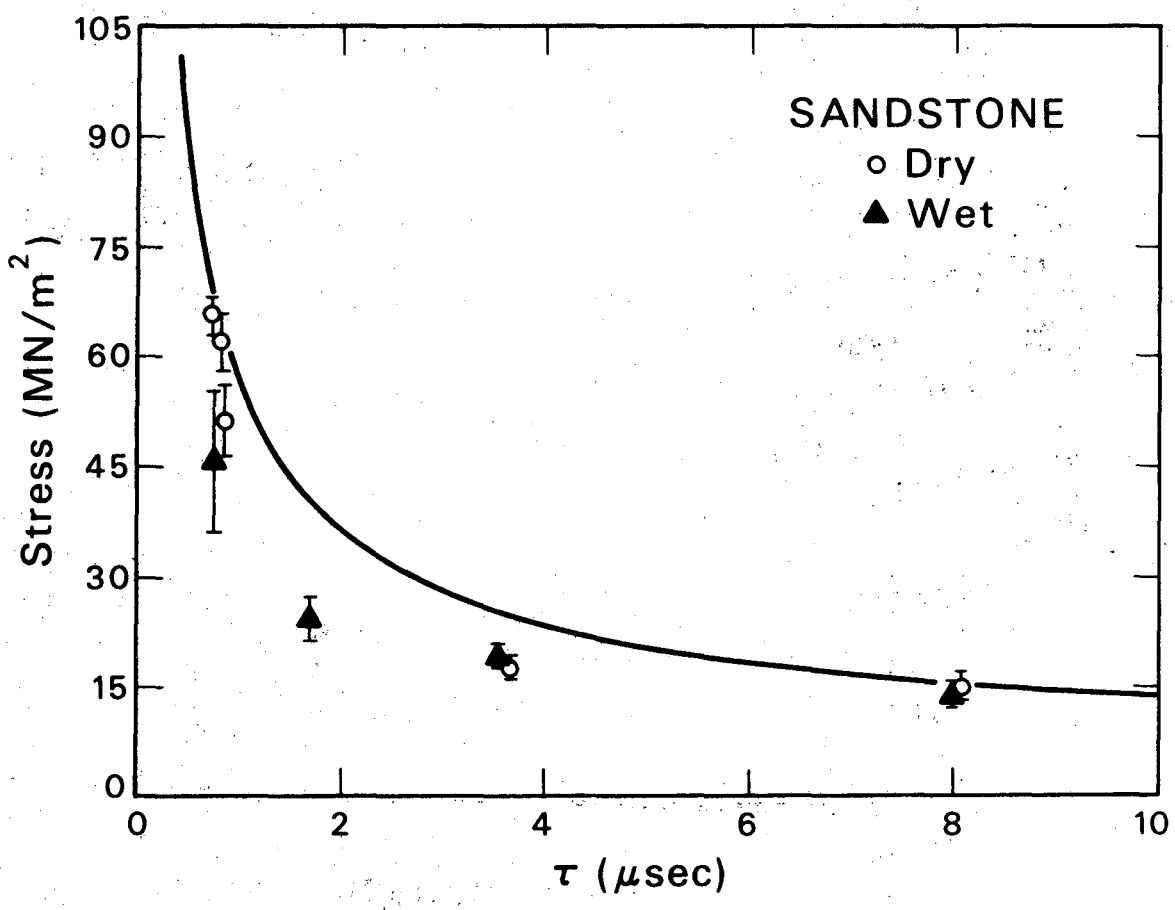

XBL 752-4675

Fig. 4-9. Predicted curve and the experimental data for sandstone.

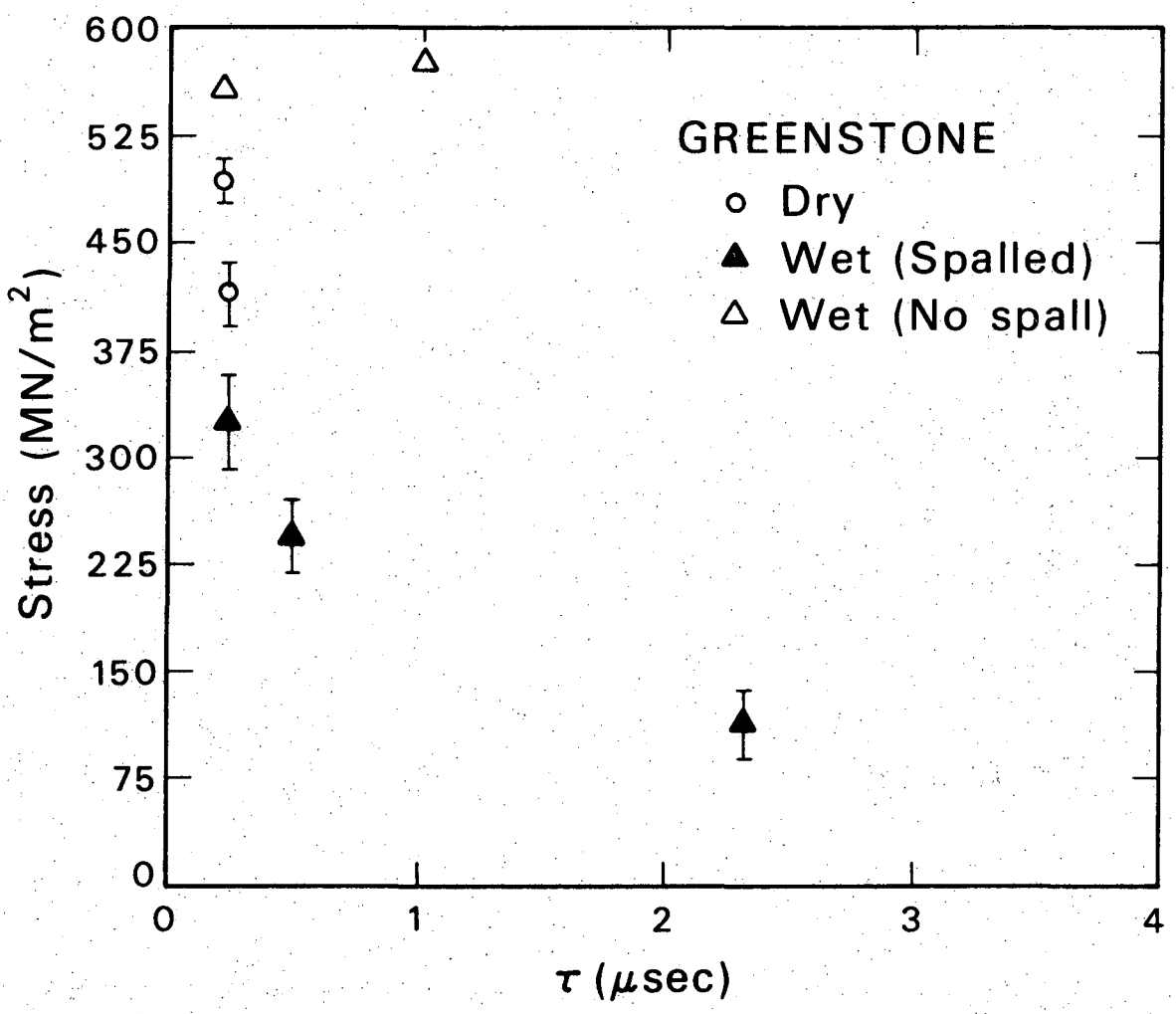

XBL 752-4674

Fig. 4-10. Experimental data for greenstone.

APPENDIX

An Extension of the Dynamic Model of Section 3.4

Consider a material with the crack distribution (i.e. the number of cracks per volume having a strength less than or equal to S)

$$N(S) = \left(\frac{S - \sigma_u}{\sigma_0}\right)^m$$

subject to a stress pulse of magnitude σ and duration τ . The smallest crack which can be initiated by this pulse is roughly

$$a_{min} \simeq K_{Ic}^2/\pi\sigma^2.$$

A crack of length $a(\geq a_{min})$ will start propagating if α (the angle that the crack normal makes with the applied stress) satisfies the condition $\alpha \leq \cos^{-1}\left[(a_{min}/a)^{1/4}\right]$. Hence, assuming a uniform distribution of crack orientation, the number of cracks per volume that will be activated can be given as

$$N(\sigma) = \int_{\sigma_u}^{\sigma} \frac{2}{\pi} \cos^{-1}\left[\left(\frac{S}{\sigma}\right)^{\frac{1}{2}}\right] \frac{m}{\sigma_0^{\,m}} (S-\sigma_u)^{m-1}\, dS \ .$$

Assume that the volume is divided into cells each of which contains one active crack. The cell fails when the crack in that cell reaches the side walls of the cell. Having the total number of active cracks $N(\sigma)$, the cell size may be found as in Section 3.4

$$d = \frac{1}{2}\left[A\ell/N(\sigma)\right]^{\frac{1}{2}}$$

The number of cells that have failed (N_{failed}) is given by

$$N_{failed} = \left[N(d) - N(2d)\right] \cdot 1 + \left[N(2d) - N(3d)\right] \cdot 2 + \left[N(3d) - N(4d)\right] \cdot 4 + \cdots$$

$$= \sum_{i=1}^{r} N(id)$$ where rd is the largest possible crack size. To find $N(id)$ at time t, the propagation law may be assumed as

$$a = \cos\alpha \sqrt{a_0^2 + c^2t^2}, \quad \text{leading to}$$

$$N(id) = \frac{2}{\pi} \frac{1}{\sigma_0^m} \int_0^{\alpha^*} \left\{ \frac{K_{Ic}}{\sqrt{\pi u}} - \sigma_u \right\}^m d\alpha$$

where

$$u = \begin{cases} \left[i^2d^2/\cos^2\alpha - c^2t^2\right]^{\frac{1}{2}} & \text{if } x > K_{Ic}^2/\pi\sigma^2 \cos^4\alpha \\ K_{Ic}^2/\pi a^2 \cos^4 & \text{if } x \leq K_{Ic}^2/\pi\sigma^2 \cos^4\alpha \end{cases}$$

and

$$\alpha^* = \cos^{-1}\left[id/\left(\frac{K_{Ic}^2}{\pi\sigma_u^2}\right)\right].$$

The fraction of cells that have failed can now be found from the total number of cells and the number of cells that have failed at time t. But without a knowledge of the damage required for complete failure, this model can not be useful.

Lindborg has developed a model which relates the fraction of cracked grains to the size of the largest crack and predicts the damage required at complete failure. Initially it was thought that his work could be used with the preceding analysis. Unfortunately upon examination it was found to contain serious errors which will now be discussed.

A Discussion of Lindborg's Paper [5-1]

Lindborg used a simple model of crack coalescence which gives the probability of having n-cells cracked - the neighbors being uncracked - as

$$q(n) = A(n)\ p^n \text{ Polynomial of } (1-p) \qquad \text{Eq. (4) in } [5\text{-}1]$$

where p is the probability of having a cracked cell, and indicated that this polynomial $P(1-p)$ can be expressed as

$$P\ (1-p) = \sum_{k=4\sqrt{n}}^{2n+2} a_k (1-p)^k \ .$$

The argument following Eq. (5) in [5-1] may be correct as far as p is concerned, but does not justify writing Eq. (4) in [5-1] as

$$q(n) = 0.5\ (5p)^n \qquad \text{Eq. (8) in } [5\text{-}1].$$

since $(1-p)^k$ is not close to unity at all. Hence the correct form reads as

$$q(n) \cong 0.5\ (5p)^n\ P(1-p)\ .$$

It is not clear how to proceed using this correct form of Eq. (8) in [5-1] since the coefficients a_k in the polynomial $P(1-p)$ are not known. A possible way is to approximate the polynomial by a single term $(1-p)^m$.

Using the coefficients for the first six cases (i.e. for $n = 1$ through $n = 6$) we can get $m = 1.1 + 4.1$.

Unfortunately the straightforward result obtained by Lindborg that failure occurs when $p = 0.20$ is not correct. Aside from the error in Eq.(8) in 5-1 , Lindborg made use of the following series expansion going from Eq.(11) to Eq.(12) in 5-1

$$1 + 5p + (5p)^2 + \cdots = (1-5p)^{-1}$$

which is true only for $5p < 1$. Thus, he automatically set the limit for p as 0.20. A quick glance at the Fig. 4 in [5-1] proves also that Lindborg's results cannot be correct; for the total number of grains $N = 100$ and for the fraction of cracked grains $p = 0.19$; for example, it is impossible to have a crack which is 25 grains long.

It is the author's belief that Lindborg's analysis can be extended correctly using the discussed approximation for $P(1-p)$ and numerical procedure in the later steps. However, it is important to realize that the model is valid only for small values of p since it assumes p to be constant at all stages of grain cracking.

LEGAL NOTICE

This report was prepared as an account of work sponsored by the United States Government. Neither the United States nor the United States Atomic Energy Commission, nor any of their employees, nor any of their contractors, subcontractors, or their employees, makes any warranty, express or implied, or assumes any legal liability or responsibility for the accuracy, completeness or usefulness of any information, apparatus, product or process disclosed, or represents that its use would not infringe privately owned rights.

TECHNICAL INFORMATION DIVISION
LAWRENCE BERKELEY LABORATORY
UNIVERSITY OF CALIFORNIA
BERKELEY, CALIFORNIA 94720